COPPE
Instituto Alberto Luiz Coimbra de Pós-Graduação e Pesquisa de Engenharia
UFRJ

APPLICATION OF FRACTURE CRITERIA TO THE SIMULATION OF BOP RAM SHEARING

Lei Zhu

Tese de Doutorado apresentada ao Programa de Pós-graduação em Engenharia Oceânica, COPPE, da Universidade Federal do Rio de Janeiro, como parte dos requisitos necessários à obtenção do título de Doutor em Engenharia Oceânica.

Orientadores: Segen Farid Estefen
Marcelo Igor Lourenço Souza

Rio de Janeiro
Junho de 2020

APPLICATION OF FRACTURE CRITERIA TO THE SIMULATION OF BOP RAM SHEARING

Lei Zhu

TESE SUBMETIDA AO CORPO DOCENTE DO INSTITUTO ALBERTO LUIZ COIMBRA DE PÓS-GRADUAÇÃO E PESQUISA DE ENGENHARIA DA UNIVERSIDADE FEDERAL DO RIO DE JANEIRO COMO PARTE DOS REQUISITOS NECESSÁRIOS PARA A OBTENÇÃO DO GRAU DE DOUTOR EM CIÊNCIAS EM ENGENHARIA OCEÂNICA.

Orientadores: Segen Farid Estefen
Marcelo Igor Lourenço Souza

Aprovada por: Prof. Segen Farid Estefen
Prof. Marcelo Igor Lourenço de Souza
Prof. Murilo Augusto Vaz
Prof. Ney Roitman
Prof. José Luis Drummond Alves
Prof. Celso Kazuyuki Morooka

RIO DE JANEIRO, RJ – BRASIL
JUNHO DE 2020

Zhu, Lei

Application of fracture criteria to the simulation of BOP ram shearing/Lei Zhu. – Rio de Janeiro: UFRJ/COPPE, 2020.

XX, 132 p.: il.; 29, 7cm.

Orientadores: Segen Farid Estefen

Marcelo Igor Lourenço Souza

Tese (doutorado) – UFRJ/COPPE/Programa de Engenharia Oceânica, 2020.

Referências Bibliográficas: p. 124 – 132.

1. Blow-out preventer. 2. Ram shearing simulation. 3. Fracture criteria. I. Estefen, Segen Farid *et al.* II. Universidade Federal do Rio de Janeiro, COPPE, Programa de Engenharia Oceânica. III. Título.

To my beloved wife and our coming child

Acknowledgement

It would not be possible to accomplish the present thesis without supports from many people.

First of all, I would like to express my deepest gratitude to my supervisor, Prof, Segen Estefen, for offering me great insight and advice through my four and a half years of study at COPPE, UFRJ. The same thanks go to my co-supervisor, Prof. Marcelo Igor Lourenço de Souza. The discussion with him has benefited me a lot in building the numerical model. His support made me feel warm in the time waiting for the review of the manuscript.

Many thanks to Prof. Duan Menglan and Prof. Shi Lin, who gave me the opportunity to study abroad in Brazil. Special thanks to the BOP manufacturer in China, Rongsheng Machinery Manufacture LTD., for helping me to complete the full-scale BOP shear experiment and provide the experimental data. The work would not have been possible without the financial support of the China Scholarship Council and CAPES/Brazilian Ministry of Education.

Thanks also go to all my friends in Brazil, for all their support and help. The time I spent with them in Brazil will be the beginning of a lifelong friendship.

I also would like to thank my wife, Yuan Zheng, for her accompanying, patience, support, and empathy through this long journey. Her presence has been a constant source of strength and motivation in the years of my Ph.D. study.

In particular, during the difficult time of the global pandemic of COVID-19, I would like to thank the medical workers who are fighting the front line day and night. Their deeds inspire the whole world. Mourning for the patients who passed away during this period, may they rest in peace.

Resumo da Tese apresentada à COPPE/UFRJ como parte dos requisitos necessários para a obtenção do grau de Doutor em Ciências (D.Sc.)

APLICAÇÃO DE CRITÉRIOS DE FRATURA À SIMULAÇÃO DE CORTE DE BOP RAM

Lei Zhu

Junho/2020

Orientadores: Segen Farid Estefen
Marcelo Igor Lourenço Souza

Programa: Engenharia Oceânica

O Blowout Preventor (BOP) submarino é de grande importância para a segurança de operações offshore de perfuração de poços de petróleo e gás. O ram de cisalhamento BOP fornece a última defesa para proteção contra explosão. Uma abordagem comum para avaliar a capacidade de cisalhamento da ram BOP é a técnica de elementos finitos, mas a precisão ainda é um desafio devido à dificuldade de selecionar e aplicar um critério de fratura adequado. O objetivo desta tese é fornecer uma abordagem completa para a aplicação de critérios de fratura para a simulação de cisalhamento de BOP. Os seguintes critérios de fratura, CrashFEM, Johnson-Cook e Mohr-Coulomb Modificado, são aplicados e os resultados obtidos são comparados. Os dados experimentais do TRIP 690 são usados para derivar os parâmetros de fratura para todos os critérios, e uma abordagem de calibração modificada, especificamente para o critério CrashFEM, é proposta com base em um teste de tração padrão do material do tubo de perfuração S135, permitindo assim a aplicação prática do critério de fratura fornecido. Para verificar o modelo numérico combinado com o critério de fratura, é conduzido um experimento de cisalhamento em larga escala do BOP. Modelos numéricos confiáveis com malha refinada são construídos de acordo com as condição de carga e contorno do experimento. A curva de pressão de cisalhamento é primeiramente comparada com a curva de pressão simulada. O resultado mostra que a correlação entre resultados numéricos e experimentais é consistente. Um estudo de caso é realizado para investigar a eficiência de cisalhamento para diferentes lâminas de ram. O modelo proposto é aplicado com sucesso para analisar a eficiência de cisalhamento de cada desenho de ram.

Abstract of Thesis presented to COPPE/UFRJ as a partial fulfillment of the requirements for the degree of Doctor of Science (D.Sc.)

APPLICATION OF FRACTURE CRITERIA TO THE SIMULATION OF BOP RAM SHEARING

Lei Zhu

June/2020

Advisors: Segen Farid Estefen
Marcelo Igor Lourenço Souza

Department: Ocean Engineering

A subsea blowout preventer (BOP) stack is of great importance for the safety of offshore oil and gas drilling operations. The shear ram BOP provides the last defense for blowout protection. Fail to cut the drill pipe or isolate the well may induce disaster damage on humans and facilities, as it happened in the case of the Macondo accident. A common approach to help to evaluate the shear capacity of the BOP ram is the finite element technique, but the accuracy is still a challenge due to the difficulty of selecting and applying a proper fracture criterion. The objective of this thesis is to provide a thorough approach to apply fracture criteria for the simulation of BOP ram shearing. The following fracture criteria, CrashFEM, Johnson-Cook, and Modified Mohr-Coulomb, are applied, and the obtained results are compared. The TRIP 690 experimental data are used to derive the fracture parameters for all criteria, and a modified calibration approach, specifically for CrashFEM criterion, is proposed based on a standard tensile test of S135 drill pipe material, thus enabling the practical application of provided fracture criterion. To verify the numerical model combined with the fracture criterion, a full-scale BOP ram shearing experiment is conducted. Reliable numerical models with refined mesh are built according to the loading and boundary conditions in the experiment. The shearing pressure curve is firstly compared with the simulated pressure curve. The result shows that the correlation between numerical and experimental results is consistent. A case study is conducted to investigate the shear efficiency for different ram blades. The proposed model is successfully applied to analyze the shear efficiency of each ram design.

Contents

List of Figures

List of Tables

List of Symbols

A, n	material constants for power hardening law
A_{cl}	ram closing area
A_{cs}	cross-sectional area of the pipe
a_0	original radius of the round bar specimen
a_f	cross-section radius at damage initiation
c, f	material parameters in CrashFEM criterion
C_1, C_2, C_3	material parameters in MMC criterion
C_f	ductile fracture scaling factor
C_r	BOP closing ratio
D	overall damage variable
d	scalar damage variable
d_0, d_1, d_2	material parameters in Johnson-Cook criterion
d_i	individual damage variables
E_l	elongation %
F_{DET}	shearing force calculated bt DET
F_{op}	operation hydraulic force
F_{rs}	ram shearing force
F_x	lateral concentrated load force
g_1, g_2, g_3	BOP geometry constants
h_0, h_1, h_2	constants for shearing force equation by regression analysis

$[I]$	identity stress tensor
k_s	material parameter in CrashFEM model
L	characteristics length of the element
M_0	fully plastic bending moment of the wall
N	external axial force
N_0	fully plastic axial force
N_p	plastic force capacity of cross-section
$N_{act}, N_{mult}, N_{max}$	number of individual damage variables
P_{cl}	closing pressure
P_{op}	operation pressure
P_{rs}	ram shearing pressure
P_w	wellbore pressure
p	hydrostatic pressure
ppf	weight per foot
q	the second deviatoric stress invariant
R	radius of undeformed tube
r	normalized third deviatoric stress invariant
$[S]$	deviatoric stress tensor
S_E	standard error
t	thickness of pipe
U_S	ultimate tensile strength
$\bar{u}^{pl}$	effective plastic displacement
$\bar{u}_f^{pl}$	effective plastic displacement at the point of failure
Y_S	tensile yield strength
$\Delta\bar{\epsilon}^{pl}$	increment of the equivalent plastic strain

δ	indentation depth
δ_d	relative distance of the blades after the full collapse
$\bar{\epsilon}_0^{pl}$	initial value of the equivalent plastic strain
$\bar{\epsilon}_f$	equivalent plastic strain to fracture
$\bar{\epsilon}_f^D(\eta)$	ductile limit curve with correction
$\bar{\epsilon}_f^d$	ductile fracture strain
ϵ_f^{dp}	measured equivalent plastic strain at damage initiation
ϵ_f^{d0}	predicted equivalent plastic strain
$\bar{\epsilon}_f^{pl}$	plastic strain at failure
$\bar{\epsilon}_f^S$	shear fracture strain
ϵ_S^+	shear fracture strain for equibiaxial tension
ϵ_S^-	shear fracture strain for equibiaxial compression
ϵ_T^+	ductile fracture strain for equibiaxial tension
ϵ_T^-	ductile fracture strain for equibiaxial compression
η	stress triaxiality
η_0	stress triaxiality of the smooth tension bar in a tension test
θ	normalized Lode angle
θ_S	shear stress ratio
θ_S^+	shear stress ratio for equibiaxial tension
θ_S^-	shear stress ratio for equibiaxial compression
ξ	half-length of dented region
$[\sigma]$	stress tensor
$\bar{\sigma}$	equivalent stress
σ_0	yield tress
$\sigma_1, \sigma_2, \sigma_3$	maximum, medium and minimum principal stress, respectively

σ_e	energy equivalent flow stress
$[\sigma_{ef}]$	effective stress tensor
σ_m	mean stress
τ	denotes the flow stress of the material in shear
τ_{max}	the maximum shear stress
ω	state variable for damage initiation

List of Abbreviations

API	American Petroleum Institute
AHSS	Advanced high-strength steels
A∗STAR	Agency for Science, Technology and Research
BOP	Blowout preventer
BSEE	Bureau of Safety and Environmental Enforcement
BSR	Blind Shear Ram
CSB	Chemical Safety Board
DET	Distortion Energy Theory
DIC	Digital image correlation
DNV	Det Norske Veritas
DVS	Double V Shear
DWH	Deepwater Horizon
EDS	Emergency Disconnection Sequence
EMC	Extended Mohr-Coulomb
ERC	Energy Risk Consulting
FE	Finite element
FEA	Finite element analysis
J-C	Johnson-Cook
LFS	Low Force Shear
LMRP	Lower Marine Riser Package

MASP	Maximum anticipated surface pressure
MMC	Modified Mohr-Coulomb
MMS	Minerals Management Service
NOV	National Oil Varco
OD	Outer diameter
OEM	Original Equipment Manufacturer
R-O	Ramber-Osgood
SEMS	Safety and Environmental Management System
U.S.	United States
VBR	Variable bore rams

Chapter 1

Introduction

1.1 Background

As the global energy demand is continually increasing, the oil and gas industry has explored to deepwater and ultra-deepwater offshore oil and gas fields. This process is associated with the use of highly complex equipment and recognized technological advancement, both challenges and risks increase with the water depth. In the worst case, the failure of equipment can cause serious consequences. Such events are unusual, but the occurrence of only one of them can compromise the continuation of offshore oil exploration and production and even cause huge loss for both economy and human lives, as was the case of the event occurred in the drilling phase in the Macondo field, in the Gulf of Mexico, in 2010. The development of new equipment, especially those related to subsea processing, must be followed by critical analysis of safe operation. In addition, proven equipment safety margins should be revisited, as new technologies are incorporated for its construction and operation.

In the exploration phase, aspects related to drilling safety should be treated as a priority. Well control and blowout prevention have become particularly important topics in the oil industry for a number of reasons. Among these reasons are high drilling costs, possible loss of life, and waste of natural resources when blowouts happen. Therefore, it is important to estimate the capacity of offshore equipment and investigate the failure mode of them.

1.2 Blowout Preventer

A blowout is an uncontrolled kick flow of formation fluids. Offshore well blowouts, which are uncontrolled releases of hydrocarbons to the environment, pose a threat to both the safety of offshore workers and the environment.

Zubaidah Ismail et.al [1] examined several accidents in the offshore drilling ac-

tivities from 1957 to 2013, for the recorded 219 accidents, blowouts represented the highest number of basic causes with 46.1%. Table1.1 denotes several notable offshore blowouts from 1990 to 2012[2]. It can be seen that offshore blowout accidents happened in several offshore oil fields, the rig type also differs from jackup to semi-submersible platform.

Table 1.1: Notable offshore blowouts from 1990 to 2012[2]

Years	Rig name	Rig owner	Rig type
1993	Actinia	Transocean	Semi-submersible
2001	Ensco 51	Ensco	Jackup
2002	Arabdrill 19	Arabian Drilling Co.	Jackup
2004	Adriatic IV	Global Sante Fe	Jackup
2007	Usumacinta	PEMEX	Jackup
2009	West Atlas / Montara	Seadrill	Jackup / Platform
2010	Deepwater Horizon	Transocean	Semi-submersible
2010	Vermilion Block 380	Mariner Energy	Fixed offshore platform
2012	KS Endeavour	Chevron	Jackup

In Brazil, the frequency of the blowout dropped since 1988, due to well control training and certification program as well as the development in well control monitoring equipment and kick detection technology. Whereas, several accidents still happened during the drilling operations, as it is shown in figure1.1 [3] .

Normally, during the drilling operation, the rig crew maintains the drilling fluid's hydrostatic pressure at a value by several engineer methods, this value is supposed to be greater than the formation pressure, to make sure the formation fluids cannot flow into the well. However, the formation pressure can exceed hydrostatic pressure in some situations, such as the crew fails to fill the hole to replace the volume removed by the drill string, or the drilling string penetrates a formation with abnormally high pressure. To solve this problem, the blowout preventer (BOP) will be activated to provide safety as a secondary well control barrier. The BOP system is an arrangement of valves, several types of preventers, connectors, and the control system.

The BOP is a critical element of well control and has a long history of application in the oil and gas industry. As reviewed by Han[4], in 1924, the ram BOP was introduced to the market by Cameron Corporation. A shear ram BOP with two

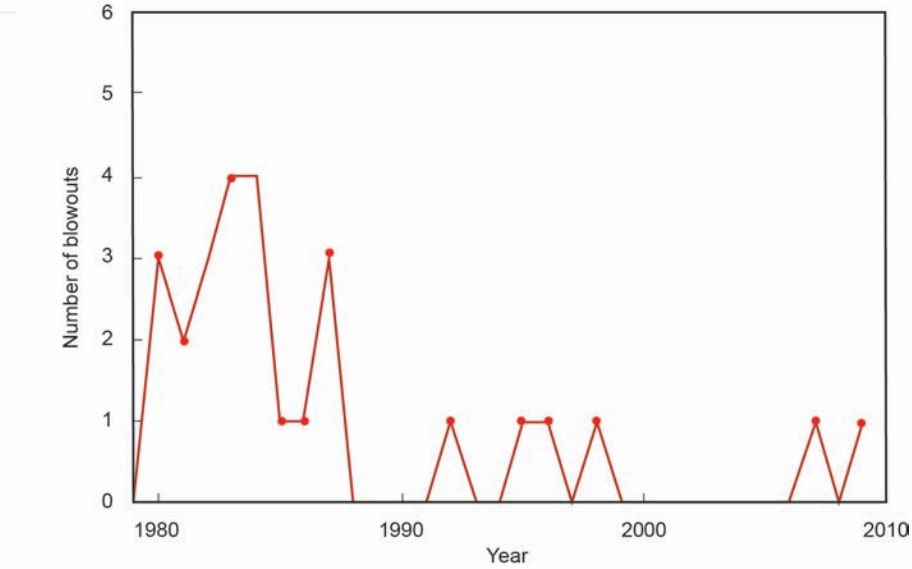

Figure 1.1: Blowouts in Brazil during drilling operations(adapted from[3])

opposed ram assemblies was invented by NL Industries Inc. in 1986. In 1990, the Azerbaijan Petroleum Machinery Research Institute reported a shear ram BOP and the rams were driven by the hydraulic cylinder pistons. These initial inventions and designs met the needs of early oil and gas exploration and laid the foundation for the development of the BOP equipment system.

A subsea BOP stack plays an extremely important role in providing safe working conditions for drilling activities in deepwater and ultra-deepwater regions. For floating drilling rigs, such stacks are commonly installed at the wellhead on the ocean floor. With the same purposes of conventional land drilling BOP stacks, they provide a means of pressure control when formation flows develop and also prevent the blowout incident by sealing the well.

Figure 1.2 [5] illustrates a typical riser and subsea BOP system. The subsea BOP system has two sections, the Lower Marine Riser Package (LMRP) and the lower BOP stack. The LMRP usually has one annular BOP, one connector to attach to lower BOP, the control system, gas bleed valves, and flex joint. The lower BOP stack is installed at the wellhead with the marine riser pipe. The riser system provides a means to return drilling fluids to the surface. Auxiliary lines on the riser provide hydraulic supply fluid. High pressure choke and kill lines provide means to bring any gas or other high pressure influx to the surface safely. Because floating rigs move, there is a motion compensation system, a telescopic joint, and a flex joint on the top and bottom of the riser string.

The subsea BOP stacks usually consist of various BOPs and other components. Annular preventers can seal off on any dimension from open hole to the largest drill pipe or casing in the wellbore, but it is designed only to seal the annulus. Ram

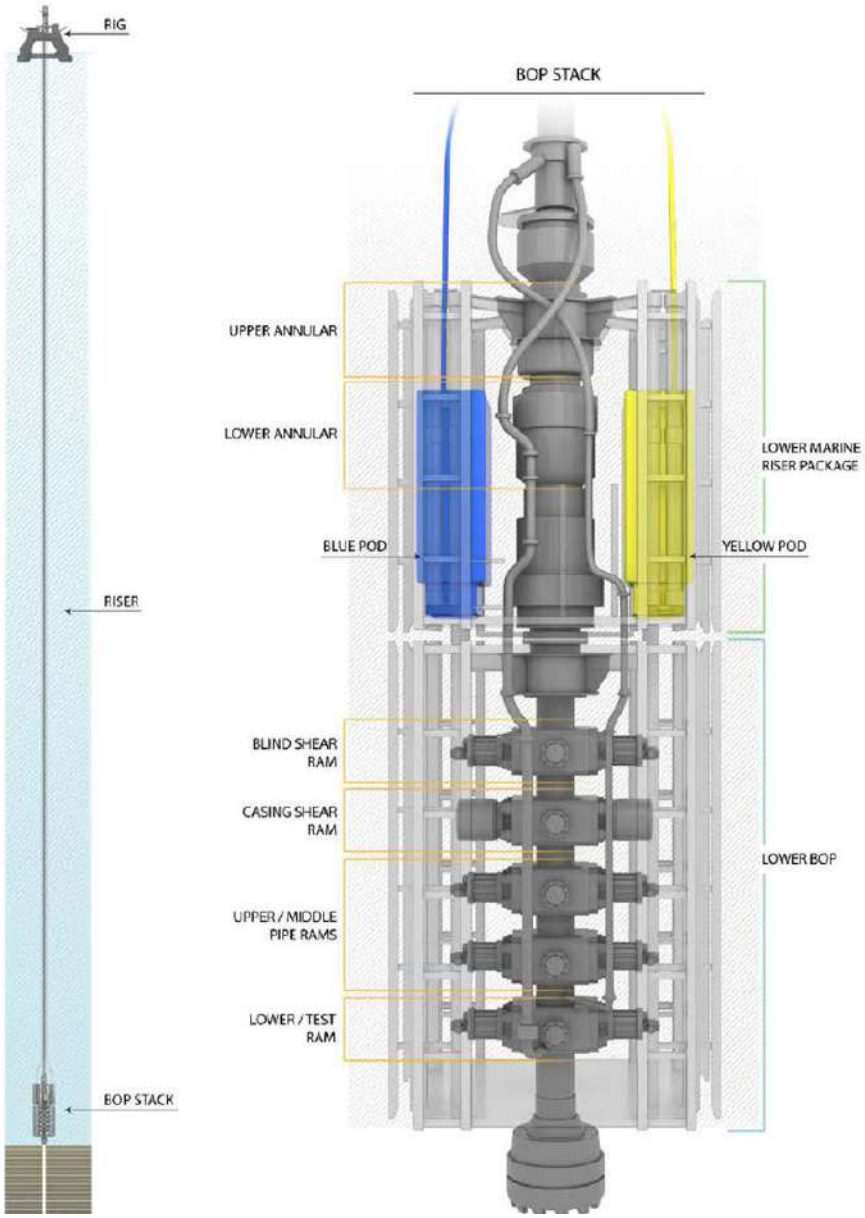

Figure 1.2: Schematic illustration of the subsea riser and BOP system[5]

BOPs are also used to seal the well through a combination of different ram types and specific operation sequence. In some emergency situation, such as subsea blowout accident or other situation that the Emergency Disconnection Sequence (EDS) need to be activated, the BOPs need to shear the drill string or other tubular inside the well and seal the wellbore. For the implementation of this last defense function, the most important components are shear rams. Those BOP rams have blades with a built-in cutting edge. If drill pipe or other tubular is still inside the wellbore during the closing operation, they are supposed to be cut and the wellbore should be sealed.

Of all the components on the blowout preventer, shear rams are the only device that is supposed to cut through the drill pipe. To prevent a blowout, they stop the

formation fluid moving forward and give the crew valuable time to recover downhole pressure balance. As for EDS, after the shearing and sealing process, the LMRP will disconnect with the BOP and leaves the BOP alone on the seabed to further control the well.

As various shear rams are used, according to the American Petroleum Institute (API) standard[6], shear rams can be classified into sealing shear rams and non-sealing shear rams. As one of the typical sealing shear rams, the Blind Shear Ram (BSR), indicated in figure 1.3 [7], has one straight and one V-shaped blade. Apart from the differences in details of dimensions, this blade is commonly used by Original Equipment Manufacturer (OEM).

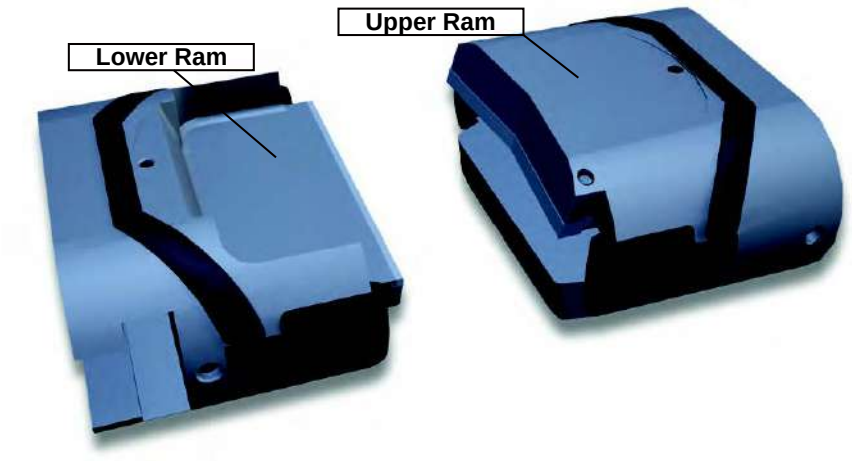

Figure 1.3: Typical Blind Shear Ram[7]

Double V Shear (DVS) ram, such as the one designed by Cooper Cameron in 2001[8], has both V-shaped blades. Several studies have reported that DVS rams can easily cut off multi-strand wire rope in the BOP, and have more shear efficiency than BSRs[9].

Non-sealing shear ram is capable of shearing or cutting certain tubular, but does not seal the well. For example, the Casing Shear Ram is capable of cutting tubular with a large, thick wall. The typical geometry of CSR is denoted in figure 1.4 [7].

A typical sealing shear ram system is demonstrated in figure 1.5 [10], the sequence of the closing operation is denoted. As the closing operation begins, the hydraulic fluid goes through the position of point 1 in the figure, enters the shuttle valve, and pushes a metal "shuttle" to one side. The fluid thus arrives at the hydraulic cylinder behind pistons, denoted in point 2, and drives the ram to move forward and shear the drill pipe. At point 3, the wedge locks can prevent the pistons from moving back. After the shearing, rubber seals on the ram will close off the well. Oil pushing up from the well adds pressure below and behind the ram, helping to keep the ram closed.

Figure 1.4: Typical Casing Shear Ram[7]

In the past, the use of a five BOP stack with one blind shear ram seems to be a standard configuration and common practice of the offshore oil and gas industry, the majority of BOP stacks had a single shear ram. Due to safety considerations, more BOPs are required in a subsea BOP stack for deepwater drilling. As in the case of Macondo accident, there were two shear ram BOPs on the Deepwater Horizon's BOP stack: one CSR and one BSR. As mentioned earlier, non-sealing CSRs can be used in a BOP stack in addition to the BSRs. CSRs are typically high-capacity shear rams capable of shearing drilling collars and casing strings. Usually, they are placed below the BSR in the BOP stack. When CSRs are installed and it is necessary to conduct the BOP shearing and closing operation, the CSRs shear the pipe and the BSRs above the casing rams are closed to seal the well. Shear rams normally require higher closing pressures to shear the pipe than the pipe rams require to create a seal on the drill pipe. Some rigs have two BOP control systems: one is a standard system for closing the shear rams to seal the well with no pipe in the BOP; the other is a high-pressure control system for shearing pipe. In a subsea BOP control system, several ways are responsible to activate the BSRs.

Due to these complicated technologies and special features, shear rams provide the last line of defense among the various devices on the subsea BOP system. The drill operators must ensure that sufficient hydraulic pressure is available to carry out the shear operation. Either fail to shear the pipe inside the well, or fail to seal the wellbore will cause disastrous consequences. Even though it is often difficult to conclude which failure of equipment ou operation is the main cause of a blowout accident, at least three notable accidents were proved to be relevant with the failure of BOP shearing and sealing operation.

The first one induced an estimated 140 million gallons of oil spilling into the ocean of Yucatan in 1979[9]. To control the blowout of an exploratory well, Ixtox 1,

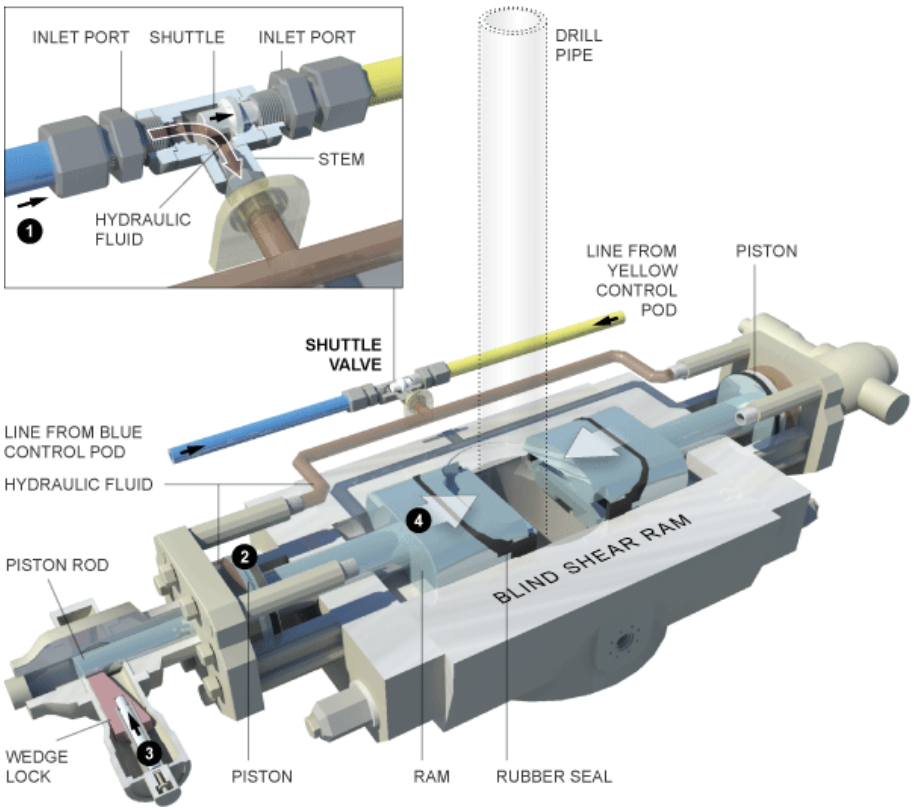

Figure 1.5: Typical Sealing Shear Ram System[10]

shear rams were activated at one point and fail to shear, possibly because the drill collars were just in the stack. At that time, this was the second-largest spill all over the world.

The second case happened in an onshore oil filed of Chongqing, China on Dec 23th, 2003 [4]. The drill pipe in the BOP stack was deformed by the shear rams, but not sheared successfully. The well did not seal and went out of control. 243 persons were killed by gas poisoning after the blowout accident.

The last accident is the most famous one: the Deepwater Horizon(DWH) blowout in the Gulf of Mexico in 2010. According to several reports, the BSR blades fail to cover the complete BOP annulus, and the off-center position of the drill string induced the failure of BOP shearing operation. The details corresponding to the failure of shear rams in this accident is reviewed in the following section.

1.3 Shear ram failure in the Macondo accident

A huge blowout happened in the operation of Macondo well on April 20, 2010, which led to enormous consequences. Eleven workers on the DWH drilling rig lost their lives, and 16 others were seriously injured. There were also enormous consequences for the companies involved in the drilling operations, to the Gulf of Mexico envi-

ronment, and to the economy of the region and beyond. The total economic impact is in the tens of billions of dollars. The flow continued for nearly 3 months before the well could be completely killed, during which time nearly 5 million barrels of oil spilled into the gulf. The Deepwater Horizon was a semi-submersible offshore drilling unit. The maximum water depth of its operation is about 8000 feet. On April 20, 2010, during the drilling operation for an exploration well in the Gulf of Mexico, the control of the well was lost, the BOP system failed to seal the well, the blowout caused explosions and subsequent fires. The rig sank two days later, further resulted in a huge oil spill. After about three months of additional efforts, the well was permanently sealed. This accident took 11 lives, hurt 16 people, and did huge damage to the environment. The BOP stack on the rig consists of seven BOP components. The sequence of those BOPs from the top to bottom are two annular preventers, one BSR BOP, one CSR BOP, and three pairs of Variable Bore Rams (VBR). After the accident, the BOP stack was raised from the seafloor and transferred to the Michoud facility. Forensic tests were conducted for shear rams used on the rig[11]. Segments of drill pipe were also recovered from the drilling string and were matched together. This process includes a combination of visual examinations of the shear and fracture surfaces, laser profilometry, and mechanical tests.

In 2011, Det Norske Veritas (DNV) published a forensic examination report for DWH BOP failure in the Macondo accident [11]. Based on the examination of the damage to the BSR blocks and the drill pipe segments, the position of the drill pipe at the time of cutting by the BSR was not at the center of the wellbore. The pressure increase produced an upward force (axial compression load) on the drill pipe. This upward force provided the forces necessary for the drill pipe to elastically buckle, forcing the drill pipe to the side of the wellbore.

According to the results of those tests and analysis, the timeline sequence of various failures was inferred. The EDS was noted to have been activated but not followed by a successful implement of the BSR shearing and sealing operation, due to the failure of both control pods. The upper VBRs were found in the closed position, a section of drill pipe was buckled and off-center between the shearing blade surface. The cross-section of the drill pipe was outside of the blade surface and not fully sheared as intended. It was speculated that the BSR was activated by the Autoshear system later, but the well was not sealed.

BSRs failed to close and seal the well during the accident and were identified as the primary cause of failure of the BOP stack according to these pieces of evidence[11]. The insufficient ability of the BSRs to shear the off-center drill pipe is was indicated.

As denoted by DNV, various OEM equations exist for an approximate calculation

of the force required to shear a drill pipe, whereas these methods only consider the most common shear situation for the BSR, the pipe is centered and without axial tension or compression. To further study the capability of shear rams to shear drill pipe in specific conditions, DNV has performed two FE models. One is an elastic buckling model of the drill pipe section between the UA and the Upper VBR. The other is a ram shearing model based on the physical evidence on the recovered drill pipe and BOP ram segments. For estimating the cause of the buckling, DNV built a Finite Element (FE) simulation and found that a compressive axial load of 113,568 lbs on the drill pipe was necessary to cause buckling. They also simulated the shearing process of DWH BSR. A FE model and an update of the off-center drill pipe shearing model were developed to illustrate the difference between the BSR cutting a centered pipe versus an off-center pipe. The shearing force and shearing pressure calculated in the center scenario simulation was compared with other related studies.

For the off-centered drill pipe, the FE model predicted a 2.8 in. block displacement between the upper and lower BSR blocks for an applied force of 1,256,750 lbs (equivalent to 5590 kN or 5280 psi), which means the close force was far beyond the BOP ability. The upper and lower BSR blocks were 2.8 in. from being fully closed. The side packers were 1.7 in. from making initial contact and sealing. The lower BSR blade was 2.2 in. from contacting the rear packers and sealing. This study compares the process of BSRs to shear a centered and off-center drill pipe and calculates the forces to cut a centralized and buckled drill pipe. It was concluded that the shearing force was increased by 41% when shearing the buckled drilling pipe compared to the centralized one.

Later, in 2011, another analysis report was published for Macondo DWH blowout, calling for improving offshore drilling safety[12]. In the report, the function of CSR of DWH was clarified: CSRs are installed in the BOP stack below the BSR so that the casing rams can be used to sever thicker pipe, and then the drill string above the casing rams can be raised out of the way so that the BSR can be closed and the well sealed. Even with the addition of a CSR, the ability to seal the well is questionable if the pipe either above or below the CSR must be moved out of the way after the CSR cuts the pipe to allow one or more BSRs to seal the well. In a well control emergency, there is no assurance that the pipe can be moved at the appropriate moment to allow the BSR to seal. Also, they identified the role of BOP failure in Macondo Blowout: the faulty design of the BSR, which would not shear and seal a modest 5.5 in. diameter drill string (well below its rating) in compression, significantly contributed to this national disaster. Given that there was only one BSR in the BOP system at the Macondo well and that it failed to stop the blowout because of its design and operational shortcomings, there is an

urgent need for those shortcomings to be corrected. The performance of the design capabilities described in the preceding recommendation should be demonstrated and independently certified on a regular basis by test or other means.

In 2014, another study denotes that, if the BSR failed to seal the well during high-velocity well flow conditions, as denoted in figure 1.6 [5], the leakage of the sealing components can result in higher pressure and furtherly damage the BOP. This extreme situation was very likely to have happened to the BOP of the Macondo well, according to the erosion area on the BOP component found during the forensic test.

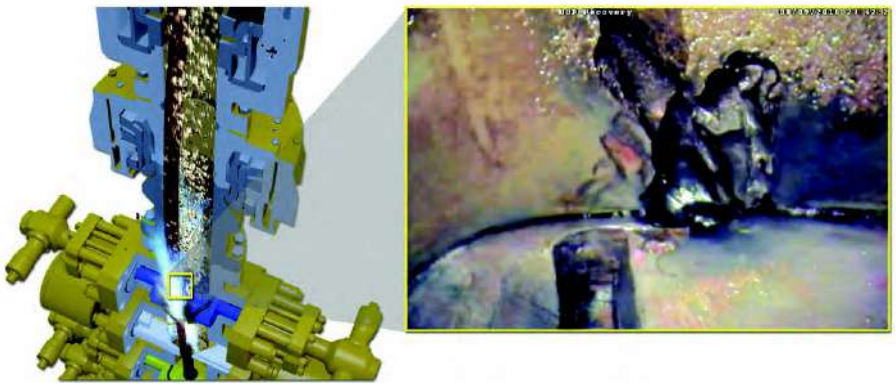

Figure 1.6: Simulation of the high-velocity well flow leakage[10]

Based on those forensic tests and numerical simulations, the primary cause of failure was identified as the blind shear rams failing to fully close and seal due to a portion of drill pipe trapped between the blocks. The drill pipe elastically buckled within the wellbore due to forces induced on the drill pipe during the loss of well control. As a consequence, the blind shear ram cannot move the drilling pipe into the blades. It is recommended that the industry examine and study the ability of the shear rams to complete their intended function of completely cutting tubular regardless of their position within the wellbore, and sealing the well. The findings of these studies should be considered and addressed in the design of future Blowout Preventers and the need for modifying current Blowout Preventers to address these findings.

After the Macondo accident, the industry updates the requirement of the shear ram test process, more departments are involved to address the demand for shear ram safety improvement. In the United States (U.S.) offshore operations, current standards include comprehensive shear-ram verification test requirements, as well as BSRs test practices recommendations. New requirements regarding shear capacity are clearly stated [13]. For example, BOP BSR ratings must exceed the Maximum Anticipated Surface Pressure (MASP) defined for the drilling operation; BSRs must be able to shear any drill pipe (excluding tool joints, bottom hole tools, and heavy

weight drill pipe or drill collars), work string, or tubing used in the field with the shear rams, they must also be able to seal well bores subsequent to shearing. Additionally, shear capability under MASP will be required for landing strings (for liners or casings); shear subs on a subsea test tree; tubing with exterior control lines/flat packs; and electric, wire, and slick line used in the field with the shear rams. At least one shear ram must be capable of sealing the wellbore after shearing under MASP conditions as defined for the operation. Any non-sealing shear ram(s) must be installed below a sealing shear ram(s). Starting no later than May 1, 2023, BOP systems must have centering mechanisms coupled within each shear ram to position pipes within the shear blade area and ensure shearing will occur.

Serious offshore accidents and the latest industry requirements indicate that the performance of shear rams in the BOP stack is still a challenge in practical engineering applications. During the deepwater oil exploration, how to make sure a successful shearing operation of the shear rams, including the sealing and non-sealing shear rams, require further study. Finite Element Analysis (FEA) plays a critical role in the failure analysis of the Macondo accident and shows large potential. Based on the understanding of these issues, the purpose of this study has been confirmed.

1.4 Objective of the thesis

The starting point of the thesis is to provide a solution to help the offshore oil and gas industry to answer the question "how to estimate if a given BOP ram can shear a given pipe successfully in the deepwater exploration activities?" Prior researches demonstrated that the process of BOP ram shearing still needs additional study. Numerical simulation using the nonlinear finite element method has been a common and promising approach, whereas difficulty arises when fracture theory needs to be applied to this complicated model. This issue built of motivation to study the modern fracture criteria to improve the understanding of the ram shearing process and to evaluate the application of proper fracture criterion to the ram shearing simulation. Therefore, the main objective of the thesis may be summarized as follows:

- Analyze the ram shearing force and discuss the necessity and advantage of fracture criteria
- Compare modern fracture criteria, identify suitable criteria in ram shearing simulation
- Propose a comprehensive application of fracture criterion including a practical parameters calibration approach

- Build a reliable FE model and provide full-scale experimental verification

1.5 Outline of the thesis

As shown in Figure 1.7, the present thesis consists of seven chapters, which are structured as follows.

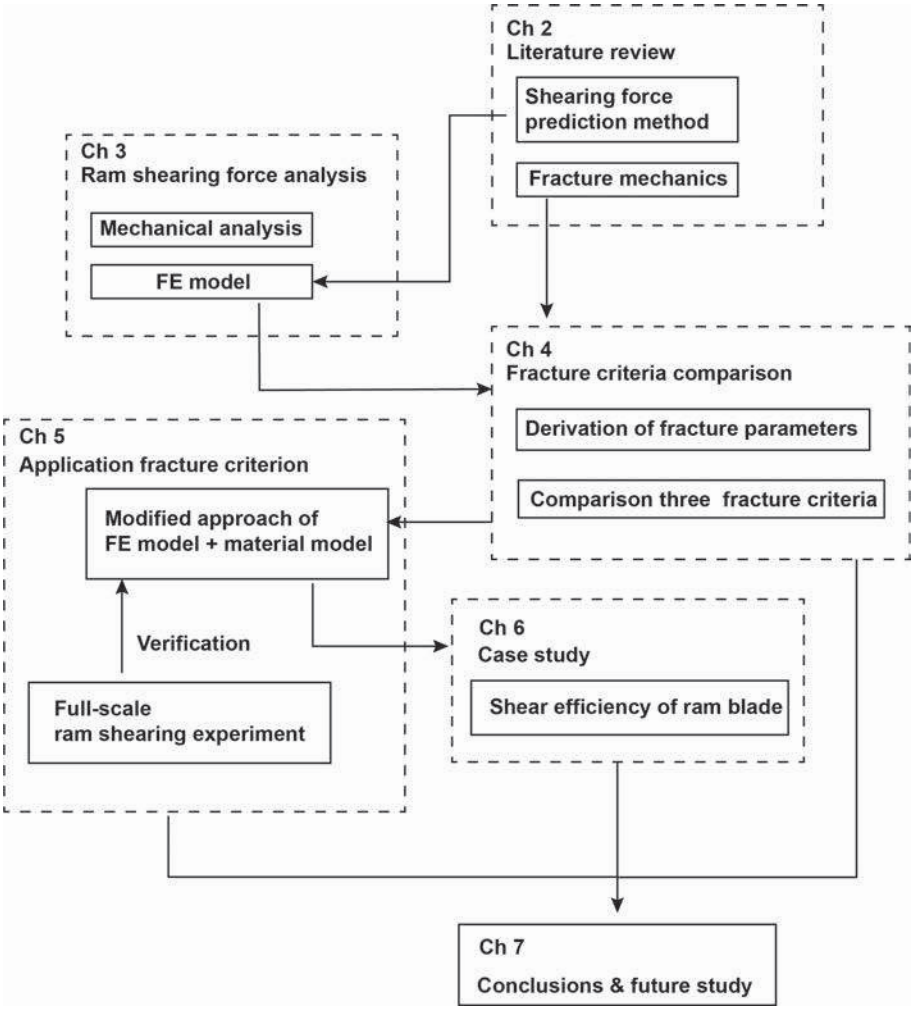

Figure 1.7: Structure of the thesis

Chapter 2 reviews the previous studies about BOP shearing capability. Full-scale BOP ram shearing experiments in the literature are listed and ram shear test data is collected. Some commonly used shearing force calculating methods are compared and analyzed. Previous FE models built for ram shearing simulation are investigated to identify the challenge and difficulties. Besides, fracture mechanics including classical fracture theory and damage mechanism are reviewed.

Chapter 3 analyzes the failure of the drill pipe during the ram shearing process to understand the fundamental elements which determine the ram shearing force. Several influence factors of the ram shearing force are investigated through a Finite

element analysis with constant fracture criterion. The simulated results are compared with actual shear ram test data and the accuracy of this method is discussed.

In Chapter 4, the CrashFEM criterion is compared with the Johnson-Cook and Modified Mohr-Coulomb criteria. Reasons for the differences among those criteria are discussed. A comprehensive application of the CrashFEM criteria for BOP shearing simulation is presented and recommendations are provided about the selection of suitable fracture criteria.

Chapter 5 presents a practical fracture parameter calibration approach, based on which the numerical model is verified by a full-scale ram shearing experiment. The shearing pressure curve is firstly compared with the simulated pressure curve. The stress distribution, damage evolution, and macro crack propagation on the pipe are also analyzed.

Chapter 6 provides a case study of the complete numerical model combined with a fracture criterion. The shearing efficiency study is conducted to investigate the influence of ram blade designation on the shearing force. This case study demonstrates the potential of the proposed numerical model in engineering applications.

The final, chapter 7, presents the main conclusions drawn in the thesis and indicates some meaningful future study that may broaden the scope of the current study.

Chapter 2

Literature review

In this chapter, existing methods to study the shearing performance of BOP shear rams are introduced with three main aspects: the experimental work, analytical solutions, and numerical simulations. The state of art for fracture theory is then reviewed, the advantage and limits of fracture mechanics and phenomenological ductile fracture criteria in the issue of BOP ram shearing is discussed.

2.1 Previous study of BOP shearing capability

2.1.1 Full-scale ram shearing test and experimental work

To predict the shear capacity of shear ram BOPs in the oilfield, the ram shearing test conducted by the OEMs is the only way. Each preventer equipped with shear blind rams should be subjected to a shearing test. As specified in the API Specification 16A standard[6], these tests should be performed without tension in the pipe and with zero wellbore pressure. There is a minimum requirement of drill pipe size and grade for each size of the BOP. Shearing and sealing shall be achieved in a single operation. The piston closing pressure shall not exceed the manufacturer's rated working pressure for the operating system. Documentation shall include the manufacturer's shear ram and BOP configuration, the actual pressure and force to shear, and actual yield strength, elongation, and weight per foot of the drill pipe samples. In the BSR test procedure, a section (approximately four feet in length) of the drill pipe is required to be suspended vertically above the preventer and lowered into the wellbore. It is permitted to loosely guide the portion of the pipe below the ram to prevent excessive bending of the pipe section during shearing. The pressure at which the pipe is sheared will be obvious from the rapid pressure change at the instant of shearing. Thus, Ram shear tests record the required shear force or shear pressure, if the operating system pressure available has been exceeded, the pipe would not shear on the rig.

In 2002 and 2004, the West Engineering published two BOP shear study reports for U.S. Minerals Management Service (MMS), aiming to answer: "Can a given rig's BOP equipment shear the pipe to be used in a given drilling program at the most demanding condition to be expected?"[9, 14] As they reported in the study, even after 2000, many operators and drilling contractors chose not to perform the shearing test when accepting new or rebuilt drilling rigs. Manufacturers, operators, and contractors use empirical equations to estimate the shear force for drill pipes. West Engineering did an investigation for 14 offshore drilling rigs, only 7 of them were found to have conducted the shearing test. For those rigs providing test data, five rigs passed and two failed to shear the pipe on the surface (71% success) upon simple analysis of the testing data. This investigation reveals an uncertainty of the safety related to the ram shear capability that may occur in the offshore drilling operation. Besides, the report also denoted the inability of shear ram BOP to shear the tool joint of drilling pipe in the drilling operation. There is not an established requirement for tool joint length. With variable lengths of tool joints, hang off to shear offsets must be checked to ensure the shear ram does not attempt to shear at the tool joint. This also does not consider the situations of automatically actuated shear sequences where the operator does not have the opportunity to ensure no tool joint is in the shear path.

As required by the latest API Specification 16A [6], shear ram test is now mandatory for any preventer equipped with blind shear rams and the documentation including actual pressure and force to shear the pipe shall be provided by manufacturers. However, this test is extremely expensive and the test frequency is not uniformly defined by the standard. After the Macondo well accident, the experimental study of ram shearing ability has become increasing.

In 2011, Frank Springett et.al [15] introduced the Low Force Shear (LFS) technology based on the comparison of several ram shear test results. This new ram blade design was reported to have higher shear efficiency and can reduce shear force to shear the same pipe. Their shear ram study had begun since 2006, and they had conducted over 500 shear tests. From their observation, both the thickness of the pipe and the blade geometry have a great influence on the shear force, while the friction of the drill pipe has little to no impact. They also tested over 40 ram block designs to optimize the shear force. FEA was reported to help predict pipe failure, but those experimental work of pipe specimens to determine the failure mode of the material was not presented.

In 2013, MCS Kenny [16, 17] did a shear ram design study for the Bureau of Safety and Environmental Enforcement (BSEE). The report included experimental and FEA numerical investigation of BOP shear ram performance and design study. In this study, they use surface BOP rams to shear an S-135 drill pipe with a diameter

of 88.9 mm in a centralized non-flowing condition. They built a system mainly including a surface blind shear ram BOP, the control panel to control the rams moving, and the pressure chart recorder to measured the pressure needed to close and open the ram. The average time of the two times of the shear test is about 6.5 seconds, from the touches of the pipe to the end of the shearing process. The highest pressure recorded to shear the pipe for the tests is 9.65 MPa and 8.62 MPa, respectively.

In 2014, Georgios et al. [18] from BP America Inc. reviewed the study in Abernethy's Weiull handbook[19] and revealed that as there is no consistent test procedure required for any regulations in the industry, some factors in the experiments test need to be controlled in order to accurately record shearing force values. For example, the ram speed can obviously affect the recorded shearing force. For two identical shear ram tests conducted for BP, half the ram speed can cause a 6.5% decrease in shearing force. For another six tests, the blades stalled during the shearing process and thus induced 70% more force than the rest. In another test the blades were stopped and restarted several times during the shearing process, the shearing force decreased 22.1% than the other. As the author suggested, a consistent test procedure is in high demand.

In 2015, Han et.al [4] conducted a study of the damage of the shear ram in the shearing process. They used FZ35-70 blind shear ram BOP to shear S135 and super 13Cr drill pipes. The maximum shear force of the BOP control system is 1769 kN, the S135 drill pipe was successfully sheared, while the super 13Cr drill pipe was not sheared. During their onshore BSR BOP shear test, obvious plastic deformation of the ram blade edges was observed and measured after the shearing operation.

The latest experimental study of ram shearing was conducted by Edward[20] from Lloyd's Register Drilling Integrity Services Inc in 2016. Different from the former studies with only full-scale shear ram test, they also made an effort to use a cell model theory to calibrate the fracture parameters for drill pipe material with the standard test specimen. When applying the latest fracture theory to the ram shearing simulation, these fracture parameters based on experimental work are critical for an accurate FE model. However, when observing the ram tensile strength data of drill pipes, they found unexpected large variation in material specimens taken from close drill pipe sections. The actual shear force recorded from the shear ram test performed on the same drill pipe was also found inconsistent.

As for the influence of flow in the wellbore, to investigate the high-pressure fluid effect on the ram shearing process, a report of BSEE collects information of the promising facilities in the U.S. that can perform ram shearing test under flowing conditions [21]. This kind of experimental work may cover the situation that may happen to the BOP shearing operation during a real blowout scenario. However,

the study found that the industry has currently conducted no tests to evaluate the flowing fluid effect; even some identified facilities may be able to perform this test after modifications to their facilities, the scaled model is preferred because full-scale testing can be complicated and expensive. Also, there is a safety concern for conducting these types of tests.

Other full-scale shear ram test results available in the literature review [9, 17, 22, 23] are collected and presented in Table 2.1. The overall data provides an interesting and valuable reference for the ram shearing force study.

Table 2.1: Actual shear ram test data

BOP Ram	Pipe specifications	Number of tests	Average value of shearing force (kN)
Hydril	DP, S-135, ϕ127mm	12	1138.35
Hydril	DP, S-135, ϕ139.7 mm	12	1929.79
Cameron SBR	DP, S-135, ϕ88.9mm	2	1320.76
Cameron DVS	DP, S-135, ϕ149.2mm	1	2486.66
Cameron CSR	Casing,Q-125, ϕ346mm	1	5966.16
Cameron ISR	DP, S-135, ϕ139.7mm	1	1395.52
Hydril BSR	DP, S-135, ϕ168.2mm	1	3549.68
Cameron ISR	DP, G-105, ϕ127mm	1	946.58
Cameron ISR	DP, S-135, ϕ127mm	1	996.40

DP: drill pipe

A general trend may be that for the same type of BOP ram, the larger the size of the pipe being cut, the greater the shearing force requirement. However, the designation of ram can also affect the shear force. For example, a possible discrepancy may be observed on the ram shearing force for cutting the S-135 drill pipe with a diameter of 88.9 mm, which is greater than shearing forces for similar drill pipes with a diameter of 127 mm. Due to data incompleteness, it is quite difficult to have a good understanding of the packed elements and, nevertheless, a good agreement may be noted among the corresponding Shear Forces and some element characteristics. Apart from unknowing the ram designs and their characteristics, the corresponding Shear Forces vary. For example, the Hydril BSR for drill pipes with diameters of 127mm and 139.7 mm give higher shearing forces than the corresponding from

Cameron ISR, despite the drill pipe weight is 24.9 ppf(pounds per foot) for Cameron and 21.9 ppg for Hydril tests.

2.1.2 OEM equations

To estimate the shearing performance of a subsea BOP, manufacturers have used several equations to calculate the required shear force and combine these calculations with BOP shear test data. This chapter presents different formulations to calculate the required shearing force and proposes an integrated approach of finite element analysis for simulating the BSR shearing process.

To carry out a closing operation, the BOP operation system offers a hydraulic pressure, pushing the ram block towards each other until the well is closed and sealed. During this process, the wellbore pressure needs to be overcome. Manufacture, therefore, built a closing ratio C_r in the design of the hydraulic piston. Basic equations in a BOP closing and opening process are summarized as follows:

$$C_r = \frac{P_w}{P_{cl}} \tag{2.1}$$

Where P_w is the wellbore pressure, and the P_{cl} is the closing pressure of BOP.

For the shear ram BOP, higher closing pressure is normally required to shear the pipe and close the well. Thus, during the shearing operation, the wellbore pressure also needs to be overcome.

$$P_{cl} = \frac{P_w}{C_r} + P_{rs} \tag{2.2}$$

Where P_{rs} denotes BOP ram shearing pressure.

In the offshore oil and gas industry, operators or designers need to make sure that the subsea BOP system has enough operation pressure to shear the pipe successfully. By ignoring the friction on the blade surface, the balance of force can be obtained on the transverse direction, as denoted in Figure 2.1.

For a well without fluid, the P_w equals to zero, thus Equation 2.2 can be denoted as:

$$P_{cl} = P_{rs} \tag{2.3}$$

Accounting for the closing area, the hydraulic pressure is calculated by

$$P_{cl} = \frac{F_{rs}}{A_{cl}} \tag{2.4}$$

where F_{rs} denotes the shearing force of the ram, A_{cl} denotes the BOP closing area. It is assumed that the closing pressure is consistent for both BOP rams.

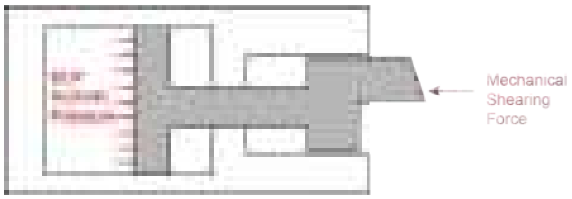

Figure 2.1: Balance of forces on a BOP shear ram

In the aspect of the BOP operation system, the operation hydraulic force acts on the closing piston F_{op}, also can be presented by the operation pressure P_{op} as follow.

$$F_{op} = P_{op} \cdot A_{cl} \tag{2.5}$$

As A_{cl} various by operator types, with the same operation hydraulic pressure, shear ram BOP may offer different values of F_{op}. Table 2.2 shows examples of BOP operators and maximum closing forces at 20 MPa [9]. This information is useful in understanding which drill pipe can be sheared in the various BOPs.

Drill operator must decide the grade of the maximum value of P_{op} for BOP shear rams, which means the maximum available hydraulic pressure to carry out the shear and seal operation. Theoretically, as a matter of safety, the following criterion must be fulfilled:

$$Max.P_{op} > Min.P_{cl} \tag{2.6}$$

Some simplified analytical solutions were built and reported that they can help to increase the reliability of the ram shearing force prediction. Generally, they are limited to special assumptions and only valid for some special situations. The accuracy of those formulas is also needed further discussed. One of the most commonly used solutions is the Distortion Energy Theory (DET). This theory says that failure occurs due to the distortion of a part, not due to volumetric changes in the part[9]. In pure shear stress, material failure occurs when the shear stress reaches 57.7% of the material tensile yield. The equation for shear force is then:

$$F_{rs} = 0.577 \times A_{cs} \times Y_s \tag{2.7}$$

Where Y_s denotes the tensile yield strength of the drill pipe to be sheared, A_{cs} denotes the cross-sectional area of the pipe.

Table 2.2: Operation force from BOP manufacturers[9]

BOP and operator type	Close area (cm^2)	Operation force at 20 MPa (kN)
Cameron 10K U w/LB	1445.16	2989.2
Cameron 10K U	1470.96	3042.6
Cameron 15K UII	2129.03	4403.7
Cameron 15K TL ST locks	1541.93	3189.4
Cameron 15K TL Ram locks	1645.16	3402.9
Cameron 15K TL Boosters	3277.41	6779.1
Hydril	1029.03	2128.2
Hydril	1217.42	2518.0
Hydril	1829.03	3783.6
Hydril	2027.09	4192.4
Hydril	2452.25	5072.7
Shaffer	992.90	2054.3
Shaffer	1218.06	2519.7
Shaffer	2453.54	5074.4
Shaffer booster	1000	2068.5
Shaffer booster	1894.83	3919.2
Shaffer booster	2198.71	4548.0
Shaffer booster	2414.19	5260.1

The DET shear equation method, while being reasonable, was found not to consistently predict the actual shear forces in many studies. However, the DET formula is still commonly used to estimate the shear force. As Frank Springett observed, for the V-shear blade ram, when using the ultimate tensile strength U_s, instead of Y_s, the DET is found to be accurate to predict the maximum required force to shear a drill pipe with high Charpy value, but much larger than that of pipe with low Charpy value. They suggest the DET with U_s method to be the upper bound of the peak shear force.

A regression analysis for shearing force prediction was conducted by West Engineering[9] . The report invented new equations for which regression analysis was used with Y_s and elongation being independent variables in predicting shearing force. In general, the formula used is as follows:

$$F_{rs} = h_0 + h_1 \times F_{DET} + h_2 \times E_l + 2 \times S_E \tag{2.8}$$

Where h_0, h_1, h_2 denote constants, F_{DET} is the predicted shearing force using DET in Kips, E_l denotes the elongation% of the pipe material, S_E is the Standard Deviation.

Table 2.3: Calculation for three grades of drill pipe[9]

Pipe Grade	Equation
S-135	$F_{\mathrm{rs}}(Kips) = -35.11 + 0.630 \times F_{\mathrm{DET}} + 4.489 \times E_{\mathrm{L}} + 2 \times 76.69$
G-105	$F_{\mathrm{rs}}(Kips) = 181.33 + 0.396 \times F_{\mathrm{DET}} + 2.035 \times E_{\mathrm{L}} + 2 \times 62.89$
E-75	$F_{\mathrm{rs}}(Kips) = -234.03 + .318 \times F_{\mathrm{DET}} + 25.357 \times E_{\mathrm{L}} + 2 \times 62.03$

Table 2.3 denotes formulas for three pipe material grades. It can be concluded that these formulas are basically DET with the correction of elongation value. Those shear data were collected before 2000, with the increase of drill pipe ductility in recent years, those formulas may limit the accuracy of the current application. A similar regression analysis based on the latest shear test data may be more significant.

ENERGY RISK CONSULTING (ERC) provides shear verification services for both surface and subsea BOP equipment [17]. This empirical equation reflects the impact of pipe thickness on the shear force, but lack theory foundation. The shearing force with or without the wellbore pressure effects are denoted as follows:

Shearing Pressure Calculation (No Wellbore Pressure Effects)

$$P_{rs} = \frac{g_3 \times ppf \times Y_s}{g_1} \tag{2.9}$$

Shearing Pressure Calculation (Including Wellbore Pressure Effects)

$$P_{rs} = \frac{g_3 \times ppf \times Y_s + g_2 \times P_w}{g_1} \tag{2.10}$$

Where g_1 denotes BOP constant corresponding to the piston closing area, g_2 denotes BOP constant corresponding to the operator piston rod opening area, g_3 denotes the shear ram type or pipe grade constant, ppf denotes pipe weight per foot.

In 2014, Georgios [18] also proposed a simplified analytical model to estimate the upper boundary for the required shear force. This model assumed that the pipe is ductile enough and shear after the cross-section of the pipe is fully flattened. No penetration of ram blades into the pipe thickness is considered before the flattening process ends. Perfectly plastic material is also assumed, which means no hardening effect of the material is under consideration. Similar to Koutsolelos' solution, these assumptions limit the application of this model.

For a subsea BOP, when the rams of the BOP are closing, other forces may be involved such as the pressure of wellbore and seawater, etc. Closing against a wellbore kick can also increase the pressure required to close the rams. In actual operation, these variables should be included since closing the shear rams should be prepared for the worst case when there is wellbore pressure under the annular. The total effect of these additive pressures can result in an increase of 20% or more to the shearing pressure established at the surface (using a 3.5 MPa wellbore kick and mud weight of 16 ppg) [14].

According to Brazilian offshore drilling experience,

- If $P_{rs} < 0.8P_{op}$, it is considered that the BOP/Ram is likely capable to shear;
- If $0.8P_{op} < P_{rs} < 0.9P_{op}$, it is considered that the BOP/Ram may be capable to shear;
- If $P_{rs} > 0.9P_{op}$, it is considered that the BOP/Ram is likely incapable to shear.

This criterion is not that accurate but much practical, for the input data is only P_{rs} and P_{op}, which is easily accessible for the OEM and operators.

2.1.3 Previous FE models

The Macondo blowout accident in 2010 made the safety of BOP become the focus of the industry again. The failure of BSR on the DWH reveals that shear rams may not be able to shear the pipe in some extreme scenarios. The investigation of the Macondo accident demonstrated the potential of FEA in ram shearing simulation, especially for some situations that may occur during offshore operation.

DNV first performed FEA on the ram shearing process based on the physical evidence on the recovered drill pipe and BOP ram segments. The model of drill pipe in buckling and off-center situation help people to recognize the capability of shear rams need additional study. To simulated the shear process of the drill pipe, DNV adopted ductile fracture and shear fracture mechanisms of a ductile material. These fracture models call for different fracture criteria with specific mathematic forms. The Johnson-Cook (J-C) damage model was utilized to capture the damage

initiation of the drill pipe material, the damage parameters were for 4340 steel, which is a base metal of API S135 grade material, but the value and derived approach was not reported.

Based on those BOP examinations conducted for the recovered segment of DWH, the U.S. Chemical Safety Board (CSB) reported their failure analysis report in 2014. It was denoted that the off-center scenario of BOP shearing had not been tested by BOP manufacturers before the accident of Macondo well. The API standard did not cover the topic of service conditions or testing protocol of shear ram BOPs. The industry had not previously recognized the phenomenon of a buckling drill pipe in a BOP may happen during certain extreme conditions and further lead to the failure of shear and seal operation. The reason for the buckling of drill pipe at Macondo was discussed, a finite element model of shear ram assemble with shear blades and rubber seal elements were built. They conducted a finite element study on the shearing and sealing capability of BSR using the ANSYS software. This study concluded that in the off-center situation that happens at Macondo, the required closing force to seal the well is more than two times of the shearing force, while the OEM equations did not distinguish the different value of force between the shearing and sealing. The required closing pressure to seal is over 37.8 MPa in this simulation, which exceeds the accumulator system supply pressure limit, 27.6 MPa.

It should be noted that, although the results of the study by CSB supported those conclusions of the former DNV study, their predicted force for the same shear ram BOP to shear the same drill pipe are different. To verify the FE model, both of those reports considered the maximum reaction force of the ram during the shear process equals to the required force to shear the pipe, and compared the calculated shear force with the Cameron empirical formula results. As Table 2 denotes, the standard error of the CSB result is 4.13% lower than the Cameron rating value, while the DNV result is 18.65% lower. If the Cameron rating value is considered to be accurate, this result indicates that for the DNV model, the shear ram should cut the pipe successfully if the pipe was in the centered position. However, the CSB model predicted the possibility that the shear process could not implement because the shearing force is very close to the rating value. The difference demonstrated the uncertainty of their FE model. The inconsistency may come from the adopted material parameters and fracture criterion selection. While the fracture mechanism adopted in the model of CSB study was not provided, the DNV conducted the simulation with the J-C damage model but did not clarify how they derive fracture parameters. The mesh size of the drill pipe in those models was not provided either. The CSB FE model is reported to have 145000 solid finite elements, while the drill pipe in the DNV model has 20030 elements, 20186 nodes. It is obvious that the numerical accuracy of these FE models needs to be improved by further study.

Table 2.4: Calculated shearing force/pressure for DWH BOP[5, 11]

Calculation method	Shearing force (kN)	Shearing pressure (MPa)	Prediction / Cameron empirical value
Cameron	3025	19.7	1
West Engineering	2262	14.6	0.74
DNV FEA	2567	16.6	0.84
CSB FEA	2900	18.9	0.96

Base on those failure studies of the DWH BSR, interest has been increased on the ram shearing simulation. A new model capable of predicting BOP shearing force reliably becomes increasingly crucial for the oil and gas offshore industry. Several FE models were built in the following years to investigate the shear performance of BOP rams. The variety was correlated with the loading condition, ram geometry, pipe position, and other aspects which may happen in an actual offshore drilling operation [4, 16, 17, 24–26].

In 2010, early-stage FE simulation was conducted by A. Tekin to achieve the estimation of shear force and optimization of ram geometry [24, 27]. He used approximated ram geometry and two kinds of drill pipe(with diameters of 127 mm and 139.7 mm) to simulate several factors on the shearing force, the fracture model was not explained clearly.

In 2012, the thesis of E. Koutsolelos explained the analysis of a shear ram and experimental determination of fracture parameters[25]. He performed a parametric study to investigate the influence of various mechanical and geometrical parameters on the resistance force and the instantaneous and final shapes of the pipe. In the FEA simulation, the MIT fracture model is applied, which based on the Modified Mohr-Coulomb (MMC) criterion combined with biaxial testing and calibration procedure. The process was performed for the TRIP690 steel as well as for the X70 grade steel. Three different cutting angles (30°, 45°, 60°) and three shape angles (120°, 150°, 180°) of BOP shear ram were performed in the simulation. Characterization of plasticity and fracture parameters of X70 was conducted by five different types of tests. These parameters of X70 then were used in the user-defined subroutine VUMAT to input the material behavior of X70 in Abaqus/Explicit. However, experimental results from small and/or full-scale cutting tests on pipes are not available in the published literature for different grades of steels. No comparison of these FE results with experimental data was performed in this thesis.

In 2013, MCS Kenny[28] did a shear ram design study for BSEE. The report included experimental and FEA numerical investigation of BOP shear ram performance and design study of BOP shear rams based on the validated simulation model. The study developed a methodology to model the shearing process and validate it with the shop test. The OEM shearing force was computed for the model under consideration and compared with the shop test and simulation and was found to be conservative. Also, a new shear ram design was proposed.

Similarly, in 2015, a 69 MPa (10000 psi) BOP shearing system was in development with tandem piston hydraulic actuators that can utilize up to a hydraulic operating pressure of 34.5 MPa, generating over one million pounds of shearing force, and shear rams designed for more efficient and robust shearing[29]. The geometry design of the ram blade is very similar to the one proposed by the Mcs Kenny in 2013.

In 2015, Chuanjun Han[4] from South-west Petroleum University of China published a study of the damage and failure of the shear ram of the blowout preventer in the shearing process. He used FEA to perform the effects of some factors: the inclination angle of the cutting edges, the V-shape angle of shear ram, and the diameter and length of the drill pipes. During their onshore BSR BOP shear test, obvious plastic deformation of the ram blade edges can be observed and measured after the shearing operation. In the shearing experiment, S135 and super 13Cr drill pipes were sheared by the shear rams. The forms of damage to the drill pipes and rams were observed and measured, such as fracture morphology, plastic strain, and surface damage.

There has been a collaborative effort between Agency for Science, Technology, and Research (A*STAR), and Lloyd's Register Energy Drilling for BOP shearing research after 2016[20, 30].They employ the MIT Extended Mohr-Coulomb (EMC) criterion for FEA simulation. The difference is that they present a micromechanics model to calibrate the undetermined parameters via a void coalescence mechanism and predict the forces for pipe shearing by finite element analyses. Theoretical work has focused on developing EMC coefficients with an intermediate level of a theory involving cell modeling of void coalescence for high triaxiality (tensile dominated) stress conditions. With this method, EMC coefficients are supposed to be determined from standard material tensile tests. However, the variation of ram tensile strength data of specimens taken from an identical drill pipe was found unexpected large. The cell model of drill pipe material is unlikely to succeed because of the basic assumption that continuous material has uniform properties on the macro scale. Liu Z. finally apply this cell modeling method to TRIP 690 steel material instead of drill pipe material and simulate the ram shearing process with the commercial software LS-DYNA. The predicted shear force was compared with the value calculated by

the DET equation.

In 2017 and 2018, McCleney et.al[31, 32] reported their FE model for the subsea BOP ram shearing simulation. They first employed the J-C fracture criterion and standard tensile specimen to build the FE model and validate the accuracy of the model with experimental work of MCS Keeny, then adopted the CFD modeling approach to study the influence of flow condition on the ram shearing force. It was concluded that the single-phase flow effects do not have a notable impact on the shearing force, but the influence of highly dynamic flow events present additional risk to the shearing operation.

2.1.4 Summary of the previous methods

The accurate value of shearing force is difficult to obtain through a full-scale shearing experiment because the situation can be very complicated inside the well. The standard shear ram tests are supposed to be performed without tension in the pipe and with zero wellbore pressure, which may cause the test to fail to replicate pipe stress conditions downhole. Historical test data, because of not having recorded critical physical properties, make the estimation of drill pipe shearing suspect in some cases. OEM equations used to estimate pressure required to shear also do not include all pertinent variables, reducing accuracy and mandating a physical shear test to establish shear requirements. Incorporating ductility and other variables can be expected to improve the accuracy of these equations[9, 14].

Considering the actual BOP shear test is generally expensive and time-consuming, a distinct advantage of FE numerical models is to have more flexibility and potential for predicting the BOP shearing force in different loading conditions and operation scenarios. However, previous BOP shearing simulations in the field have shown that some factors affecting the results are still under investigation. Some inconsistencies still arise in those numerical models, the discrepancy is mainly found in fracture criterion application. For example, a suitable fracture criterion is still required for the present FE model, uniform procedure of identification for drill pipe damage parameters has not been established.

According to the literature review above, the FE model provided in previous studies to predict ram shearing force is listed combined with the fracture criteria adopted and the respective parameters calibration or derivation method in Table 2.5.

It is visible that models verified with full-scale experiment lack a reliable calibration method, while those studies which provide parameter calibration fail to conduct a full-scale verification experiment.

Another important aspect is that the numerical accuracy of the above FE models

Table 2.5: FE models and fracture criteria

FE model	Fracture criteria	Parameter calibration/derivation	Test / FE
MIT[25]	MMC	fracture tests	No test
MCS Kenny[28]	CrashFEM	Scaled based on Aluminum	0.87
A*STAR[30]	EMC	Cell model +fracture tests	No test
McCleney[31]	J-C	Engineering judgment	1.005

needs further investigation in applications for ram shearing force prediction. BOP simulation result would be more reliable if the FE model were proposed with a thorough mesh sensitivity study, which will assure the mesh size convergence. Considering the large size of pipes and BOP rams, the computing resource requirement is also a limitation to those models in the engineering applications.

2.2 Fracture mechanics

Almost all studies on the ram shearing process have to solve one same issue, to predict when the pipe material will fail under the large deformation caused by the extrusion of ram blades. This failure criterion determines the peak value of the shearing force curve, which received the most attention when predicting the safety of the shearing operation of BOP rams. Accordingly, an accurate failure criterion is required to obtain based on fracture mechanics.

2.2.1 Classical fracture mechanics

Classical fracture mechanics can be traced back to the 1920s when Griffith [33] made an effort to study the fracture of a plate with an elliptical hole. He denoted it was not possible to predict fracture by a critical stress or strain criterion [34]. An energy balance based method was then proposed by Griffith to deal with the fracture of a linear elastic brittle material. The plastic work at the crack front found to be an important variable in the studies of Orowan [35] and Irwin [36]. Based on these findings above, Irwin introduced a single parameter known as the stress intensity factor that can determine the local stresses around the crack tip. The critical value was found depends on the material property, the geometries and loading modes.

Three fracture modes were proposed in the literature, mode I correspond to a

pure opening mode which was most discussed and analyzed, while the research on mode II and mode III is still not adequate. Application of those linear elastic fracture mechanics has some limits, for example, the stress intensity factor was found only valid when the annular region around the crack tip is large compared to the plastic zone.

The elastic-plastic fracture mechanics was introduced to address the demand for dealing with a fracture with large plastic deformation. An important concept in this area is the J integral. Rice [37] proved that J can be used to measure the toughness for a non-linear elastic material. But when applied to plastic materials, this method is not valid in the plastic zone near the crack tip where loading is non-proportional.

Another way to study plastic fracture is Slip line theory. McClintock [38] reviewed the plasticity aspects of fracture mechanics and summarized those solutions to slip line fracture mechanics. To study the crack initiation and growth, Bao then introduced crack tip response functions, but this analytical prediction assumed material without strain hardening, which limits its application. These studies based on fracture mechanics described above usually are applied to solve issues in structures with a sharp crack, which is not in the same case as BOP ram shearing.

Numerical simulation of large deformation and fracture initiation process is another approach to study the fracture and failure and receive increasing interest in the last decades. As observed in the full-scale ram shearing test, the fracture cross-section reveals large plastic deformation. The pipe section close to the contact point with ram blades is sequenced and flattened into an elliptical shape. However, the shape of cross-section before the pipe rapture is not identical, which differs from one test to another. Thus, those assumptions above limited their application in ram shearing study.

2.2.2 Damage mechanics

The concept of damage was firstly proposed by Kachanov [39] in building a theoretical model for the rupture process. He assumed that the microcracking under complex loading conditions can be distinguished into two stages, the stable stage that microcrack gradually develops, and the unstable stage that fracturing accelerates significantly. The stable stage is the main part of the lifetime for the specimen, and the microcracking does not affect creep strain. A scalar parameter was proposed to characterize the damage of the material. Thus a certain value of a scalar parameter can correspond to the fracture localize at the moment of rupture.

Based on the damage concept, Lemaitre [40] proposed an isotropic ductile damage model to study the ductile failure of large scale structures. He denoted that previous microscale fracture models built by McClintock [38], as well as Rice and

Tracey [37], provided good physical mechanisms, but may have difficulty to apply due to lack of accurate local stress calculation. He used the effective stress vector and thermodynamics to derived the damage process of the crack initiation. Both the damage and plasticity are assumed to be isotropy, validation was given for both radial loading and general loading scenarios. An important hypothesis of this study is that the processes of plasticity and damage may be independent, which yields the uncoupled damage criterion.

As reviewed by Lin et al. [41], after those pioneer work presented above, various damage mechanisms have been proposed and developed in the next few decades, which refers to damage due to multiplication of mobile dislocation, damage due to creep constrained cavity nucleation and growth, damage due to continuum cavity growth, damage due to superplastic void growth and damage due to ductile void growth. It should be noted that dominant damage mechanisms vary significantly between different deformation conditions, including the material property, the loading path, the temperature, and the strain rate, etc.

As in the case of the BOP ram shearing process simulation, a progressive damage mechanism is employed in this study to capture the fracturing effect of the dill pipe. Similar to many previous damage models, the plasticity and damage are assumed to be independent during the deformation process. It should be noted that, when solving rupture of ductile metal in complicate loading condition, damage initiation criterion is correlated with the concept of the ductile fracture initiation. The theory of the phenomenological ductile fracture criterion is reviewed in the following section. Formulas of progressive damage framework are expressed in the following section.

Assuming the equivalent plastic strain to fracture $\bar{\epsilon}_f$ as the damage initiation of plastic strain, damage initiation is defined in the following form:

$$\omega = \int \frac{d\bar{\epsilon}^{pl}}{\bar{\epsilon}_f(\eta)} = 1 \tag{2.11}$$

where ω is a state variable that increases monotonically with plastic deformation. $\bar{\epsilon}_f(\eta)$ can be represented by each fracture criterion.

When the damage initiation criterion is met, the model uses a scalar damage variable, d, to simulate the degradation of stiffness. After damage initiation, the damage variable is assumed to increase in the following form:

$$\dot{d} = \frac{L\dot{\bar{\epsilon}}^{pl}}{\bar{u}_f^{pl}} = \frac{\dot{\bar{u}}^{pl}}{\bar{u}_f^{pl}} \tag{2.12}$$

where $\bar{u}_f^{pl}$ corresponds to the effective plastic displacement at the point of failure.

It should be mentioned that as the present paper aims to investigate the effects of different damage initiation criteria, a linear form of damage evolution is there-

fore assumed for every single or combined failure mechanism. The overall damage variable, D, is adopted to capture the combined effects of all active criteria and is computed in terms of individual damage variables, d_i, for each criterion as follows:

$$d_{mult} = 1 - \prod_{i \in N_{mult}} (1 - d_i) \tag{2.13}$$

$$D = \max\{d_{mult}, \max_{j \in N_{max}} (d_j)\} \tag{2.14}$$

The above expressions indicate an overall damage mechanism in a multiplicative and a maximum sense, where N_{mult} and N_{max} denote the sets of active mechanisms by:

$$N_{act} = N_{mult} N_{max} \tag{2.15}$$

The effective stress tensor, $[\sigma_{ef}]$, is defined to denote the undamaged stress tensor in the current increment as

$$[\sigma_{ef}] = (1 - D)[\sigma] \tag{2.16}$$

Elements are removed from the mesh once the maximum degradation has occurred ($D = 1$) because the material has lost its load-carrying capacity at this point.

2.2.3 Phenomenological ductile fracture criterion

Ductility is an inherent property of a material, it represents the microstructural characteristics of the material itself and the ability to withstand the amount of plastic deformation before fracture. In the microscope scale, ductile damage corresponds to void nucleation, growth, and coalescence under high-stress triaxiality, or shear band formation under low-stress triaxiality. In the macroscope scale, ductile damage is reflected by the degradation of material stiffness or strength.

In order to predict the damage initiation, a well-constructed criterion is critical. Different damage models have been proposed in the literature to predict the fracture initiation in structural metal. While existing other approaches, the phenomenological fracture criterion is increasingly used to the finite element model due to its simplicity, especially in the industrial application. Failure is assumed to occur when one predictor variable reaches a critical value, the damage variable is uncoupled from plastic and hardening variables.

In the previous application of uncoupled fracture criterion, equivalent strain to fracture (also called fracture strain) is widely used to define the material ductility.

In recent years, several numerical models have been built by researchers to predict the required force for the BOP shearing operation. Considering the actual BOP shear test is generally expensive and time-consuming, a distinct advantage of those numerical models is to have more flexibility and potential for predicting the BOP shearing force in different loading conditions and operation scenarios. However, some inconsistencies still arise in those numerical models, the discrepancy is found in both predicted shearing force value and verification method of the simulation results.

Two of the most critical aspects are that fracture criteria selection standard are not clear and the derivation of experimental based fracture parameters are not provided. BOP shearing operation includes the failure of the drill pipe between the rams, extensive plastic deformation, and complete rupture at the shear position close to the shear rams that have been observed in the BOP shearing tests [4, 17]. Drill pipe materials are generally advanced high-strength steels (AHSS), which are characterized by both high yield stress and large elongation. To simulate this process with the FE model, pipe elements generally experience fracture onset and evolution, until the pipe rupture. The combination of an accurate constitutive model with a ductile fracture model under a complicated stress state is essential to capture deformation and ram contact force responses [42].

Based on damage mechanics, other phenomenological damage models were introduced, such as the Johnson-Cook model [43] and the Void Growth Model [44] . Since the simplicity of these models and facilities to implement, they have been widely used for fracture prediction in forming processes of structural metals as well as other applications [45, 46] .

Stress triaxiality (the ratio of the hydrostatic pressure to the von Mises stress) is commonly used as a strong predictor of the plastic strain to cause void growth leading to ductile fracture. Bao [34, 47, 48] designed complete tests to calibrate the fracture strain in the whole range of stress triaxiality and found different fracture mechanisms operating for the onset of fracture prediction at different stress triaxiality ranges, which means that triaxiality-based criteria need to be corrected. Complementary stress state variables were introduced by other scholars to address this demand. Hooputra et al. [49, 50] proposed an integral fracture criterion, which is called CrashFEM. Damage is calculated separately according to ductile fracture and shear fracture mechanisms. A shear stress ratio was proposed to capture the fracture mechanism of the shear band localization. Wierzbicki and Xue [51, 52] studied the effect of deviatoric stress ratio and introduced the Lode angle parameter (or the normalized third stress invariant), as a correction of the ductile fracture. Bai and Wierzbicki [53] proposed a new model of metal plasticity and fracture with pressure and Lode dependence. Calibration methods were used to postulate the 3D

asymmetric fracture locus. These fracture models presented above have been verified with mechanical tests and applied to specific engineering applications. However, the fracture loci of AHSS material are not commonly provided in the literature and often differ considerably from one author to another for a similar grade [54–58]. Selecting a proper fracture criterion for BOP ram shearing is, therefore, an essential and necessary task for obtaining reliable simulation results. Although lots of researchers have conducted comparative studies and parameter calibration of fracture models in metal forming and crashworthiness simulation, the influence of fracture model selection is still in blank in the simulation of the BOP ram shearing process.

A modern fracture model generally has several fracture parameters and needs a series of mechanical tests to calibrate these parameters for the respective pipe material. The application of the ductile fracture model in the BOP shearing simulation, which meets academic requirements is, therefore, even a tougher job, with high processing time. The most popular criterion for the former FE models for BOP ram shearing is the J-C fracture model, and fracture parameters are usually determined according to numerical investigation and engineering judgment [4, 16, 28, 31, 54, 55]. The discussion to apply the MMC fracture criterion for the BOP shear force prediction [20, 25, 30, 42, 59] , the efforts to reduce the calibration cost, and to increase the accuracy of the numerical model are still undergoing. Another promising choice is the CrashFEM criterion, which has been used by many researchers in crashworthiness simulation [60, 61] and proved to be capable of predicting fracture along the nonlinear strain path [62, 63].

Formulas of the ductile fracture criteria adopted in the current thesis are presented as follows.

An expression of spherical and deviatoric components can be used to describe a specific stress state $[\sigma]$ as follows:

$$[S] = [\sigma] + p[I] \tag{2.17}$$

where $[S]$ and $[I]$ corresponds to the deviatoric and identity stress tensor, separately. p is the hydrostatic pressure related to m, the mean stress, as:

$$p = -\sigma_m = -\frac{1}{3} tr[\sigma] = -\frac{1}{3}(\sigma_1 + \sigma_2 + \sigma_3) \tag{2.18}$$

where σ_1, σ_2 and σ_3 are the principal stresses; σ_m denotes the first invariants of the stress tensor.

The other two invariants of the stress tensor $[\sigma]$ used to formulate the present fracture criteria are defined as:

$$q = \bar{\sigma} = \sqrt{\frac{3}{2}[S] : [S]} = \sqrt{\frac{1}{2}[(\sigma_1 - \sigma_2)^2 + (\sigma_2 - \sigma_3)^2 + (\sigma_1 - \sigma_3)^2]} \tag{2.19}$$

$$r = \left(\frac{27}{2} det[S]\right)^{1/3} = \left[\frac{27}{2}(\sigma_1 - \sigma_m)(\sigma_2 - \sigma_m)(\sigma_3 - \sigma_m)\right]^{1/3} \tag{2.20}$$

Three essential parameters to describe the fracture criteria in the literature [50, 53] are stress triaxiality parameter, η, normalized lode angle parameter, $\bar{\theta}$, and shear stress ratio parameter, θ_s. They are defined with respect to the three invariants presented above as:

$$\eta = \frac{-p}{q} = \frac{\sigma_m}{\bar{\sigma}} \tag{2.21}$$

$$\bar{\theta} = 1 - \frac{2}{\pi} \arccos\left(\frac{r}{q}\right)^3 \tag{2.22}$$

$$\theta_s = \frac{(1 - k_s \eta)\bar{\sigma}}{\tau_{max}} \tag{2.23}$$

where τ_{max} denotes the maximum shear stress, and k_s is a material parameter. Notably, in the plane stress condition, η, $\bar{\theta}$, and θ_s are related through [53, 54]:

$$\theta_s = \frac{\sqrt{3}}{\sin\left[\frac{\pi}{6}(3 + \bar{\theta})\right]}(1 - k_s \eta) \tag{2.24}$$

Based on this review of ductile damage and fracture criterion, this study considers the three most widely used criteria in the ram shearing simulation, which refers to the J-C criterion, the MMC criterion, and the CrashFEM criterion. Their formulas are introduced in the following section.

The ductile and shear fracture criteria proposed by Dell et. al [63] reflect the effect of anisotropy, state of stress, and strain path based on various experimental results for aluminum alloy. In this paper, a simplified form only accounting for stress triaxiality is adopted due to the property of the material.

Ductile fracture criterion

Ductile fracture criterion correlates fracture initiation with nucleation, growth, and coalescence of voids. It assumes that the ductile fracture strain, ϵ_f^d, is a function of stress triaxiality η:

$$\bar{\epsilon}_f^d = \frac{\epsilon_T^+ \sinh[c(\eta^- - \eta)] + \epsilon_T^- \sinh[c(\eta - \eta^+)]}{\sinh[c(\eta^- - \eta^+)]} \tag{2.25}$$

where c is assumed as a constant material parameter. ϵ_T^+ and ϵ_T^- define the boundary conditions of the equivalent fracture strain for the equibiaxial tension and equibiaxial compression conditions as follows:

$$\bar{\epsilon}_f^d = \begin{cases} \epsilon_T^+, & \eta = \eta^+ \\ \epsilon_T^-, & \eta = \eta^- \end{cases} \tag{2.26}$$

For isotropic materials, the stress triaxiality in equibiaxial tensile and compressive states is $2/3$ and $-2/3$ respectively.

Shear fracture criterion

Shear fracture criterion assumes that fracture initiates due to shear band localization. The equivalent strain at fracture ϵ_f^s is a function of shear stress ratio as follows:

$$\bar{\epsilon}_f^s = \frac{\epsilon_S^+ \sinh[f(\theta_S - \theta_S^-)] + \epsilon_S^- \sinh[f(\theta_S^+ - \theta_S)]}{\sinh[f(\theta_S^+ - \theta_S^-)]} \tag{2.27}$$

where ϵ_S^+ and ϵ_S^- have similar definitions to equation 2.26. The parameters θ_S^+ and θ_S^- correspond to the values of θ_S at $\eta = \eta^+$ and $\eta = \eta^-$, respectively.

Johnson-Cook criterion

The original Johnson-Cook criterion corresponds to critical equivalent fracture strain to a function of stress triaxiality, strain rate, and temperature [43]. In this study, according to BOP shear test observation, the BOP shearing process is assumed with constant temperature and quasi-static strain rate. A simplified form only accounting for stress triaxiality effect is therefore adopted as follows:

$$\bar{\epsilon}_f = d_0 + d_1 exp(d_2 \eta) \tag{2.28}$$

where d_0, d_1 and d_2 are material parameters.

Modified Mohr-Coulomb fracture criterion

MMC fracture criterion considers both stress triaxiality and the lode angle effect on fracture locus. The plastic strain to fracture was derived in the space of as $(\bar{\epsilon}_f, \eta, \bar{\theta})$ [53, 64]:

$$\bar{\epsilon}_f(\eta,\bar{\theta}) = \left\{ \frac{A}{C_2}\left[C_3 + \frac{\sqrt{3}}{2-\sqrt{3}}(1-C_3)\left(\sec(\frac{\bar{\theta}\pi}{6}) - 1\right)\right] \times \left[\sqrt{\frac{1+C_1^2}{3}}\cos(\frac{\bar{\theta}\pi}{6}) + C_1\left(\eta + \frac{1}{3}\sin(\frac{\bar{\theta}\pi}{6})\right)\right]\right\}^{-\frac{1}{n}} \tag{2.29}$$

In the plane stress condition, one can relate the parameters η and $\bar{\theta}$ through [53, 54]:

$$-\frac{27}{2}\eta(\eta^2 - \frac{1}{3}) = \sin(\frac{\pi\bar{\theta}}{2}) \tag{2.30}$$

Then, equation 2.29 becomes:

$$\bar{\epsilon}_f(\eta,\bar{\theta}) = \left\{ \frac{A}{C_2} f_3 \left[\sqrt{\frac{1+C_1^2}{3}} \cdot f_1 + C_1\left(\eta + \frac{f_2}{3}\right)\right]\right\}^{-\frac{1}{n}} \tag{2.31}$$

where

$$f_1 = \cos\left\{\frac{1}{3}\arcsin\left[-\frac{27}{2}\eta(\eta^2 - \frac{1}{3})\right]\right\} \tag{2.32}$$

$$f_2 = \sin\left\{\frac{1}{3}\arcsin\left[-\frac{27}{2}\eta(\eta^2 - \frac{1}{3})\right]\right\} \tag{2.33}$$

$$f_3 = C_3 + \frac{\sqrt{3}}{2-\sqrt{3}}(1-C_3)\left(\frac{1}{f_1} - 1\right) \tag{2.34}$$

As for the plane strain condition, a more straightforward form is derived as:

$$\bar{\epsilon}_f(\eta,\bar{\theta}) = \left\{ \frac{AC_3}{C_2}\left[\sqrt{\frac{1+C_1^2}{3}} + C_1\eta\right]\right\}^{-\frac{1}{n}} \tag{2.35}$$

Chapter 3

Analysis of the ram shearing force

According to the requirements of industrial applications, the ram shearing process, and prediction of the maximum shearing force are very important issues. In this chapter, mechanical analysis of ram shearing force is conducted based on the failure process of drill pipe material in the shearing operation. By observing the fracture morphology of the drill pipe as well as the tube deformation in the BOP ram shearing experiment process, the failure of drill pipe is correlated with the typical punch and die process. Based on this analysis, a finite element model with constant damage criterion is established to simulate the ram shearing process and to predict the maximum shearing forces. Considering those boundary conditions and loading conditions which may occur in an actual offshore drilling operation, Sensitive study is conducted by investigating the influence of the drill pipe size, axial pre-load condition, off-center condition, and the shear failure parameter. Numerical simulation results are compared with actual shear ram test data. The limitations of the FE model with constant damage criterion is discussed.

3.1 Analyzing the failure of drill pipe in the ram shearing process

To conduct the mechanical analysis of ram shearing force, the failure of drill pipe in the ram shearing process is required to investigate first. A successful closing process includes two steps, first is the blades pass each other under the driving force of hydraulic pressure, while the sharp edge of rams shears the pipe. The second is the rams continue moving until the ram block ends meet. The current analysis is supposed to focus on the first step which is directly related to the mechanical shearing force. Note that the failure process of the drill pipe is consistent with the shearing process of the rams. The failure of the drill pipe is equivalent to the success of the shear.

According to observation in the full-scale ram shearing experiment, the drill pipe body experiences various stages during the cutting process, which is shown in Figure3.1. Assuming the pipe is set in the center of the BOP, in this process, the magnitude of the shearing force, the speed of the rams, the area of contact between the blade of the ram and the pipe, and the deformation of the pipe material all experience nonlinear changes.

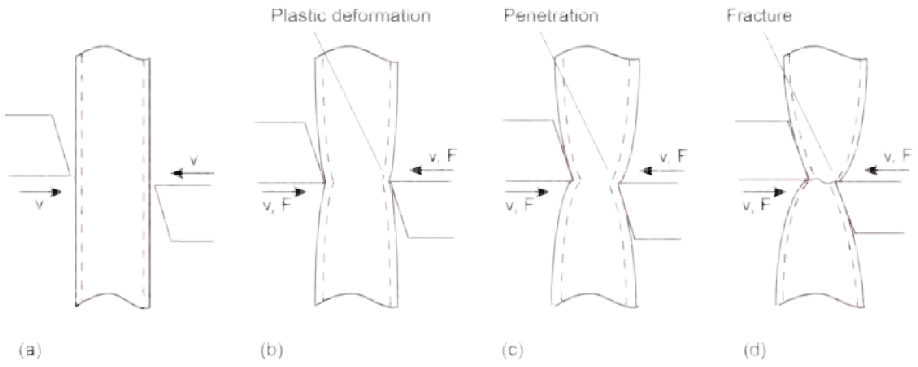

Figure 3.1: Four stages during the cutting process

In detail, rams are initially forced forward by the hydraulic pressure of the BOP control system, as shown in Figure 3.1 (a). In Figure 3.1 (b), ram blades begin to deform the drill pipe causing an initial elastic and progressive plastic deformation. In Figure 3.1 (c), the pipe necking occurs due to the extrusion of rams. To some degree, the local material at a certain position (close to the blade shear tip) can not stand the extreme deformation, ram blades move further and begin to penetrate the drill pipe material. In Figure 3.1 (d), the material fractures under the force of ram blades, macro cracks develop until the total separation of the drill pipe section.

In these stages, the shearing force changes dramatically with the deformation of the pipe and during the penetration process. The following analysis will focus on these two stages.

It can be observed in the ram shearing test, the local pipe section in contact with the ram blade experience large plastic deformation before rupture. An obvious example is that in the shearing experiment of a prior study by Han Chuanjun, the drill pipe that was not cut also showed large plastic deformation. As demonstrated in Figure 3.2, even the super 13Cr drill pipe was not successfully cut by the blind shear ram in the respective operation pressure, obvious plastic deformation occurs to the drill pipe material.

The analysis of plastic deformation of the pipe body during the extrusion process by Wierzbicki [65] can be employed to understand the pipe deformation process

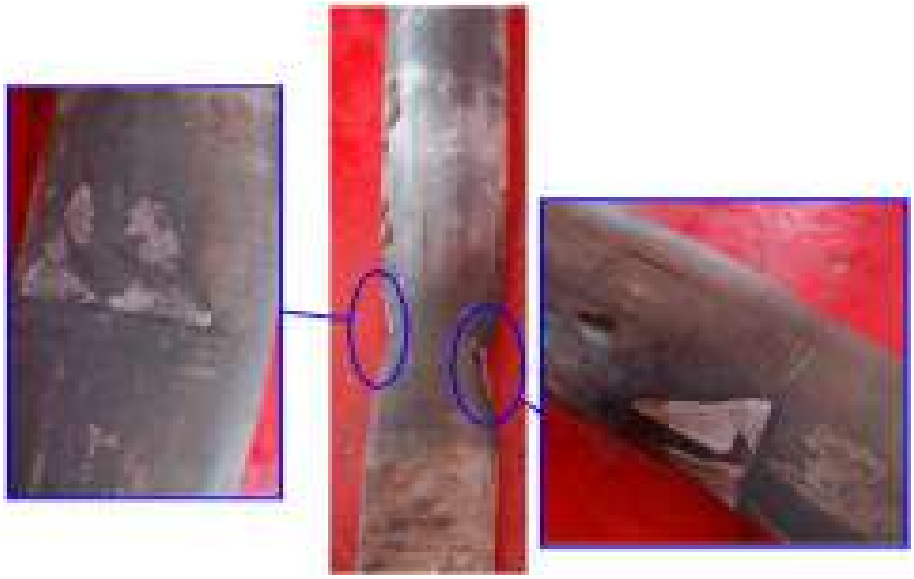

Figure 3.2: Plastic deformation in a full-scale experiment to shear a super 13Cr drill pipe[4]

before a fracture occurs. In their analytical model, the pipe is considered as idealized rigid-plastic material subjected to lateral concentrated loading conditions. With a changing contact area, the load-deflection characteristics of tubes are expressed as a function of the external axial force:

$$F_x = \frac{8M_0}{R} + \frac{4\pi N_0 R\delta}{3\xi}\left[1 - \frac{1}{4}\left(1 - \frac{1}{N_p}\right)^3\right] \tag{3.1}$$

Where F_x denotes the lateral concentrated load force, δ is the indentation depth, ξ is half-length of the dented region, M_0 denotes the fully plastic bending moment of the pipe wall, R denotes the radius of the undeformed pipe, N_0 is the fully plastic axial force.

To minimize the crushing force in the indentation process, the locally dented zone adjusts its length to fulfill $\frac{\partial F_x}{\partial \xi} = 0$ and the relation between ξ and δ is given by

$$\frac{\xi}{R} = \left\{\frac{2\pi\delta}{3t}\left[1 - \frac{1}{4}\left(1 - \frac{N}{N_p}\right)^3\right]\right\}^{\frac{1}{2}} \tag{3.2}$$

Where t is the thickness of the circular pipe, N denotes external axial force, N_p is the plastic force capacity of the cross-section.

In the case of a freely sliding tube ($N = 0$), it is possible to express the shape of the dented zone as well as the amount of overall shortening of the tube in terms of elementary functions. The deflection profile of the dented region can be found by knowing the dependence of ξ on δ.

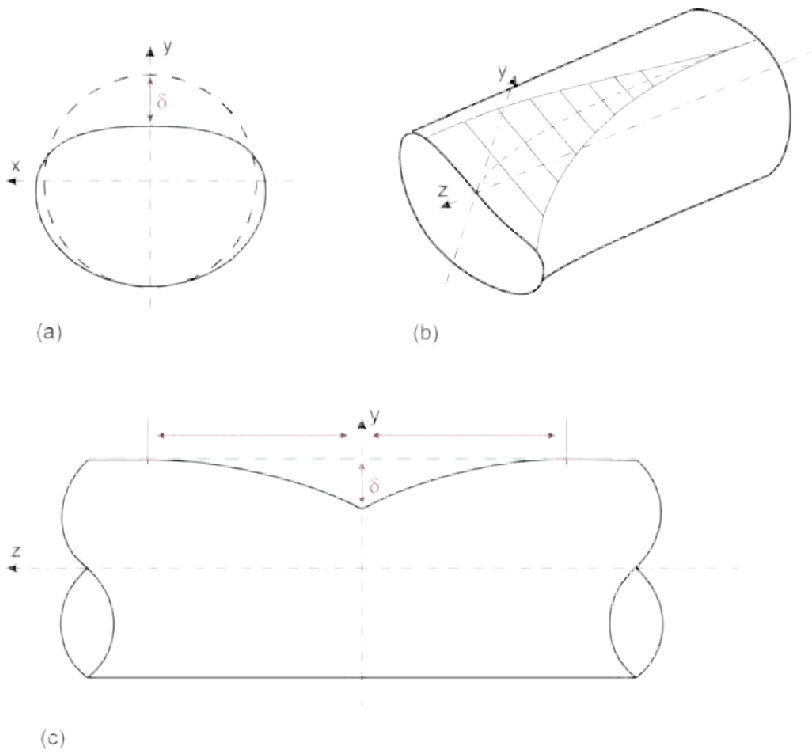

Figure 3.3: Mechanical analysis of pipe plastic deformation under lateral concentrated load[65]

$$\frac{\xi}{R} = \sqrt{\frac{\pi\delta}{2t}} \tag{3.3}$$

The geometry of the plastic deformation of a pipe under lateral concentrated loading condition is shown in Figure 3.3. Even some specific parameters affect the deformation, the overall cross-section deformation similar to that on a drill pipe in the ram shearing process. The analytical analysis suggests the lower bound of a drill pipe length to calculate the ram shearing force. For example, when a Double-blind ram shearing a drill pipe ($\phi 127mm$), if the ductility of the pipe material is large enough that the pipe is fully extruded into a plate before fracture, the theoretically largest dented zone can be calculated by Equation 3.3, where $\delta = R - 2t$, $R/t = 6.9$, Thus $\xi = 2.77R = 176mm = 0.176m$, the value of the necking zone pipe length is $0.352m$. However, the initial crack may already occur because ram blades invade the tube material in the process of indentation deformation. In this case, the failure of the drill pipe body will be induced by fracture initiation and propagation before it is completely deformed.

For the S135 drill pipe, the typical thickness of the pipe body is about $9.2mm$. When the ram blades shear the pipe body without initial macro-cracks, the strain localization induces fracture initiation and propagation, and further cause the failure of the pipe material. It is difficult for the full-size drill pipe to track the failure

process. In this section, the characteristics of typical AHSS sheet blanking produce is employed to study the fracture and thickness of the tube during ram shearing.

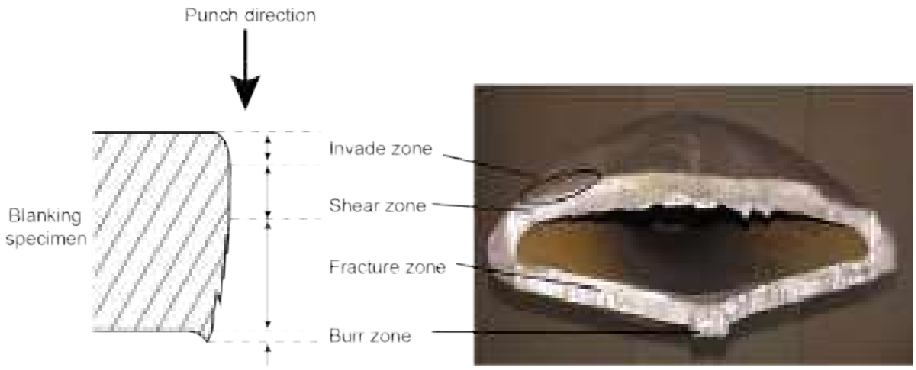

Figure 3.4: Correlation cross-section of the pipefish with blanking specimen

The left part of Figure 3.4 is a typical cross-section of a blanking specimen [66].It can be seen that a few feature areas are left along the cutting direction after the punch shearing process completes. The rollover zone represents the plastic deformation by the time when the punch edge invades the material. The shear zone is a smooth and shiny area created during material shearing. The fracture zone is caused by the fracture of the material and generally forms a certain angle. The burr zone is induced by large plastic strain at the end of the shear. The proportion of these zones is influenced by many parameters, such as punch corner radius and clearance.

The right part of Figure 3.4 is a cut cross-section of a drill pipe extracted from the ram shearing experiment. Different zones are observed from the cross-sectional morphology which can be related to the characteristics of the blanking specimen. The corresponding parts can be clearly found in both figures. The invade zone has obvious traces of pressing on the edge of the blade. The shear zone is smooth and the fracture zone is rough, and the grain direction is consistent with the misalignment direction of the pipe material. Burrs appear on the cross-section, indicating that the material is stretched to a great extent before the complete fracture surface formation.

From the comparison in Figure 3.4, although several zones on the sheared pipe section are not distributed along the thickness direction, all the corresponding areas of the blanking specimen can be found. Theoretically, if the pipe material is sufficiently flattened before fracture takes place, the ram shearing process can be simplified to a blanking process of a drill pipe material sheet with a thickness of $2t$. This analysis is critical to understand the ram shearing process as well as establish the numerical model.

To review the fracture generation and propagation in an AHSS material blanking process, the study of Wang and Wierzbicki [67] provides an experimental observation

and numerical analysis. As it is shown in Figure 3.5, the blanking process of a DP780 steel sheet is demonstrated, the color code of the contour is ϵ_{xy}, the tool clearance is 20%.

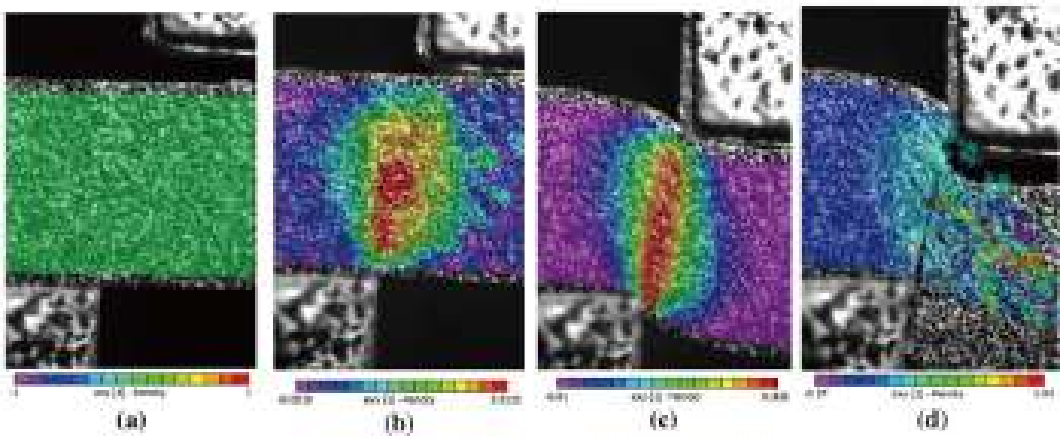

Figure 3.5: Digital image correlation analysis of the fracture process in their blanking test[67]

The fracture process in their blanking test is recorded and analyzed by a digital image correlation (DIC) deformation measurement. As shown in figure 3.5 (b), at the beginning of the process, the deformation of the specimen is mainly concentrated in the tool gap area, but there is not much deformation in the area away from the area. Figure 3.5 (c) shows that severe strain localization appeared in this area before fracture, and a high shear stress concentration was formed in a narrow area extending in the moving direction of the tooltip. Once the fracture occurred, the crack immediately propagated and caused the separation of the specimen. This crack generation and propagation process are very quick that the camera did not capture it in the test.

The blade angle also affects the ram cutting process. Cracks on the pipe body thereby may not only propagate in the thickness direction. A typical example is V-shaped blades, which are commonly adopted in the classical ram design. In this case, the pipe cross-section with a V-shaped edge will occur if it is completely crushed by rams. Suppose a perfectly plastic drill pipe sheared by Double-V ram blades, cracks may be obtained first at the position of blade contact, the fracture in the thickness direction of the pipe is shown in Figure 3.6 (b). After the fracture is formed in the thickness direction, the dislocation will extend along the circumference of the pipe body, and the extension direction is perpendicular to the ram movement direction, as shown in Figure 3.6 (c).

Note that in the blanking process, the maximum punch force was found to occur before macrocrack propagation. As discussed by Atkins [68], based on the punch force-punch displacement curve extracted from the quasi-static blanking experiment

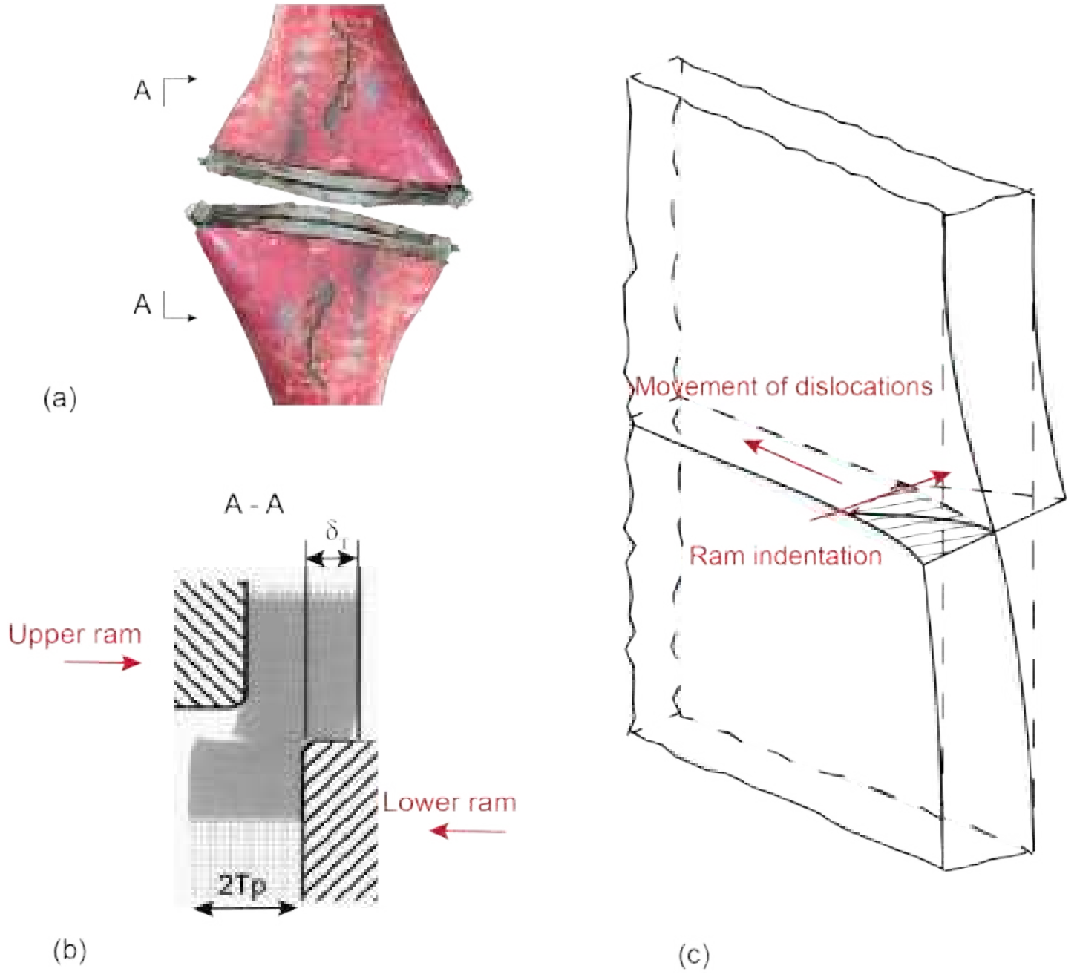

Figure 3.6: Simplified schematic of the fracture process on a completely crushed pipe

of Slater and Johnson [69], the peak value of the punch force is correlated with the plastic load instability and is not connected with cracking. When the punch penetrates the specimen, the punch load on the curve is still increasing. Because the shear area decreases, the material work hardens. The peak punch force will be obtained if the decrease in load caused by the reduction of the sheared area outweighs the increase in load associated with work hardening. It is also revealed that once crack propagation begins, the plastic deformation becomes smaller and the energy consumed includes work of cracking and work of flow.

Corresponding to the blanking test process, Koutsolelos [25] provided a simplified analytical model to calculate the BOP ram shear force. The shearing force is expressed as below.

$$F_{rs} = \tau \times A_{cs} = \tau\pi R(2t - \delta_d) \tag{3.4}$$

Where δ_d denotes the relative distance of the blades after the full collapse, τ

denotes the flow stress of the material in shear, which can be expressed as bellow.

$$\tau = \frac{\sigma_0}{\sqrt{3}} = \frac{1}{\sqrt{3}U_S}\int_0^{U_S}\sigma(\epsilon)d\epsilon \tag{3.5}$$

where the σ_0 denotes the energy equivalent flow stress. Assuming the maximum shearing force corresponds to $\sigma_d = 0$, the maximum shearing force can be estimated as follows.

$$max.F_{rs} = \frac{2\pi}{\sqrt{3}}Rt\sigma_0 \tag{3.6}$$

It should be mentioned that this solution was built based on the assumption that the maximum shearing force is obtained after the pipe is fully flattened by the blades, thus simplifying the issue to a plane strain situation, which limits the validation of this method. In fact, BOP shear ram blades are rarely designed to fully collapse the pipe before shearing it.

Back to Figure 3.1, the above mechanical analysis seems to capture the force changes in Figure 3.1 (b) and (c) under proper assumptions. Besides, analysis in the AHSS sheet blanking punch force suggests that the maximum shearing force appears to occur in the plastic load instability stage before crack initiates, which means that the peak value of shearing force is properly correlated with stage shown in Figure 3.6 (c). However, according to the observation in various full-scale ram shearing experience with BSR as well as DVS, the plastic deformation accumulated in this stage depends on the mechanical property, especially the ductility of the drill pipe material.

According to observations in various ram shearing experiments, in the pipe extrusion stage, the critical plastic deformation at which the ram blades commence to penetrate the dill pipe material is inconsistent from one case to another. This may depend on ram design, pipe dimension, and pipe material property. For a specific ram geometry, the ductility of the drill pipe material may influence this sequence. Former studies of West Engineering and George are [9, 18] consistent in the conclusion that the ductility of drill pipe material has a large impact on the ram shearing process. Because of the discrepancy in ductility, the final fracture morphology of two drill pipes with the same diameter has an obvious discrepancy, even though they belong to the same material grade and cut by the same shear ram, as shown in Figure 3.7. Besides, the maximum shear pressure of the drill pipe with lower ductility, denoted in Figure 3.7 (a), is 13.4 MPa (1950 psi), is less than half of the high ductility pipe, denoted in Figure 3.7 (b).

The ductility of drill pipes cannot be visually discerned without a mechanical test. Both elongation and Charpy impact value can reflect the ductility of pipe material. In the study of Springett [15], shearing experiments are conducted on

(a) (b)

Figure 3.7: Fracture morphology of two drill pipe with the same material grade but different ductility[9]

two drill pipes with nearly identical ultimate and yield strength, elongation, and reduction in area. The only notable difference in material property is the Charpy impact value. The experimental results show that the specimen with a 50% higher Charpy value is also 50% higher in the maximum shear force. It also can be observed in Figure 3.8 that the discrepancy of cross-sections on cut fishes quite consistent with that in Figure 3.7. In the ram shearing process, a higher ductile pipe is sheared after it has completely deformed. Macrocracks occur on the sides of the lower ductility pipe, the plastic deformation in the extrusion stage is thereby interrupted.

The above analysis shows that a practical ram shearing mechanical model needs to consider the reaction force caused by the large plastic deformation of the pipe during the flattening process and to determine the extent to which the pipe is sheared by the blade and begins to crack. If the critical deformation at the beginning of fracture can be obtained, the maximum shear force can be estimated according to some dimensional parameters corresponding to this critical value. According to some experimental results, the starting point of the fracture of the pipe has a high correlation with the ductility of the pipe, which is a natural property of the material and can only be obtained from mechanical tests. Besides, the relative position of the pipe and blade, the pipe size, the blade shape, and the loading condition also affect the maximum shearing force. Thus it is very difficult for the analytical method to provide a practical estimation of the shearing force.

By correlate the peak force of BOP ram shearing with the peak punch force in the blanking process, it is reasonable that the peak shearing force will be obtained if the decrease in load caused by the reduction of sheared area outweighs the increase

Figure 3.8: Fracture morphology of two drill pipe with different Charpy impact values[15]

in load associated with plastic hardening. Accordingly, the reduction of shear area is determined by the crack initiation and propagation caused by ram invade, while the increased load induced by plastic deformation is basically influenced by the plasticity and ductility of the pipe material. To capture both of these two the phenomenon, the numerical model combined with a failure criterion is more suitable. In the following section, the ram shearing process will be investigated with the numerical analysis method. In the following section, the ram shearing process will be investigated with the numerical analysis method.

3.2 Simulated shearing process with a constant failure criterion

To characterize ductile fracture of steel materials, numerous finite element models have been developed. In recent years, a number of finite element models were built to attain the ram shearing process and shearing force prediction. This is especially a suitable method considering the complicated loading and boundary conditions of the drill pipe and the nonlinearity in ram loading and displacement, contact area between rams and the pipe, large plastic deformation on the drill pipe as well as the

material stiffness before and after the damage initiation.

In this part, a numerical simulation for the shearing process of a drill pipe is implemented in order to calculate the maximum shearing force and to investigate the sensitivity of several factors to the shearing force curve. To make the analysis available, a constant failure criterion is employed in the current chapter. The simulation results are compared with actual BOP shearing data and the accuracy of this model is discussed.

3.2.1 FE model

Either a ram pressure-ram displacement curve or a ram force-ram displacement curve can represent the BOP ram shearing process in the macroscope. The peak shearing force value on the curve can be correlated with the shearing force offered by the operating system in the safety aspect.

In the current chapter, the ram under investigation is a typical Cameron model BSR. An estimation of this ram geometry provided by Tekin [24] is adopted. As it is shown in Figure 3.9, one blade edge is V shape, while the other is blind, geometry is demonstrated. Sealing elements are ignored, and only upper and lower shearing blades are simulated. The FE model set up and the geometry of rams are shown in the figure.

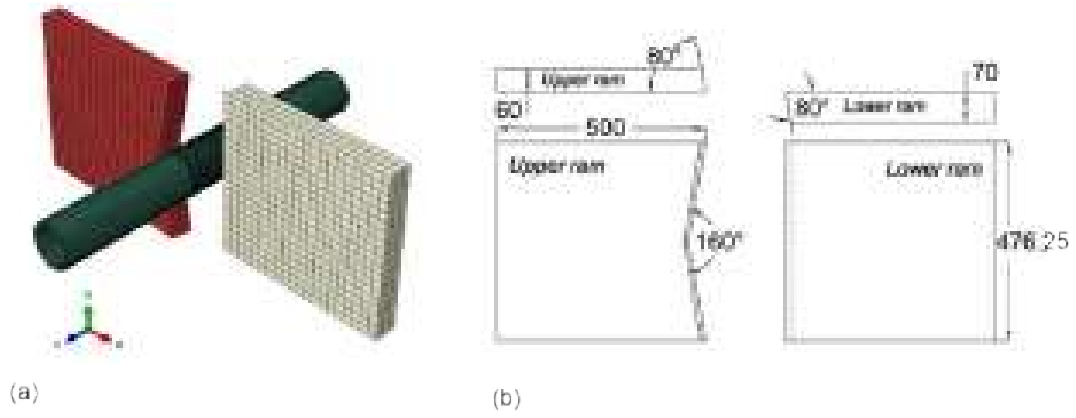

Figure 3.9: FE model set up and Geometry of BOP rams (in mm)

The length of the pipe is 1 m in the simulation. There are totally three diameters of drill pipe investigated and they all belong to API S135 grade. The dimensional parameters, as well as mechanical properties of those drill pipes, are listed in Table 3.1.

In order to carry out this FE simulation, 3D solid elements C3D8R are used. They are 8-node linear brick elements, with reduced integration and hourglass control. It is shown that they are more suitable than shell elements without out-of-plane

Table 3.1: Diameters and material properties of the drill pipe

Material grade	OD (mm)	Thickness (mm)	Yield strength (MPa)	Tensile strength (MPa)	Elongation %
S-135	88.9	9.35	1071.45	1113.5	19.5
S-135	127	9.20	1014.22	1099.71	23.1
S-135	139.7	9.17	1052.83	1101.78	20

degrees of freedom, which are too stiff for the actual material from the drill pipe [25].

Considering that the insufficient number of elements may cause a large deviation as well as convergence problem, while the very fine mesh will imply excessive computer time, the pipe mesh was divided into two main parts with coarse and fine meshes, as it is shown in Figure 3.10. The mesh size of the shear zone is 5 mm $\times$ 2.5 mm, and there are 4 elements through the thickness of the pipe. The mesh size for other parts of the pipe is 5mm $\times$ 10 mm.

3.2.2 Material property of drill pipe

Normally, both of the material of ram blade and drill pipe are high strength alloy steel, while the ram blade is much stronger. For simplicity, the deformation of the rams is neglect, and the rams are taken as rigid bodies. The material of drill pipe steel was modeled through elastic-plastic J2 flow theory with isotropic hardening. Figure 3.11 shows the true stress versus plastic strain curve [24] for API S135 drill pipe material employed in the numerical analysis. The Young modulus and Poisson‘s ratio are assumed to be 210 GPa and 0.3 respectively.

Failure of the tube in the BOP implies a successfully shearing operation. To conduct a numerical simulation for the ram shearing process, a failure criterion is necessary and important. A simplified failure criterion is presented as follows.

$$\omega = \frac{\bar{\epsilon}_0^{pl} + \sum \Delta \bar{\epsilon}^{pl}}{\bar{\epsilon}_f^{pl}} \tag{3.7}$$

Where $\bar{\epsilon}_0^{pl}$ is any initial value of the equivalent plastic strain, $\Delta \bar{\epsilon}^{pl}$ is an increment of the equivalent plastic strain, $\bar{\epsilon}_f^{pl}$ is the strain at failure, and the summation is performed over all increments in the analysis.

This failure criterion can be employed in both fast dynamic processes and nonlinear analyses. It is assumed that the fracture plastic strain of material is constant

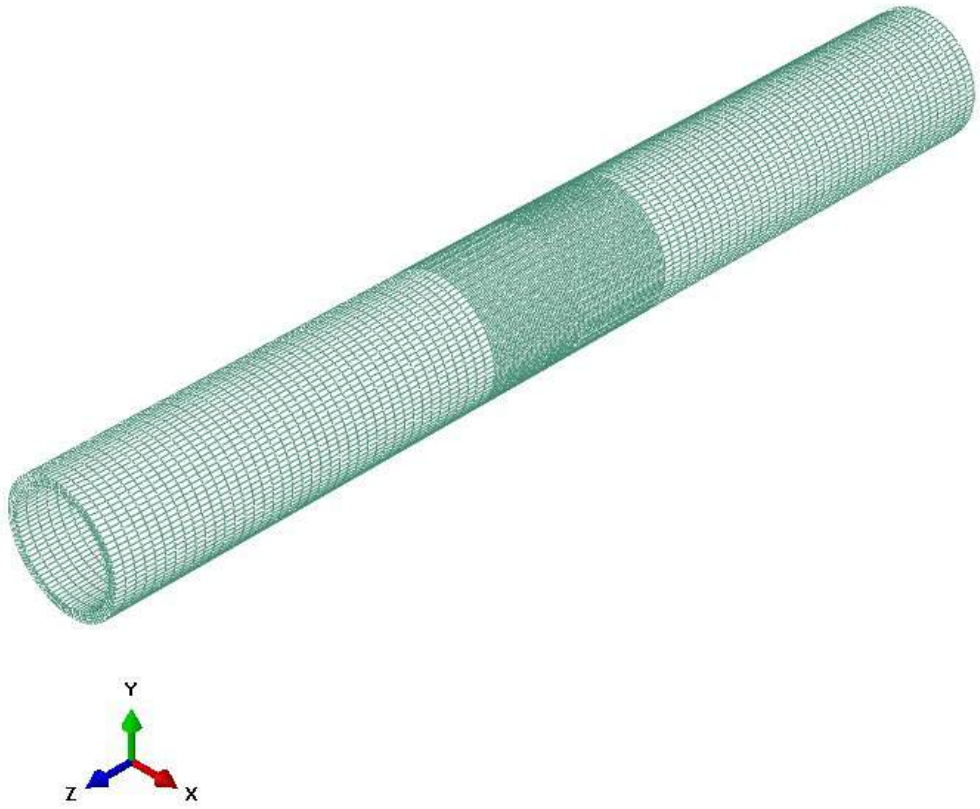

Figure 3.10: Mesh of the drill pipe in the FE model

during the shearing process, for all pipe elements. When the shear failure criterion is met at an integration point, all the stress components will be set to zero and that material point fails. Combined with the "Mesh Deletion" method, the element will be deleted when all nodes fail, thus the onset of the macro-crack can be presented by the deleted elements.

Since the application of failure criteria is complicated, to make the FE model for ram shearing simulation accessible, this simplified failure criterion is conducted in chapter 3. The shear failure value 0.3 was assumed for the current numerical simulation based on an optimization study. The accuracy and sensitivity of this shear failure parameter are discussed at the end of chapter 3.

3.2.3 Loading and boundary conditions

The FE model is built with the assumption that the ram shearing process is under a quasi-static loading condition. The initial distance between the ram and the pipe is set to be infinitely small to obtain computational efficiency. The pipe is supposed

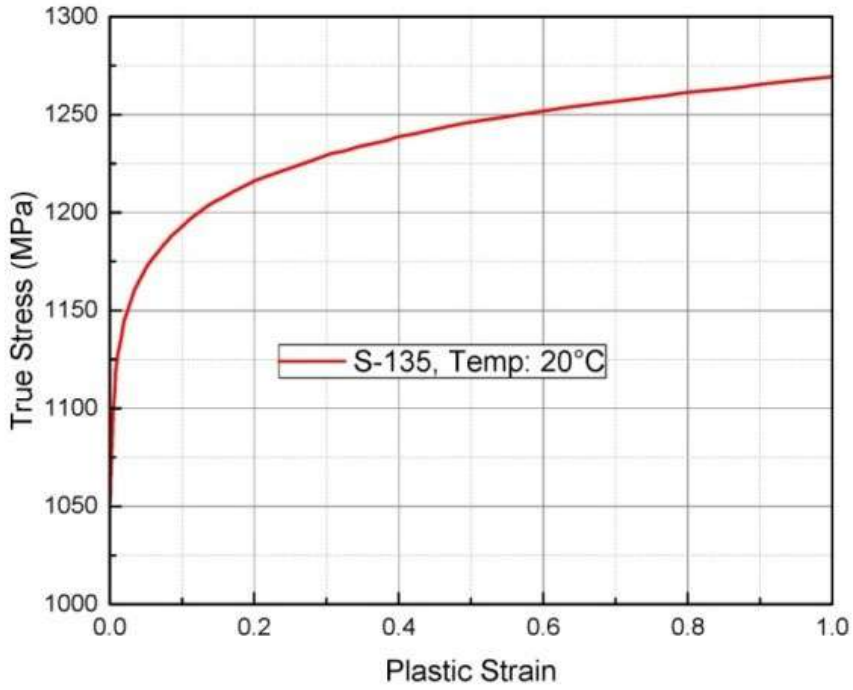

Figure 3.11: Stress vs. strain curve of the S135 drill pipe material

to be fixed, along with the central position of the BOP rams. Both the pipe's upper and lower boundaried are fixed in all degrees of freedom. In addition to the direction of shearing the pipe, the other degrees of freedom of the rams are fixed. Prescribed displacement of the rams along the x-axis is conducted to ensure that the ram moves to a position where the pipe can be completely cut off.

In the simulated cutting process, initial contact develops between the drill pipe and the blades. The contact area increases nonlinearly until the pipe is fully flattened, there may be another contact between the opposite inner surface of the pipe due to the ram extrusion. To solve the contact issue in ram shearing simulation, the tangential and vertical contact formulas offered by Abaqus were used to perform the contact simulations and calculate the contact pressure generated.

In the offshore drilling operation, the ram shearing may happen in some emergency situations, in which the drill pipe may be static in mud or in an empty well, under tension or compression, in the center of the well or at an off-center position. In this numerical simulation, several scenarios are classified and simulated by different boundary and loading conditions, thus the reaction force curve under ram displacement is generated for each scenario. The maximum shearing force can be obtained by extracting the peak force value on the curve. A basic model is first built with three centralized drill pipes without any axial load, the outer diameter(OD)

of the pipe is 88.9 mm, 127 mm, and 139.7 mm, respectively. The sensitivity of several loading scenarios to the maximum shearing force is then discussed including the axial load on the pipe ends, the off-centered distance of the drill pipe, and the shear failure parameter.

3.2.4 Simulation results of the basic model

The dynamic explicit method was employed in this simulation, the analyses are conducted on the nonlinear FE code Abaqus, which are suitable for the BOP shearing process.The simulation results are presented as follows.

Three simulations are conducted as a basic model, the geometry and mesh method has been covered above. To set the boundary condition, the top and bottom of the drilling pipe are fixed in all directions. Tool clearance between rams is set to be zero, no axial load is added to the pipe.

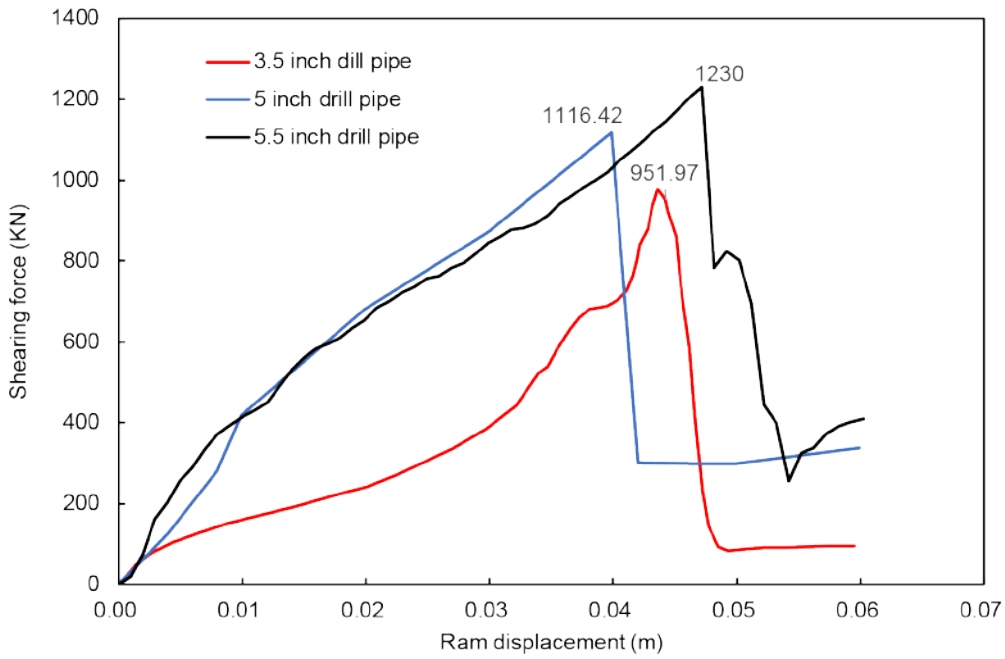

Figure 3.12: Shearing curve of changed sizes of drill pipes

To characterize the ram shearing process in the macro scale, the shearing force curve with ram displacement for the basic loading condition is presented in Figure 3.12. There is a reaction force on both rams, only the ram with the maximum reaction force is drawn. In the shearing force curve, the reaction force increases nonlinearly to a peak value. Upon failure of the pipe, the reaction force will suddenly drop to a much smaller value, which depends on the geometry and material of the BOP sealing elements. In the current case, after the separation of the pipe, rams continue to move forward, both of the upper and lower pipe fishes will bend and

resist ram moving. The reaction force of the ram may remain to a constant value or continue to rise, but this does not affect the maximum shear force in the analysis. The maximum sharing force of the pipe with a diameter of 88.9 mm is 976.8 kN, when the diameters are 127 mm and 139.7 mm, the peak force values are 1116.4 kN and 1230 kN respectively. This means the force requirement for shearing operation may increase with drill pipe outer diameter. It seems that with the same material, larger diameter and thickness of the dill pipe causes more difficulty for BOP shearing.

The simulation results can help to understand the BOP shearing process. Take the deformation process of the drill pipe ($\phi 139.7mm$) in Figure 3.13 as an example. After the initial contact of the drill pipe and the blades, the reaction force on the ram develops. As the local stress in the contact zone increases, the pipe is extruded by the rams and flatten to an oval shape. The deformation develops until a critical value, some local elements close to the ram blade edge begin to be removed. This element deletion process is similar to macro-crack on the pipe, which propagates until the total separation of pipe finally happens.

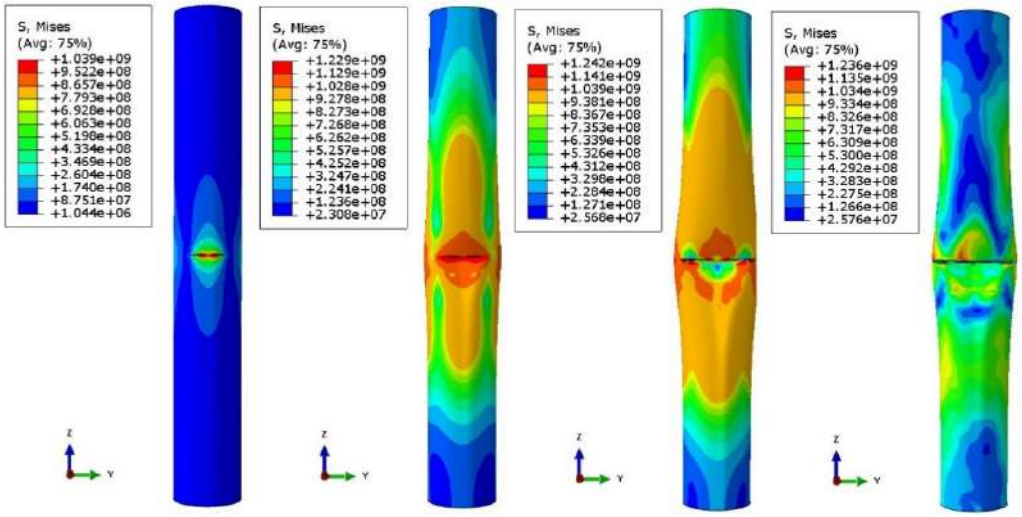

Figure 3.13: Stress distribution and deformation on the 139.7 mm OD drill pipe

To discuss the accuracy of the simulated maximum shearing force, actual data of ram shear test results [15, 19–24] [9, 28] is collected and compared with simulated results as Table 3.2 shows.

To gain a better understanding of those results from FE simulation, qualitative and quantitative analysis are shown below.

A very good alignment is observed for the shearing forces of the 127 mm OD drill pipe. For drill pipe with 139.7 mm OD, the alignment is poor for the Hydril ram and reasonable for the Cameron ISR (see also that pipe weights are different: 21,9 ppf for Hydril and 24,7 ppf for Cameron). For the drill pipe with 88.9 mm OD, the alignment is acceptable. In summary, possible discrepancies mentioned above

Table 3.2: Actual data of ram shear test results compared with simulated results

BOP ram	Pipe OD (mm)	Number of tests	Experimental force F_{rs} (kN)			FE force F_{rs} (kN)	FE / Test
			μ_c	σ_c	σ_c/μ_c		
Hydril	127	12	1138.35	26.06	0.023	1116.40	0.98
Hydril	139.7	12	1929.79	221.00	0.114	1230.01	0.64
Cameron	88.9	2	1320.76	105.73	0.080	976.80	0.74
Cameron	139.7	1	1395.52			1230.01	0.88
Cameron	127	1	996.40			998.70	1.002

μ_c: Average value; σ_c: Standard deviation.

should be considered in this context, parameters of the numerical model may cause a large distance between results, such as damage criterion, material parameters, and interaction properties.

In order to discuss the accuracy of FE simulation, the maximum shearing forces of the three S135 drill pipes are compared with the corresponding OEM calculation results, as shown in Table 3.3. In general, the OEM seems to be very conservative against the FE.

Table 3.3: Difference in maximum shearing force between FE analysis and OEM formula

Pipe OD (mm)	FE force F_{rs} (kN)	OEM force F_{rs} (kN)	FE / OEM
88.9	976.8	1859.3	0.52
127	1116.4	2707.8	0.41
139.7	1230	3124.2	0.39

3.2.5 Sensitivity analysis of loading conditions

Effect of pre-Load on drill pipe

During the drilling operation, the weight of the drill string is put on the hoisting equipment and bit weight is adjusted by the weight gauge. Normally, the natural point is supposed to be on the drill collar. Thus, except for weight on the drill bit that creates a compression load on the drill bit section, the drill string is under axial

(vertical) tension load during the drilling operation. Once formation fluid begins to enter the wellbore, it will create some forces in the vertical direction, which pushes the drill string upwards. Therefore, the axial tension load will decrease gradually while the compression force is increasing. In the present simulation, the result of the required shearing force assuming either compression or tension is described below.

In this part of ram shearing simulation, the upper bound of the pipe is fixed in all degrees of freedom, while the pipe is free along the axial direction at the lower bound. A uniformly distributed load of 100 kips (444.8 kN) axial tension or compression force is applied to the cross-section at the pipe's lower bound. Three different sizes of the drill pipes were considered. The results for these simulations are indicated in Table 3.4, where the positive and negtive pre-load values indicate tension and compression cases.

Table 3.4: Results for the pre-load simulation of different pipe sizes

Pipe OD (mm)	Pipe pre-load (kN)	FE force (kN)	Difference
88.9	0	976.8	
88.9	444.8	970.94	0.6%
88.9	-444.8	969.96	0.7%
127	0	1116.4	
127	444.8	1076.26	3.6%
127	-444.8	1064.67	4.7%
139.7	0	1230.01	
139.7	444.8	1131.61	8%
139.7	-444.8	1100.86	10.5%

In these groups of simulations, the results for each pipe size tend to be similar. Required shearing force without tension or compression is a little higher than that of pipes under compression or tension. This result is consistent with the conclusion in the study of Kousolelos [25].

Pipe in an off-center position

For the complexity of the drill string movement inside a well, cutting through non-centralized drill pipe also is possible to happen during the offshore drilling operation.

DNV [11] found that this led to the BSR being unable to completely shear and then close the well in the Macondo accident of 2010.

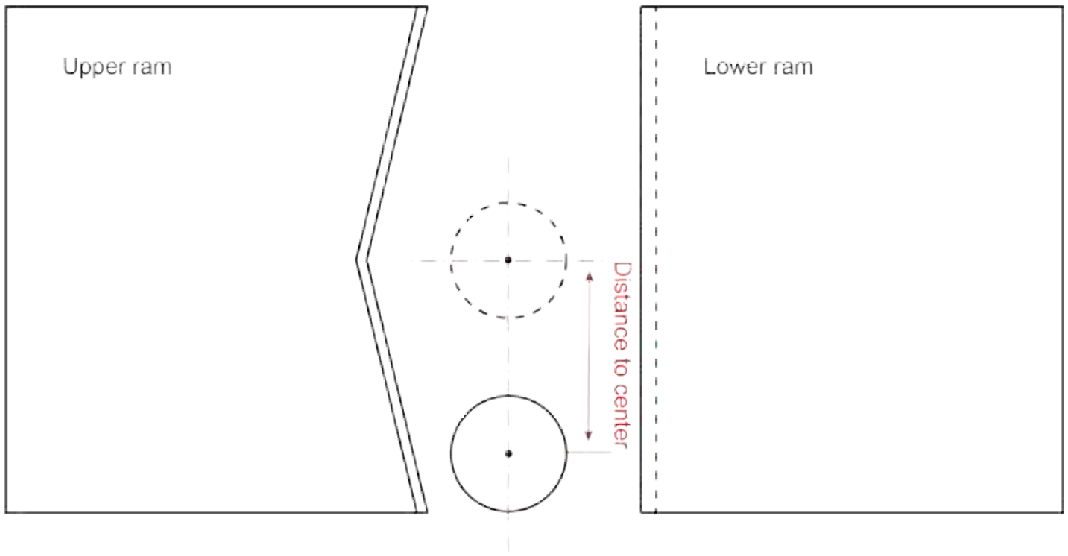

Figure 3.14: Non-centralized pipe position denoted by distance to the center

Accordingly, the non-centralized pipe position will affect the required shearing force. Due to the various load adding on the drilling pipe, the distance between the drilling pipe and the center point of the wellbore may be different. The positions of the drill pipe and rams indicated by the "distance to center" are shown in figure 3.14. The influence of the drill pipe with various distances to the central position is investigated in the current group of simulations, the distances are set to be 127mm, 200mm, and 240mm separately. The S135 drill pipe with a 127mm OD in Table 3.1 is adopted, the mesh and other input parameters of the model remain unchanged to the basic model.

In Figure 3.15, a group of shearing curves for drill pipes with 127 mm OD fixed at the top and bottom positions are shown in different colors. The red curve represents the shearing process of the centralized pipe, the required shear force is 1116.4 kN. At the position of 127 mm to the center, where the drilling pipe is still fully cut, the required shear force is 934.2 kN(represented by the blue curve), which means it requires 16.7% lower force to be cut. At the position of 200 mm to the center, according to the simulation, the pipe is not fully cut, but most of the pipe still can be sheared inside the BSR. As the black line shows, the shearing process curve is very close to the curve at the position with 127 mm to the center. At the position of 240 mm to the center, most of the pipe is outside the BSR, where the shearing force is no longer the main cause of the ram reaction force. In this situation, the maximum reaction force is much lower, as it is shown by the purple line.

It should not be ignored that in the situation where the pipe is not fully cut by

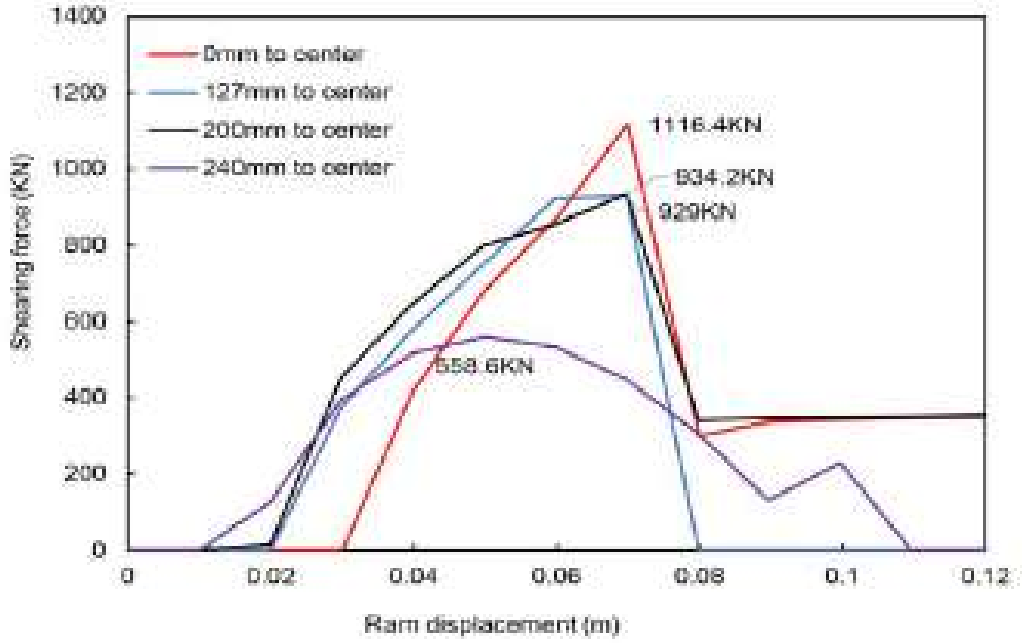

Figure 3.15: Shearing force curve with an off-center condition, 127mm OD pipe

the ram, the BSR is probably not able to seal the well (after shearing the pipe), which may cause the failure of the well control. This risk requires further attained in the ram designation, especially in those situations where the ram width can not fully cover the wellbore diameter.

Difference between BSR and DVS

Ram geometry designation also influences the shearing force because the angle of the blade edge may change the mechanic of shearing. Accordingly, the BSR and DVS are the most common designations adopted by various BOP manufacturer, their required force to shear a drill pipe with 139.7 mm OD is compared through numerical simulation. The only difference between the current V shear ram FE model with the basic Blind shear ram model is that the lower blind ram is replaced by another V-shaped ram illustrated in Figure 3.9. The shearing force-ram displacement curves for these two models are denoted in Figure 3.16.

It can be observed that even the shearing force of the DVS exceeds the force of BSR in the elastic and plastic deformation stage, the former curve decrease earlier than the later one. The maximum shearing force for the DVS is 975.35, which is only 79% of the force for the blind shear ram. This means that the pipe is easier to shear with the former ram type in the current scenario. A more comprehensive shear efficiency study is presented in Chapter 6.

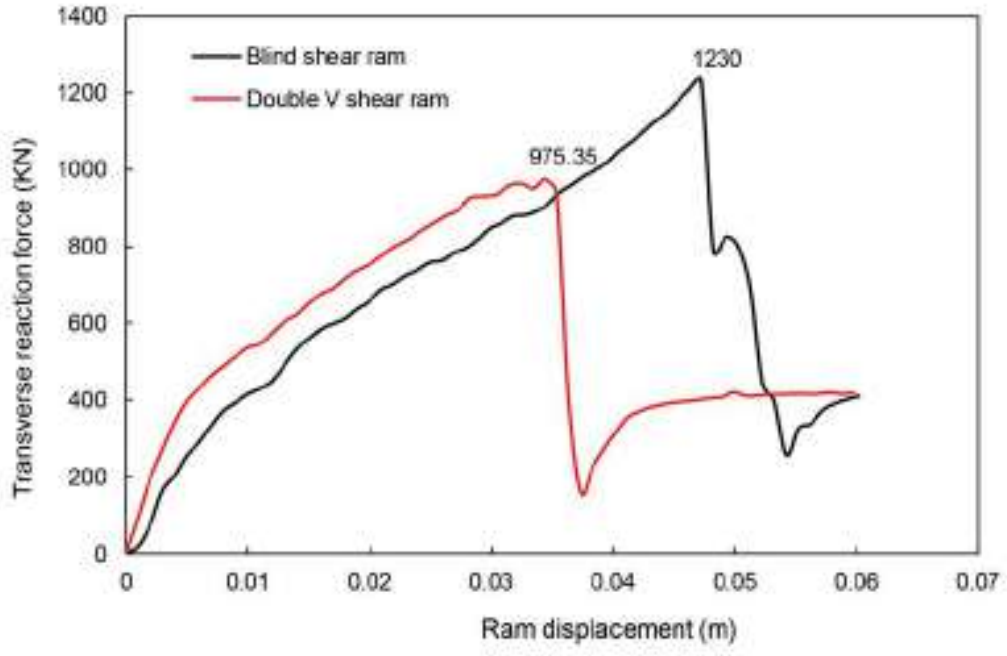

Figure 3.16: Shearing force curve for two ram types

3.2.6 Sensitivity analysis of shear failure parameter

The shear failure criterion is adopted in this chapter because it is easy to implement in the finite element analysis. Only one parameter, the equivalent strain at failure, needs to be provided. However, the limit of this failure measure is also obvious. The assumption that the equivalent strain to fracture is a constant value contradicts a lot of experimental observations of previous studies [54, 55] . Even though similar constant equivalent strain criteria are still used in many leading nonlinear FE software such as Abaqus, LS-DYNA, and PAM-CRASH, the application of them needs to be discussed, the determination of the critical strain value should be very careful. In this part, the influence of the shear failure parameter on the shearing force is investigated.

Based on the previous numerical model in this chapter, in order to improve numerical accuracy, a more sophisticated mesh design is provided, as shown in Figure 3.17. According to the simulated plastic deformation of the pipe in the basic model, the pipe is divided into three areas along the Z-axis. The mesh grid is distinguished by these areas and gradually refined along the Z-axis to the pipe center. The transition parts between the three areas are adopted to make sure the continuity of the instance. For the pipe areas from the upper and lower bound of the pipe to the center where the plastic deformation is still neglectable, a rough mesh grid with a size of 10 $\times$ 10 $\times$ 2.3 mm is conducted in order to decrease calculation time. For those elements close to the ram contact areas, the mesh size is refined to 2.3 $\times$ 2.3

× 2.3 mm. The mesh grid near the central layer between two rams area is critical, because a coarse grid may cause excessive distortion of the elements and affect the convergence of the calculation. The mesh size in this area is 1.15 × 1.15 × 1.15 mm. See Chapter 4 for a complete mesh design and convergence analysis.

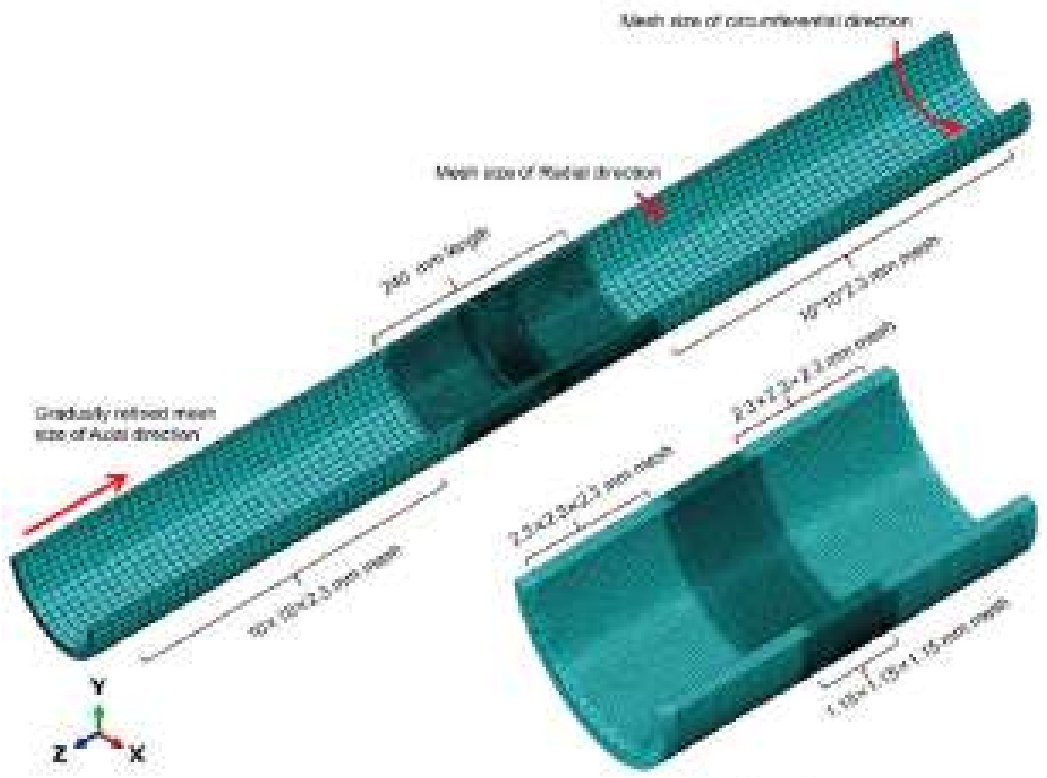

Figure 3.17: Mesh grid divided by three regions

In addition to mesh division, the pipe size and ram dimensions are the same as the basic model in this chapter. The drill pipe with 127 mm OD is adopted, the only difference in the material property is that the choice of shear failure parameters here are 0.4, 0.5, and 0.6 respectively.

Figure 3.18 shows the shearing force curves corresponding to different shear failure values. From the comparison, before the maximum value appears, the three curves are generally consistent with each other. Since the value of the shear failure parameter determines the critical plastic deformation to the failure of elements in each model, the peak value of each curve corresponds to different ram displacements. Besides, in the current group of simulations, a larger shear failure value is correlated with the higher peak value in shearing force, which means the pipe is more difficult to shear.

Figure 3.19 records the stress distribution and pipe deformation at the time when the pipe is completely separated in the ram shearing numerical simulation corresponding to the three parameters. The letters (a) (b) (c) in the picture corre-

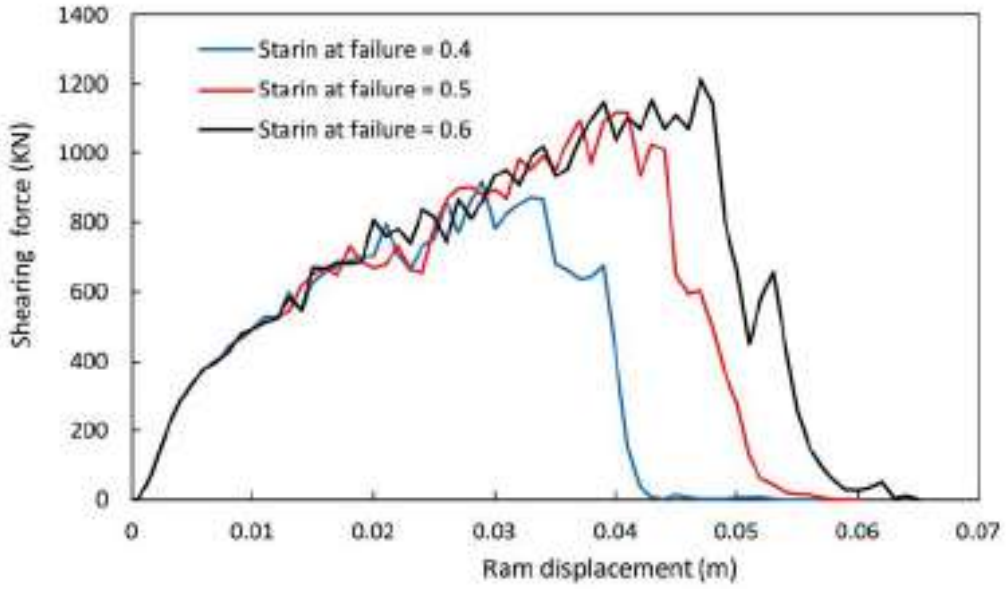

Figure 3.18: Shearing force curve for three shear failure parameter values

sponds to the simulation results when the value of shear failures are 0.4, 0.5, and 0.6, respectively. In these side-view profiles, it can be observed that although all the three models have local large plastic deformations due to ram extrusion, the accumulation of deformation at the time of failure is obviously different. In Figure 3.19 (a), since the shear failure value is small, the cumulative plastic deformation is the least. There is still a high-stress concentration area extending along the Z-axis on the side of the pipe wall as the pipe is separated The direction of macrocrack progression is mainly on the cutting plane of the blade, the crack develops along the circumferential direction and finally separates the pipe. The pipe is not completely deformed, the opposite sides of the pipe inner surface are far from each other. When the value of shear failure is slightly larger, as shown in Figure 3.19 (b), the pipe is further squeezed due to more plastic deformation accumulation before it is completely separated. Macrocracks not only extend in the circumferential direction but also in the axial direction along the Z-axis, at the side of the necking pipe. When the value of shear failure increases to 0.6, the pipe is completely flattened, as shown in Figure 3.19 (c), while the development of macro cracks is basically the same as in Figure 3.19 (b).

From the above comparative analysis, it can be seen that the value of shear failure determines the accumulation of critical value of plastic deformation, which further determines the maximum value of the shearing force curve. This shows that for the numerical model based on the constant criterion, this value seems to reflect the ductility of drill pipe material. Thus the value of shear failure is very important for the prediction of the maximum shear force accurately.

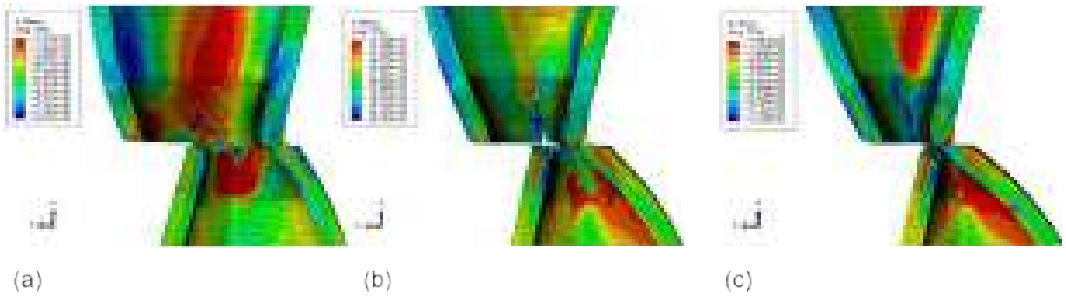

Figure 3.19: Side view of pipe cross-section upon rupture

The problem of constant fracture strain criterion is that it is impossible to obtain the critical strain value from a well designed experimental test, due to the fact that the equivalent strain to fracture is highly correlated to the stress state during a deformation of the material. Prior theoretical analyses and experimental results have shown that the material's fracture strain is not constant but changes under different loading conditions [34, 37, 54, 55]. Failure criteria which are more suitable for ram shearing simulation are discussed in the following chapter.

3.3 Summary

In this chapter, the mechanical analysis of the shearing force is conducted to understand the failure of the drill pipe during the ram shearing process. From some observations in full-scale ram shearing experiment, the plastic deformation and fracture morphology of the sheared drill pipe is analyzed. By correlating the ram shearing process with a typical blanking process, the peak value of the shearing force for a perfect ductile pipe corresponds to the plastic load instability before macrocrack initiation. It is reasonable that the peak shearing force will be obtained if the decrease in load caused by the reduction of sheared area outweighs the increase in load associated with plastic hardening.

Based on the mechanical analysis above, the FE numerical model is built to calculate the shearing force and investigate the influence of the loading conditions. Some observations from the obtained simulated results are listed as follow:

- With the same grade, the larger outer diameter of the drill pipe generally needs higher shear force to cut
- The required shearing force without tension or compression is higher than that of pipe under compression or tension
- In the non-centralized position inside the blade clearance, the pipe needs lower shearing force to be cut. For specific well configuration, if it is in the non-centralized position beyond the width of the blade, likely the pipe will not be

fully cut, and the blind shear ram may have difficulty reaching the condition to seal the well

- For a constant failure criterion, the failure parameter value reflects the material's resistance to failure and strongly influences the maximum shearing force

The actual shear ram test results are collected and compared with the simulated shearing force to discuss the accuracy of the FE model. It can be seen that FE simulation gives more possibilities to understand the shearing process of BSR and has the potential for identifications of specific and important aspects (e.g. compression, tension, offset, the shape of rams). However, the current model has limitations due to the demand for experimental work for failure parameter calibration. A more accurate failure criterion of the drill pipe in the shearing process simulation is still required.

Another important aspect is that the numerical accuracy of the above FE models needs further investigation in applications for ram shearing force prediction. BOP simulation result would be more reliable if the FE model were proposed with a thorough mesh sensitivity study, which will assure the mesh size convergence. Considering the large size of pipes and BOP rams, the computing resource requirement is also a limitation to those models in the engineering applications.

Chapter 4

Comparison of three fracture criteria in ram shearing simulation

4.1 Derivation of fracture parameters from experimental data

Base on the analysis of the BOP ram shearing process and required shearing force in Chapter 3, the FE model is built but the failure criterion still requires to improve. This Chapter focus on providing proper fracture criteria and the respective application approach for the ram shearing process. By adopting the progressive damage framework, the simulated ram shearing process is divided into several steps, shown in Figure 4.1. With the hydraulic pressure from the BOP operation system, BOP rams move towards each other. After they have contact with the drill pipe, the elastic and plastic deformation of the pipe happens in a row because of the extrusion force from the ram. The failure of the drill pipe can be furtherly seen as damage initiation and evolution. The damage is assumed to initiate when the accumulation of the equivalent plastic strain of an element arrives a critical value ϵ_f, as expressed by Equation 2.11.

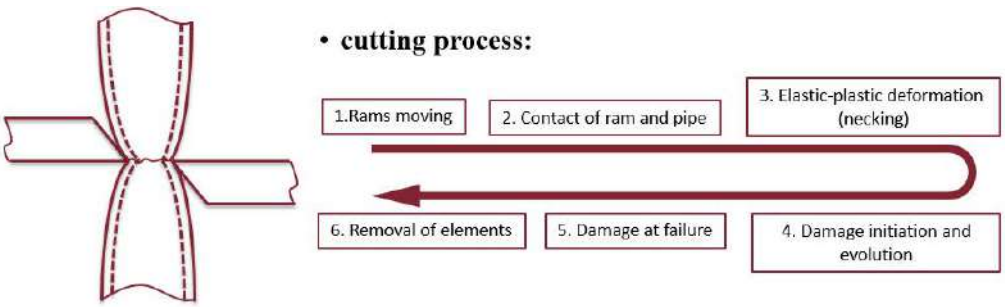

Figure 4.1: Steps of Shearing Process

This chapter demonstrates a thorough approach to apply the fracture criteria into

BOP shearing simulation. Three commonly used criteria are adopted as uncoupled phenomenological fracture models. Experimental data from TRIP690 material are employed to obtain the fracture parameters and to plot the fracture limit curve. A mesh study is then carried out for the convergence of the proposed model. The pipe mesh is gradually refined along the axial direction, a node-based explicit finite element submodel technique available in Abaqus software is adopted to decrease the CPU time.

4.1.1 Approach of fracture parameter calibration

The material adopted in this investigation is a cold-rolled retained austenite (TRIP) steel, that belongs to the category of the AHSS, grade RA-K 40/70, standard HCT690T. The plastic and fracture properties of this material have been fully characterized in previous studies [70]. Besides, TRIP690 material provides the close property with API E grade steel [25] and exhibits little anisotropy in both plastic and fracture properties [54]. It is, therefore, chosen as the material for the present study.

Bai and Wierzbicki [55] use five types of TRIP690 specimens for calibrating plastic flow and fracture parameters, which include dog-bone specimen, flat specimen with cut-outs, punch test specimen, butterfly specimen in tension and butterfly specimen in simple shear. Through a hybrid experimental-numerical method [71, 72], the equivalent plastic strain to fracture and the triaxiality were obtained for each test, as shown in Table 4.1. Their experimental data is employed in the present study to derive fracture parameters of CrashFEM ductile and shear criteria. For the J-C criterion, Bai and Wierzbicki [54] have calibrated the fracture parameters with TRIP690 steel material. Those calibrated fracture parameters for MMC and J-C criterion mentioned above are used for a comparative investigation in later sections.

4.1.2 Derivation of MMC fracture parameter

As it is shown in Figure 4.2, the 3D MMC fracture locus was then plotted through a surface fitting optimization process [53]. It should be mentioned that the original authors used the Vumat code to implement the MMC criterion into FE software to simulate the ductile fracture. In the current study, a more simple way to apply this criterion is employed. The fracture locus, which is a function of triaxiality and Lode parameter is implemented in the Abaqus code as a ductile fracture criterion[73, 74].

The 3D MMC fracture locus of TRIP 690 material is converted to a series of fracture curves, shown in Figure 4.3. Each of the colored lines corresponds to a certain lode angle and represents the equivalent plastic strain as a function of stress triaxiality. Thus, in the framework of damage mechanics, the equivalent plastic

Table 4.1: Experimental data on TRIP 690 steel for fracture parameters calibration[25]

No.	Specimen	Stress state	ϵ_f	η	$\bar{\theta}$	$\theta_s(K_s = 0.05)$
1	dog-bone	tension	0.751	0.379	1	
2	flat	tension	0.394	0.472	0.496	1.66
3	disk	equibiaxial tension	0.950	0.667	-0.921	1.80
4	butterfly	tension	0.460	0.577	0	1.58
5	butterfly	pure shear	0.645	0.9640	0	1.73

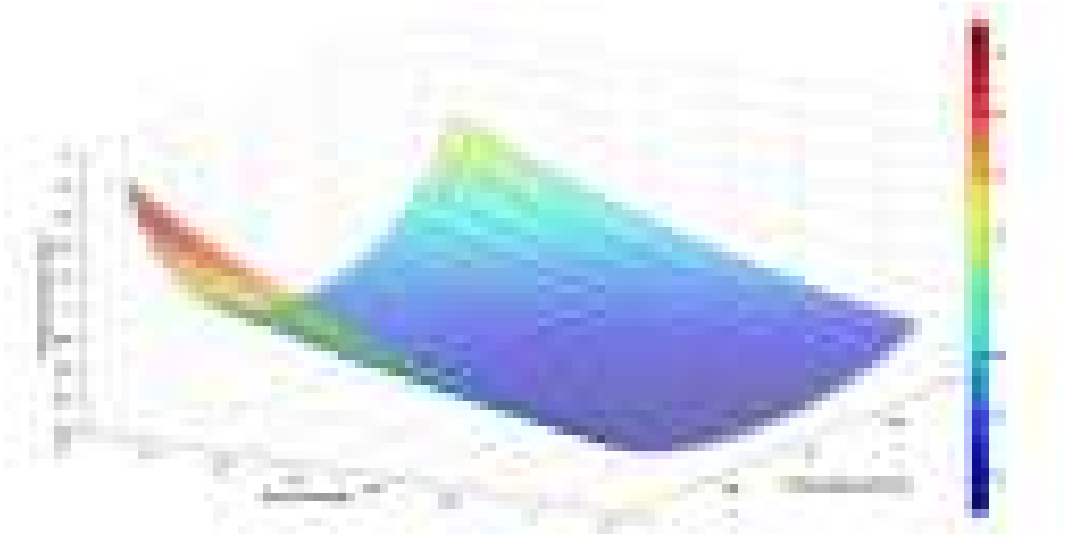

Figure 4.2: MMC 3D fracture locus of TRIP 690 material[25]

strain at the onset of ductile damage is calculated as a function of the Lode angle and stress triaxiality.

4.1.3 Derivation of CrashFEM fracture parameter

For the CrashFEM criterion, the derivation process of remaining fracture parameters for ductile and shear criteria will be discussed in the following section. It should be mentioned that experimental test #3 characterizes the stress state for equibiaxial tension, the value of the parameter ϵ_T^+ in equation 2.25 and ϵ_S^+ in equation 2.27 are therefore obtained directly from the punch test data.

There is no clear conclusion in the literature clarifying the boundary of ductile and shear fracture mechanisms' effect in the fracture criteria. Bao and Wierzbicki

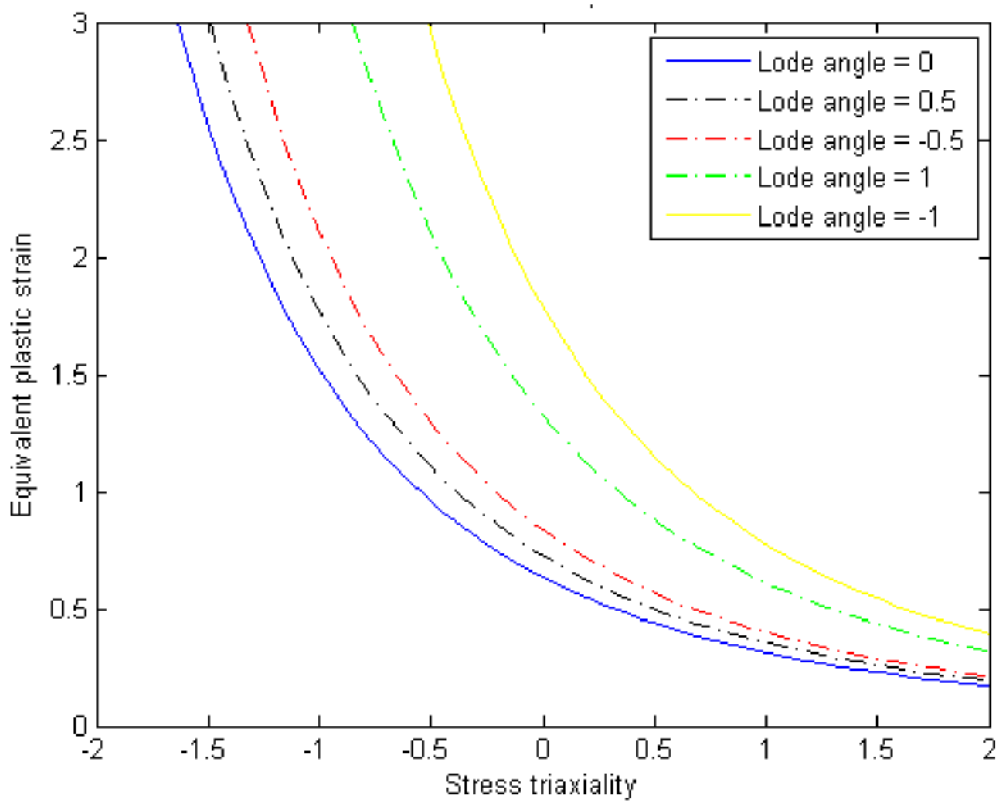

Figure 4.3: MMC ductile limit curve of TRIP 690 material

[48] carried out a series of tests in a wide range of stress state. A calibrated fracture locus for this material in equivalent strain-stress triaxiality space is plotted. Specific experimental data points for ductile and shear fracture parameter derivation are therefore chosen according to reference [48].

For the ductile fracture criterion, Hooputra et al. [49, 50] conducted three experiments with different stress triaxiality: Erichsen test, three-point bending, and notched tensile specimens. In this thesis, the stress state of elements in the experimental test data $\#1-4$ corresponds to the ductile fracture mechanism. These data points are, therefore, used to obtain the remaining parameter: ϵ_T^-, and c. The best-fitting ductile limit curve for all these points is obtained through the least square fitting method. Figure 4.4 shows a comparison between the fitting result and the one calibrated by Hooputra et al. [50].

As the #1 data is relatively far from the plane stress condition, the value of θ_s obtained through equation 2.24 may have an unacceptable error. Experimental test data points $\#2-5$ are therefore used to derive shear fracture parameters: k_s ,ϵ_s^-, and f. The shear stress ratio at each data point is calculated through equation 2.24. A series of material parameter k_s are assumed according to prior study [50, 54] and the best fitting result is obtained when $k_s = 0.05$, as indicated in Table 4.2.

Figure 4.5 shows the approximated shear fracture limit curve according to this

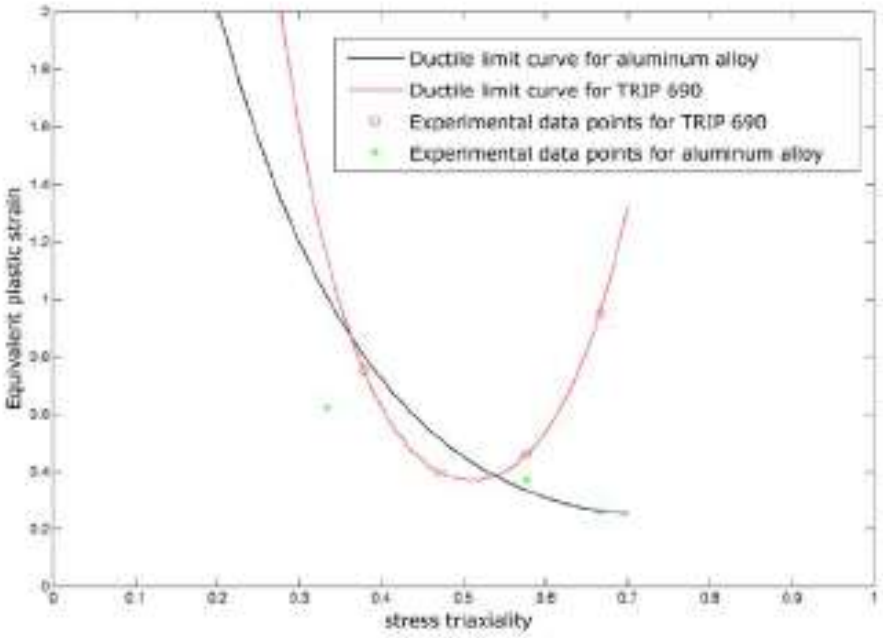

Figure 4.4: Ductile fracture limit curve derived from experimental data

Table 4.2: Curve fitting results for the assumed value of K_s

Assumed value of k_s	Least square fitting for shear fracture	R^2
0.01	$\bar{\epsilon}_f^s = \frac{0.95\sinh[f(\theta_S - 2.04)] + \epsilon_S^- \sinh[f(1.96 - \theta_S)]}{\sinh(-0.08f)}$	-0.02243
0.033	$\bar{\epsilon}_f^s = \frac{0.95\sinh[f(\theta_S - 2.132)] + \epsilon_S^- \sinh[f(1.868 - \theta_S)]}{\sinh(-0.264f)}$	0.3492
0.05	$\bar{\epsilon}_f^s = \frac{0.95\sinh[f(\theta_S - 2.2)] + \epsilon_S^- \sinh[f(1.8 - \theta_S)]}{\sinh(-0.4f)}$	0.9742
0.0667	$\bar{\epsilon}_f^s = \frac{0.95\sinh[f(\theta_S - 2.2668)] + \epsilon_S^- \sinh[f(1.7332 - \theta_S)]}{\sinh(-0.5336f)}$	0.5411
0.1	$\bar{\epsilon}_f^s = \frac{0.95\sinh[f(\theta_S - 2.4)] + \epsilon_S^- \sinh[f(1.6 - \theta_S)]}{\sinh(-0.8f)}$	0.7883

result and the one calibrated by Hoouptra et al. [50] are compared. Table 4.3 provides a summary of fracture parameters derived from the experimental data for TRIP 690 steel.

To compare the fracture limit curve in the same space, the shear fracture limit curve is represented into (ϵ_f, η) space according to equation 2.24. As for the case of MMC criterion, the calibrated TRIP 690 fracture locus is projected into (ϵ_f, η) space

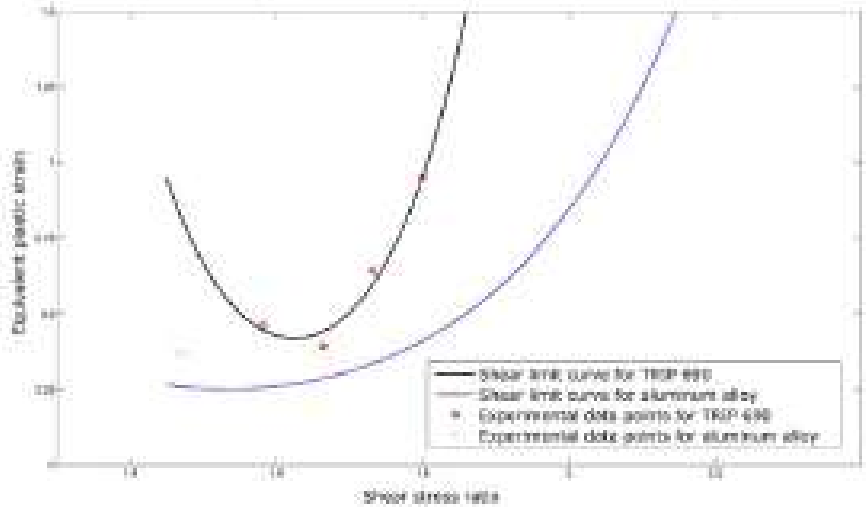

Figure 4.5: Shear fracture limit curve derived from experimental data

Table 4.3: Summary of derived fracture parameter

Fracture criterion	Calibrated Parameters
Ductile Fracture	$\epsilon_T^+ = 0.950, \epsilon_T^- = 31800, c = 10.26$
Shear Fracture	$\epsilon_s^+ = 0.950, \epsilon_s^- = 25.06, f = 8.313, k_s = 0.05$
MMC[25]	$A = 1275.9MPa, n = 0.2655, C_1 = 0.12, C_2 = 720MPa, C_3 = 1.095$
J-C[64]	$d_0 = 0.1271, d_1 = 0.5161, d_2 = 0.7599$

in plane stress and plane strain conditions, based on equations 2.30 - 2.35. Figure 4.6 illustrates the fracture limit curve for all fracture criteria mentioned above.

The solid red line corresponds to the CrashFEM shear fracture criterion, whereas the dotted red line represents the CrashFEM ductile fracture criterion. The two branches of the fracture locus alternate in different stress triaxiality range. When the value of stress triaxiality falls in the range between 0.3 and 0.6, the curve representing the ductile fracture branch is lower than the shear fracture branch. Out of this range, the shear fracture branch becomes the lower one. One can easily indicate that both CrashFEM fracture limit curve and MMC fracture locus include most of the experimental points, whereas the Johnson-Cook fracture limit curve passed only by two experimental points. Wierzbicki et al.[54] made an effort to calibrate J-C fracture locus on 2024-T351 aluminum alloy with a wide stress triaxiality range experimental data. Except for the pure shear and tension test, the J-C fracture locus was found to miss almost all experimental points. According to these calibration

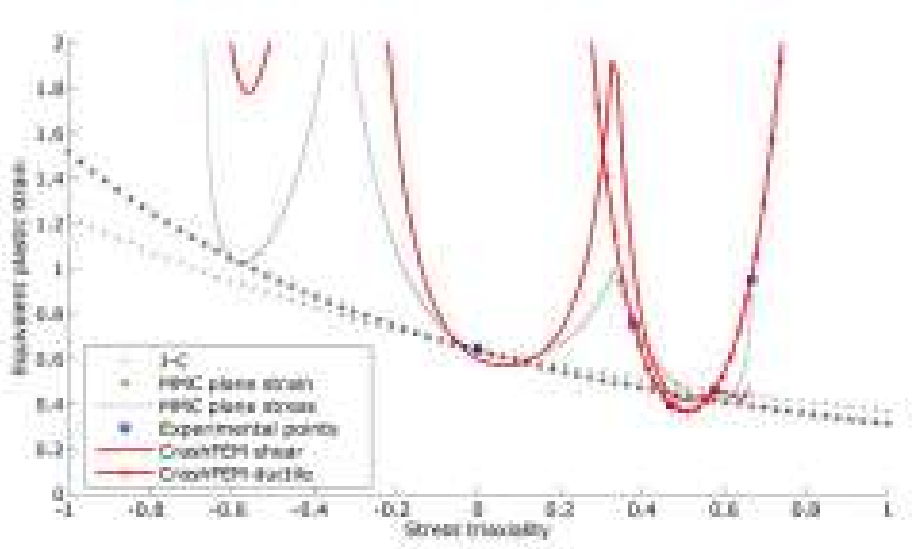

Figure 4.6: Comparison of the fracture limit curve for three criteria in the space of stress triaxiality and plastic strain

results for J-C fracture locus on 2024-T351 aluminum alloy [54] and TRIP 690 steel [55], it appears that the J-C criterion provided a lower bound for the fracture limit curve. Besides, based on Figure 4.6, the J-C criterion generally proposes a similar tendency as the MMC plane strain curve. The effect of applying different fracture criteria in the BOP shearing FE simulation will be discussed in the following sections.

4.2 FE model with fracture criterion

In this section, the CrashFEM criterion with derived parameters is applied in the Abaqus software[74], the geometry and boundary conditions of pipe and rams in the FE model are described. Several numerical simulations are carried out to investigate the mesh size sensitivity considering three selected fracture criteria.

In the actual subsea BOP operation in offshore oil and gas exploration activity, the shearing operation is supposed to stop serious accidents, such as sudden blowout events or fatal emergencies which need to activate the EDS. Those operations generally correspond to complicated loading boundary conditions with oil and gas flow effects. According to API standard [6], BOP shear test is usually conducted before a subsea BOP is installed in the offshore oilfield and provides a simple loading condition for tube shearing inside BOP. These tests shall be performed without tension in the pipe and with zero wellbore pressure. A typical full-scale BOP shear experiment [14] set up is selected for the load and boundary condition of the present BOP shearing simulation.

In the BOP shear ram test, the drill pipe is centralized in the BOP bore un-

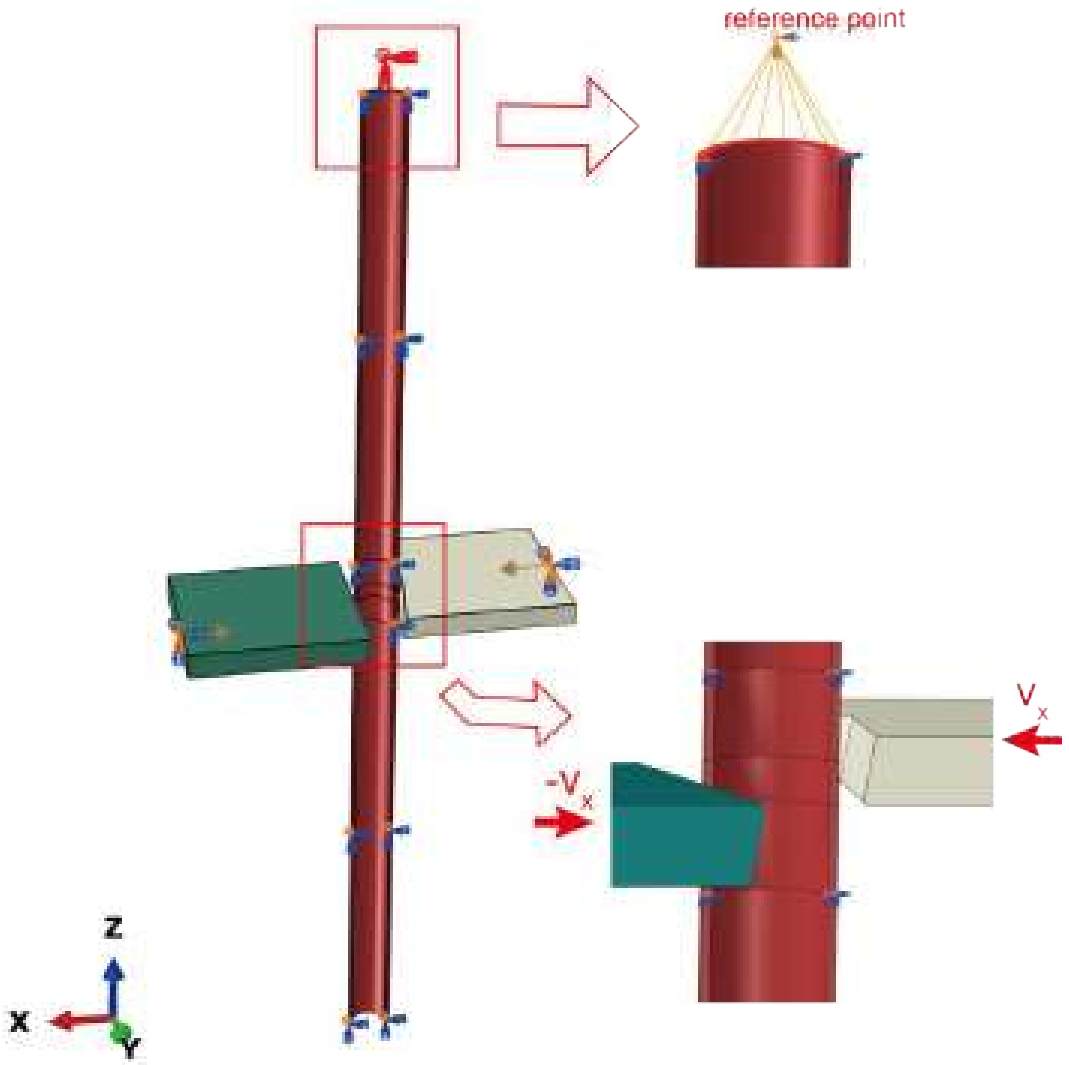

Figure 4.7: Schematic image for loading and boundary condition of the FE model for BOP ram shearing

der nonflowing well condition. BOP rams are moved by hydraulic pressure via a control panel. The average time recorded from the rams' contacting the drill pipe to ultimately closing the wellbore is 6.5 seconds. The investigation of the influence of different fracture models on the BOP shear force assumes that the ram velocity is constant during the quasi-static shear process, where the ram's inertia is not an influencing factor. Also, due to the low velocity of the ram the strain rates are low and viscous effectcs on the material behaviour can neglected. As illustrated in Figure 4.7, the loading and boundary conditions of the FE model follows the BOP shear ram test. The drill pipe, the V-shaped upper ram, and the blind lower ram in the assembly are illustrated with red, grey, and green, respectively. The central axis of the pipe is considered coincident with the central position of the BOP rams. The initial distance between the ram and the pipe is set to be infinitely small to obtain

computational efficiency. The pipe's upper bound is fixed, while the lower bound is free. The coupling option is applied to the cross-section at the upper bound to avoid over-constraining. Due to symmetry, only half of the pipe is considered. The symmetry boundary condition is assumed on the pipe midplane. By applying the prescribed velocity V_x, constant velocity control of the ram movement is introduced, as shown in Figure 4.7. In the present model, $V_x = 0.1m/s$, the sign of V_x represents the direction along the x-axis. The simulated shearing process begins with the rams initially in contact with the pipe surface and stops after the pipe is separated.

The geometry of the blind shear ram adopted in Chapter 3 (illustrated in Figure 3.9) is employed in the current chapter. Drill pipe geometry with 127 mm OD is selected in the present FE model. As discussed in Chapter 3 via the model of Wierzbicki, the length of the deflection zone in the pipe axial direction can be expressed as a function of ram indentation distance. Thus the pipe must be enough long to eliminate the pipe bound effect. It is found that when the pipe length is set to be 3 m, the transverse stress on the top and bottom of the pipe is neglectable, compared with the stress on the shearing area of the pipe. The length is therefore set to be 3 m, and other pipe geometries are listed in Table 3.1.

The material of the pipe is assumed to be TRIP 690 steel and modeled through elastoplastic J2 flow theory with isotropic hardening. The parameters of the plastic model are calibrated by Bai [55] through the dog-bone tensile test as $\sigma = 1275\epsilon^{0.2655}$, and the Young modulus and Poisson's ratio of TRIP 690 are assumed to be 210 GPa and 0.3, respectively.

The rams are taken as rigid bodies, due to the following considerations. Compared with the deformation and damage of the drill pipe, the deformation on the shear ram is neglectable expect in very small regions. It should be mentioned that the shear ram blade is made of hardened high alloy steel material with much higher mechanical strength than the pipe material in this study. Besides, the CPU time will be increased significantly when the deformation of the shear ram is taken into consideration, especially for the models with refined mesh size in the shear section on the pipe. The deformable shear ram model will increase the complexity of contact formulation between the shear ram and the pipe surface, as well as the total number of elements in the FE model, both of which may make the work more difficult.

The earlier mentioned fracture criteria with parameters derived from TRIP690 steel experimental data are applied in the FE model through a progressive damage model in Abaqus. It should be mentioned that the MMC fracture locus is used in the present thesis as a particular form of ductile damage initiation criterion just for the sake of comparison. The complete MMC fracture model application procedure is illustrated by Bai [53].

A damage evolution parameter is also required in Abaqus to capture the post-

damage effect. To eliminate the complexity of damage evolution mechanism effect, a linear form for the damage variable increment is adopted, as defined in equation 2.12. Li and Wierzbicki [75] conducted an experimental and numerical investigation on the influence of the effective plastic displacement at the failure point, U_f, on the mixed-mode stable tearing test. It was found that changing U_f by four orders of magnitude produces only a moderate effect on the load-displacement curve. In this thesis, the value of U_f is assumed to be 0.1 mm, for all the damage initiation models.

4.3 Mesh design and sensitivity investigation

BOP shearing simulation is characterized as a three-dimensional nonlinear analysis. The Continuum three-dimensional 8-noded linear elements with educed integration (C3D8R) are selected to simulate the deformation and rupture of the drill pipe. The rigid three-dimensional 4-noded surface elements (R3D4) are used to simulate the movement of the rams. Considering the structural scale of the model, a node-based submodeling technique provided by Abaqus 6.14 [74] is adopted to investigate the mesh sensitivity in one specific part of the pipe.

For the global model, a gradually refined mesh is carried out, as illustrated in Figure 4.8. After a series of simulations, it is found that only the elements inside a local area correspond to large plastic deformation. The mesh size sensitivity study is therefore carried out in this small section, labeled in Figure 4.8 as the "shear section." As for the submodel, the length is designed to cover all plastic deformation in the shearing process. A hybrid approach including both analytical estimation 3.3 and numerical simulation is carried out to pre-identify the plastic deformation. The contact area between rams and the pipe is also included. The length of the submodel is therefore set to be 0.24 m.

The global model is run first to obtain the overall pipe deformation due to the applied loadings and boundary conditions. The shearing process of the tube is then analyzed in the submodel according to the applied response from the global model. According to a numerical comparison, the difference between the reaction force calculated by the global model and the submodel with the same mesh size is negligible, as the error is less than 3%.

To demonstrate the mesh effect of an FE model for BOP shearing simulation, three series of submodels concerning the respective fracture criteria are conducted, and the mesh of the pipe is refined in separate submodels until convergence is obtained. As pointed out by Besson [76], the aspect ratio has an essential role in ductile tensile rupture; varying aspect ratio probably has a negative influence on the mesh size convergence. A mesh refinement effect with unit aspect ratio is therefore carried

out in this work. The original element number in the pipe thickness direction is 4, and the mesh is refined in all three directions to maintain a unit aspect ratio in the shearing section. The total number of elements in the global model is 132800, and the number of elements in the submodel is 18444.

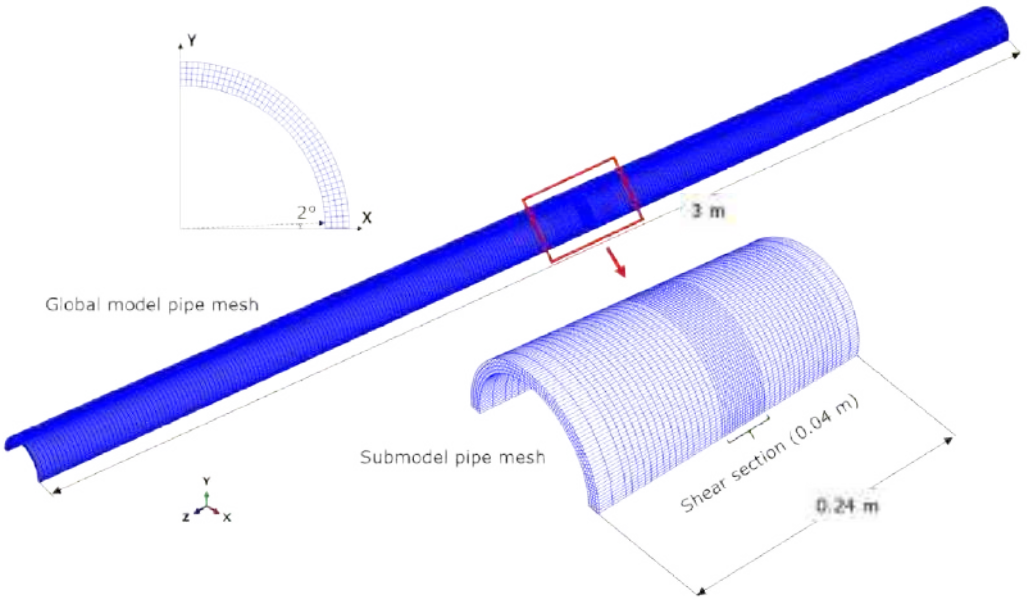

Figure 4.8: Schematic Illustration of the mesh design for the global model and submodel

Beginning with a 2.3 × 2.3 × 2.3 mm mesh (4 elements though the thickness), the mesh grid is refined gradually for the FE submodel with each fracture criteria until the peak value of the latest curve is consistent with the last one. The corresponding shearing force curve change in a form as shown in Figure 4.9 to 4.11.

It can be observed that with the number of elements through pipe thickness increasing, the simulated shearing force curve generally gets lower, the peak value of shearing force decreases. It is visible that the convergence of the mesh effect for the three fracture criteria is not obtained at the same mesh size. For the model with MMC and J-C criteria, the first accepted thickness element number for the balance of convergency is eight, which means the accepted refined mesh size is 1.15 × 1.15 × 1.15 mm, as shown with the red line in Figure 4.9 and 4.11. For the model with CrashFEM criterion, the mesh effect is only converged after the mesh size is refined to 0.78 × 0.78 × 0.78 mm, shown with a black line in Figure 4.10. It should be noted that the CPU time increases significantly after there are more than 8 elements through the thickness.

Figure 4.12 shows the maximum transverse contact force predicted at different mesh sizes for the respective fracture criterion. It can be seen that when predicted by a specific fracture criterion, lower shear forces are generated from a more significant

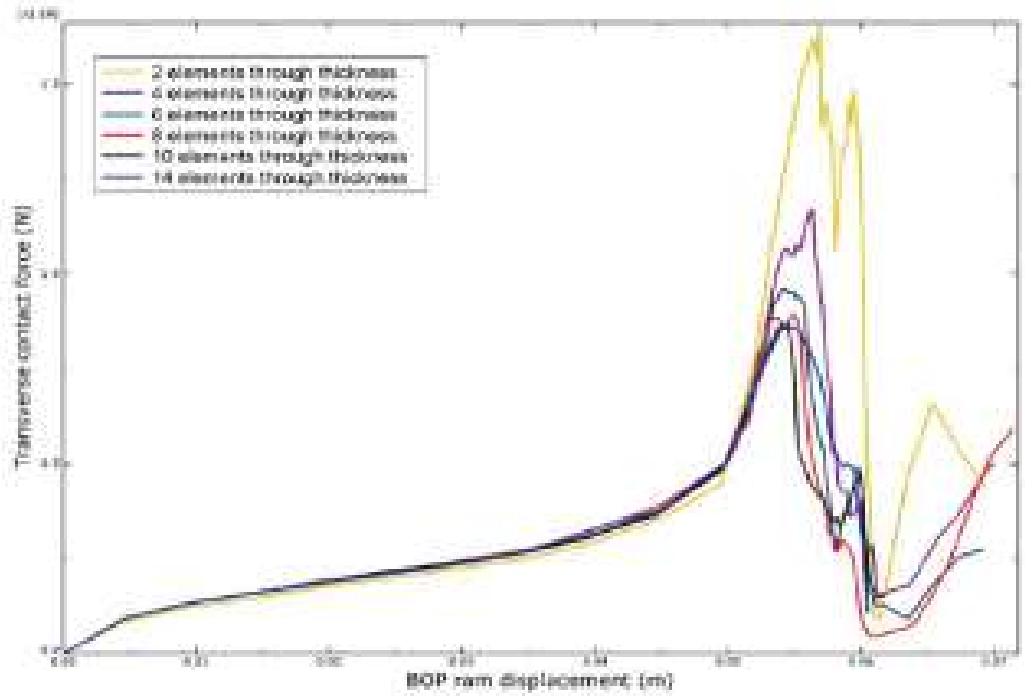

Figure 4.9: Simulated shearing force curve with a refined mesh effect (MMC)

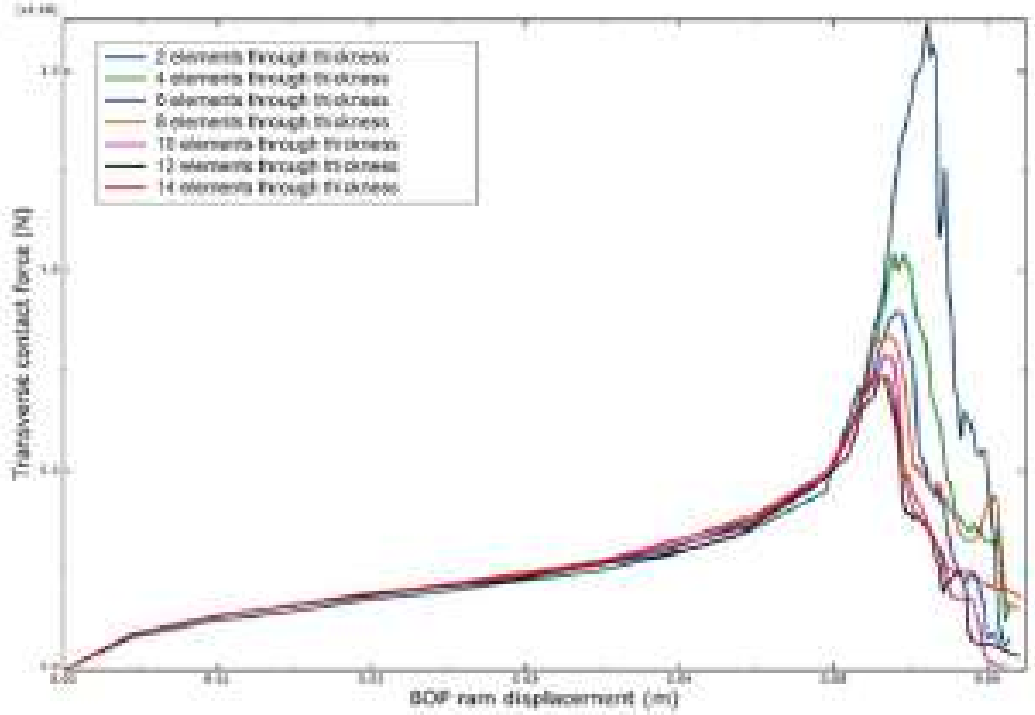

Figure 4.10: Simulated shearing force curve with a refined mesh effect (CrashFEM)

number of elements until the converged mesh size is obtained. The selection of fracture criterion has an influence on the mesh sensitivity. When predicted by the Johnson-Cook or MMC criterion, the BOP shearing force converges when element

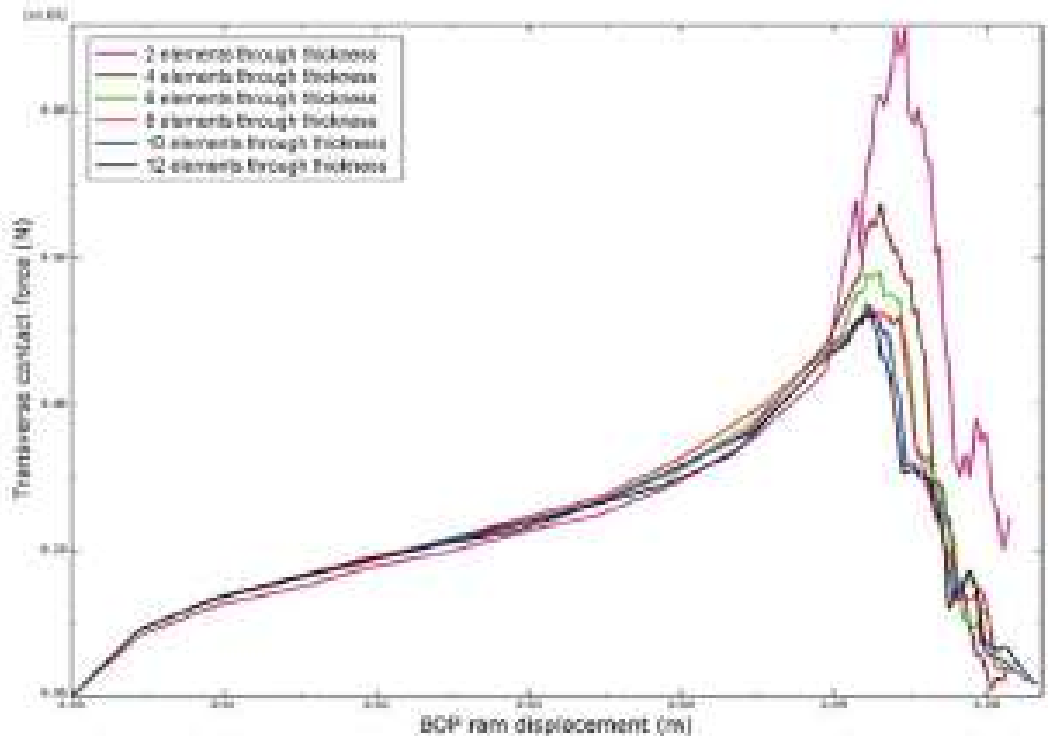

Figure 4.11: Simulated shearing force curve with a refined mesh effect (J-C)

size equal to or is smaller than 1.15 mm (number of elements through pipe thickness equal to 8). As for the CrashFEM criterion, the converged BOP shearing force is obtained with a mesh size of 0.78 mm. These element size values are chosen for the BOP shearing simulation in the following section.

Based on the difference in the three fracture criteria, the investigation is separated into two main parts. The first is to analyze the effect of applying a single branch of CrashFEM criterion individually and to compare the results with the combined CrashFEM criterion. The second part is to compare the simulation results obtained from different fracture criteria with their converged mesh size and analyze the influence of selected fracture criteria on the force prediction for ram shearing.

4.4 Separate and combined applications for CrashFEM criterion

To investigate the independent influence of each branch mechanism in the CrashFEM criterion, several simulations have been carried out with the same loading and boundary conditions. Figure 4.12 presents the transverse contact force-displacement curve of BOP rams, obtained with CrashFEM ductile fracture criterion, shear fracture criterion, and combined fracture criterion, respectively. The combined fracture criterion follows the overall damage mechanism defined in Equation 2.13, 2.14. It

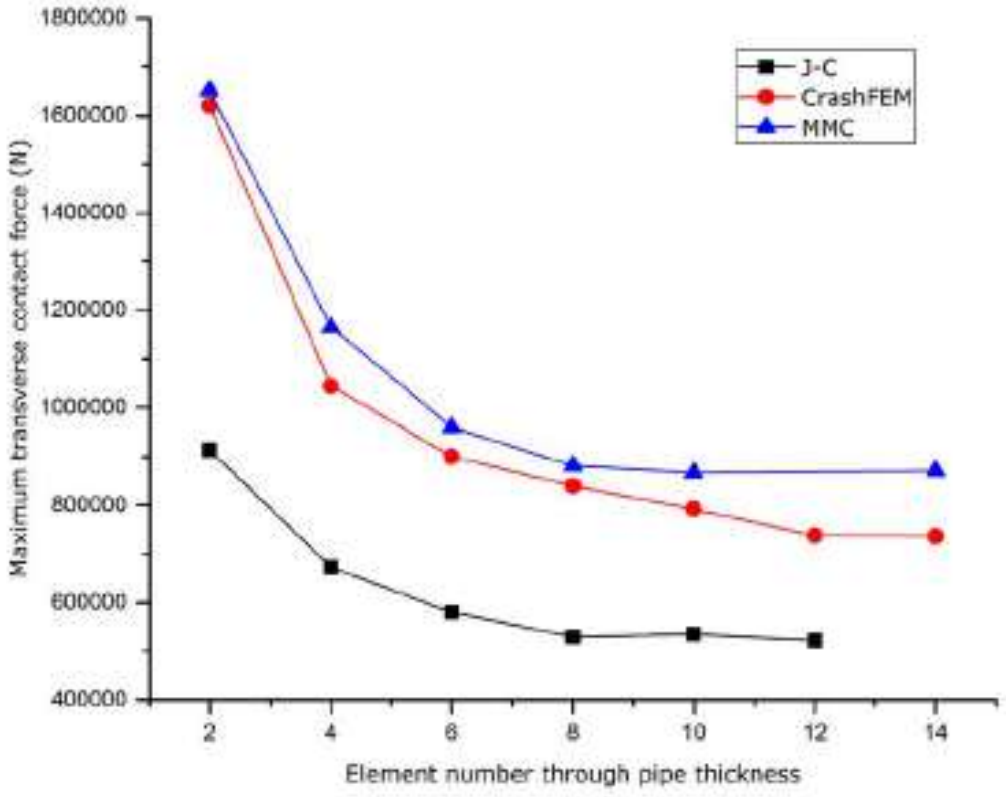

Figure 4.12: Maximum shearing force as a function of the number of elements through pipe thickness

can be figured out that, with the ductile fracture criterion, a higher shear force than the one simulated with shear fracture criterion is obtained, and the overall criterion generally indicates the least shear force value.

It should also be mentioned that the peak value predicted by ductile and shear fracture criteria separately are obtained for different ram displacements. As the red dash line marks in Figure 4.13, the shear criterion predicts an earlier decrease in the contact force curve, with ram displacement of 0.549 m. At this ram displacement value, a damage profile along a surface node path is then plotted to illustrate this difference in Figure 4.14. The position of this path in the cross-section surface, denoted as path A, is demonstrated in Figure 4.15.

Note that damage initiates when the corresponding criterion reaches the maximum value of 1, as Equation 2.11 indicates. It can be observed that at the moment when the ram displacement equals 0.549 m, the shear damage initiates at several nodes located with normalized distance 0.5 and 0.7 along with path A; whereas ductile damage has not predicted any damage in the same path.

The analysis above may reflect that both fracture mechanisms have an influence on the BOP shearing process, and the combined fracture criterion representing an

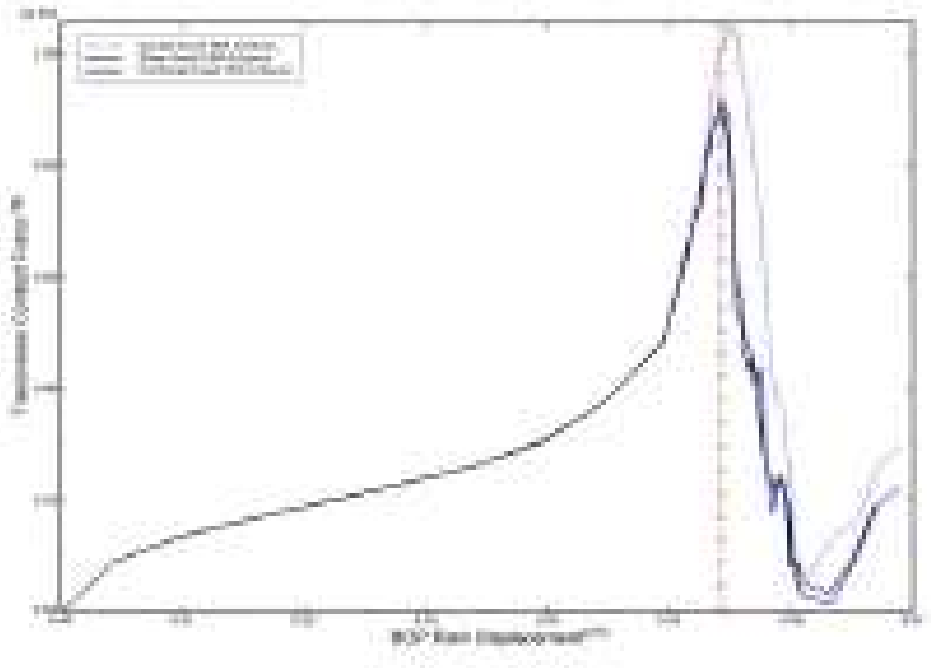

Figure 4.13: Force-displacement curve for overall CrashFEM criterion and independent branches

overall fracture model is necessary to increase the accuracy of the shear force prediction. The combination of ductile and shear fracture criterion is therefore adopted in later sections to simulate the BOP shearing process.

4.5 Comparison of simulation results for different fracture criteria

The analysis above provided a foundation for fracture criteria application. A comparative study is finally conducted among the Johnson-Cook, combined CrashFEM, and MMC fracture criteria in this section. Three FE models with corresponding fracture criteria are implemented in Abaqus/explicit code. Analyses in mesoscopic and macroscopic aspects are carried out successively, the role of fracture criteria in BOP shearing simulations is then discussed.

Two specific nodes, marked in Figure 4.15, are selected to demonstrate the triaxiality and strain history during the BOP shearing process. Node B indicates the elements on the contact surface between rams and pipe, and node C represents those elements on the inside layer and far from ram blades. Both points are located at the fracture area where elements experience elastic deformation, plastic deformation,

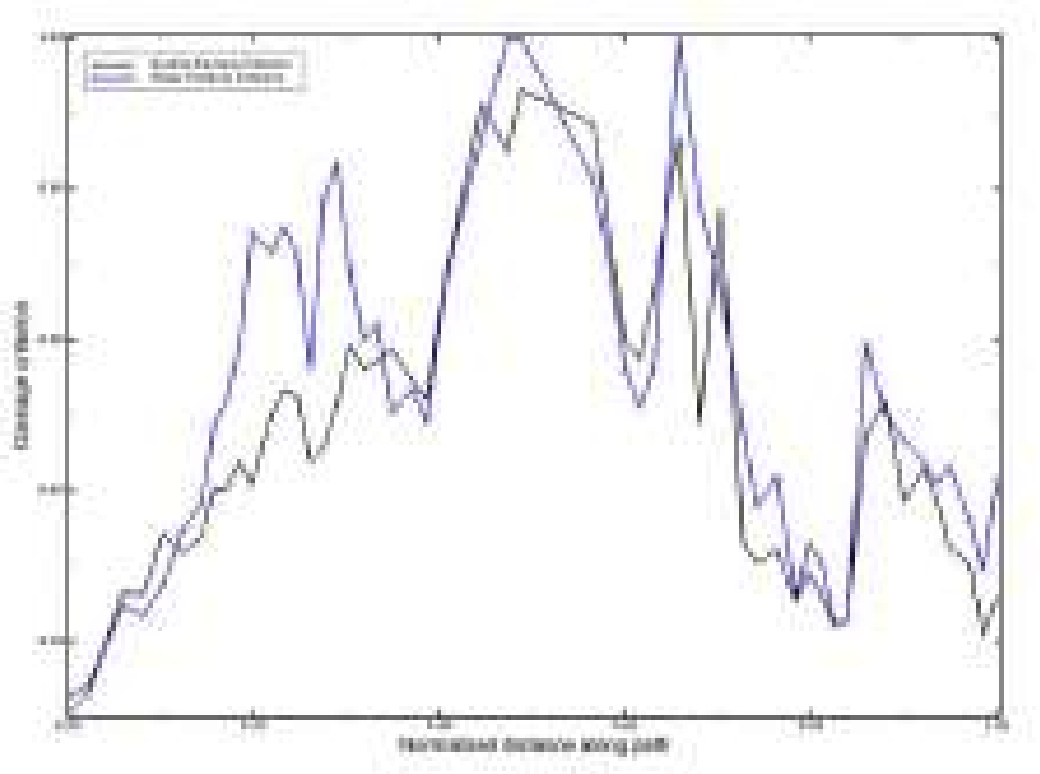

Figure 4.14: Ductile damage initiation profile along the outside surface on the symmetrical cross-section

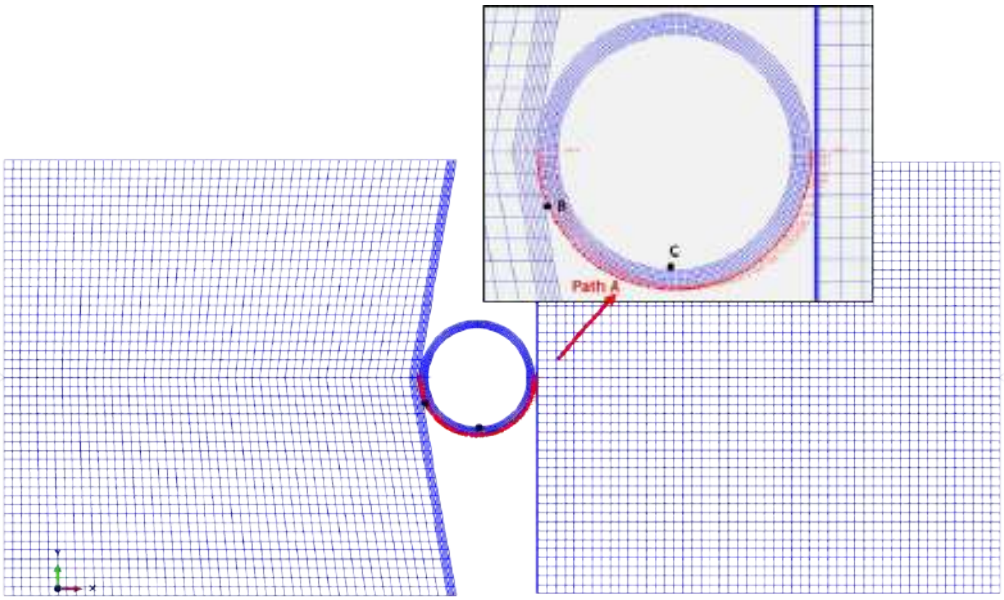

Figure 4.15: Schematic illustration of points and path position under investigation

and stiffness degradation due to damage accumulation in the ram shearing process.

Figure 4.16 plots the triaxiality history with respect to equivalent plastic strain at point B for each criterion. The general agreement in the stress state is observed

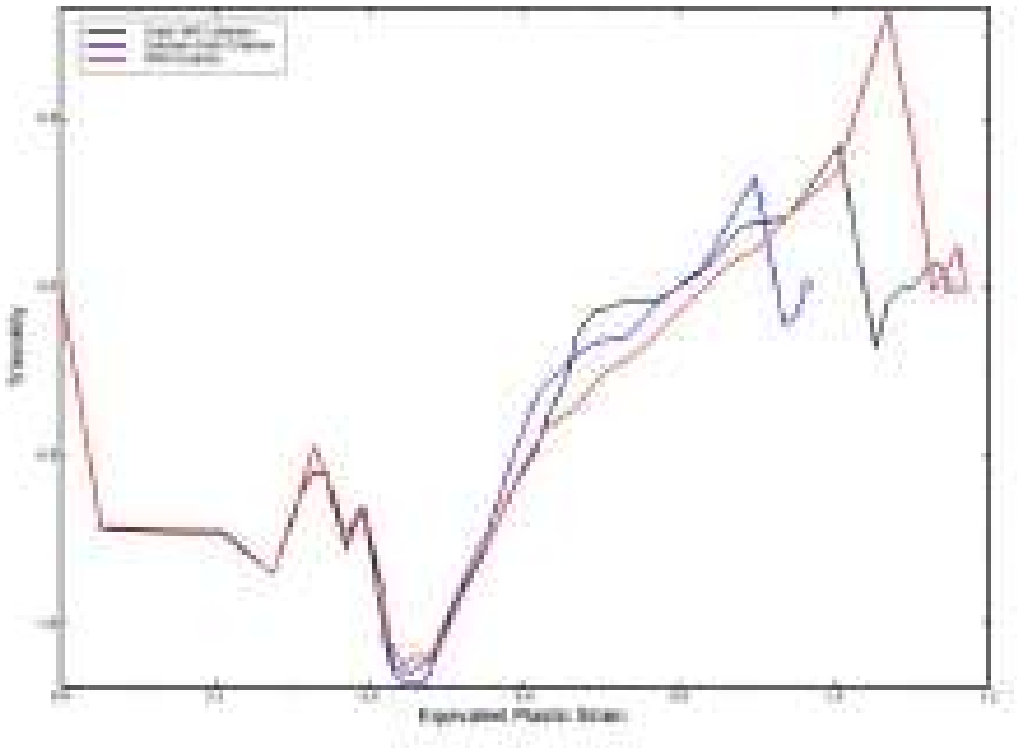

Figure 4.16: Triaxiality history curve at point B as a function of equivalent plastic strain

up to the equivalent plastic strain 0.8. Beyond this point, the triaxiality history curve predicted by the J-C criterion ends with a smaller strain value and the other two criteria, although do not match each other, have the respective fracture points very close. Note that all points end with a triaxiality close to zero, which indicates that fracture initiates in a pure shear condition.

As for the case of point C, triaxiality as a function of equivalent plastic strain drawn in Figure 4.17 has a similar tendency to Figure 4.16. A much smaller plastic strain is predicted by the J-C criterion, the value is only half of the others. Analysis of these two points provides a concept for local plastic strain accumulation during the shearing process at the fracture area. Damage distribution analyses may demonstrate the differences in the structural level.

Figure 4.18 shows the damage distribution for the shearing process considering the three fracture criteria. To obtain a better illustration of the damage area evolution, the deformation of the pipe body and elements deletion are not shown. The three series (a), (b), and (c) correspond to damage predicted by the J-C, CrashFEM, and MMC criterion respectively. Four small images in each series of figures indicate different time points, the fracture initiation for the first element, the maximum fracture reaction force, the damage evolution, and the full rupture of the pipe. It can be figured out that the damaged area predicted by the J-C as well as the CrashFEM

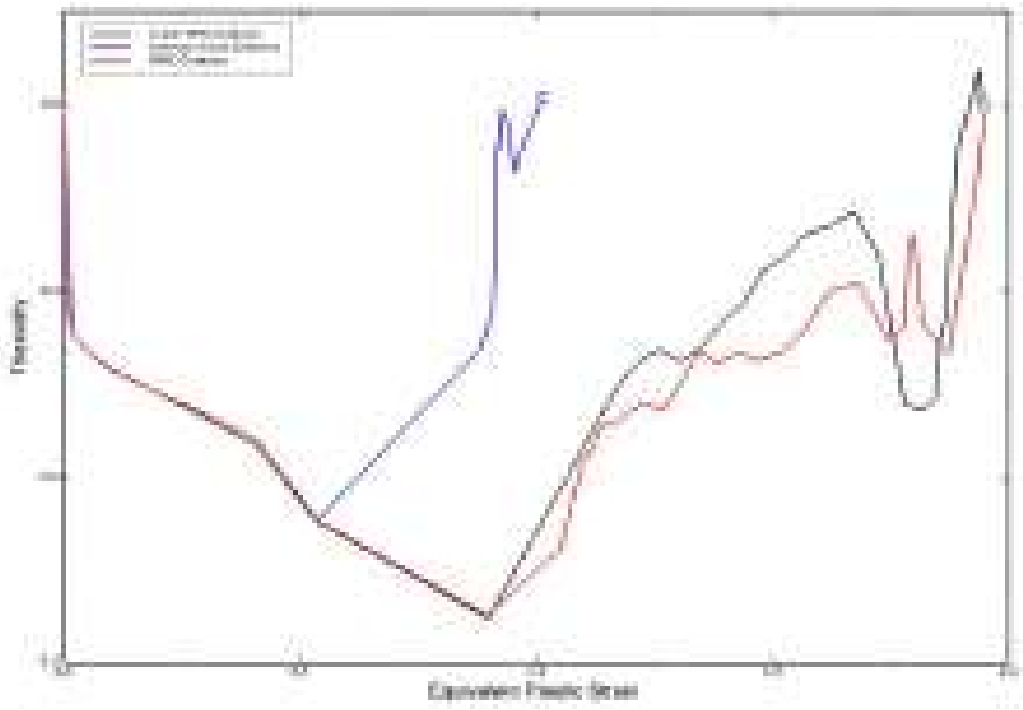

Figure 4.17: Triaxiality history curve at point C as a function of equivalent plastic strain

criterion evolute not only in the circumference direction but also along the radial direction at the location where the pipe elements distort due to the ram extrusion in the transverse direction. In these two cases, the evolution end with a broader damaged area distribution. As for the MMC criterion, damage accumulation is satisfied for the least number of elements, and the final damaged area is also smaller than the others.

To demonstrate the crucial role of damage initiation criteria, analysis of results in the macroscale is then conducted. Figure 4.19 shows the cut off deformation after rupture is obtained in numerical simulation present above. The contours in black denote the pipe cross-section before the ram shearing process, while the contours in blue illustrate the deformed pipe cross-section when the pipe is separated. Larger deformation was observed in simulations with both MMC and Crash FEM criteria, whereas the J-C criterion predicted a smaller pipe deformation due to the damage initiate earlier.

Figure 4.20 records the transverse contact force curve concerning ram displacement for the FE model with the three fracture criteria. Due to the boundary condition of the pipe, the reaction force of the two rams are slightly different, averaged force curve is calculated as the transverse contact force, and the peak force value of this force curve corresponds to the BOP ram shearing force. Note that all the

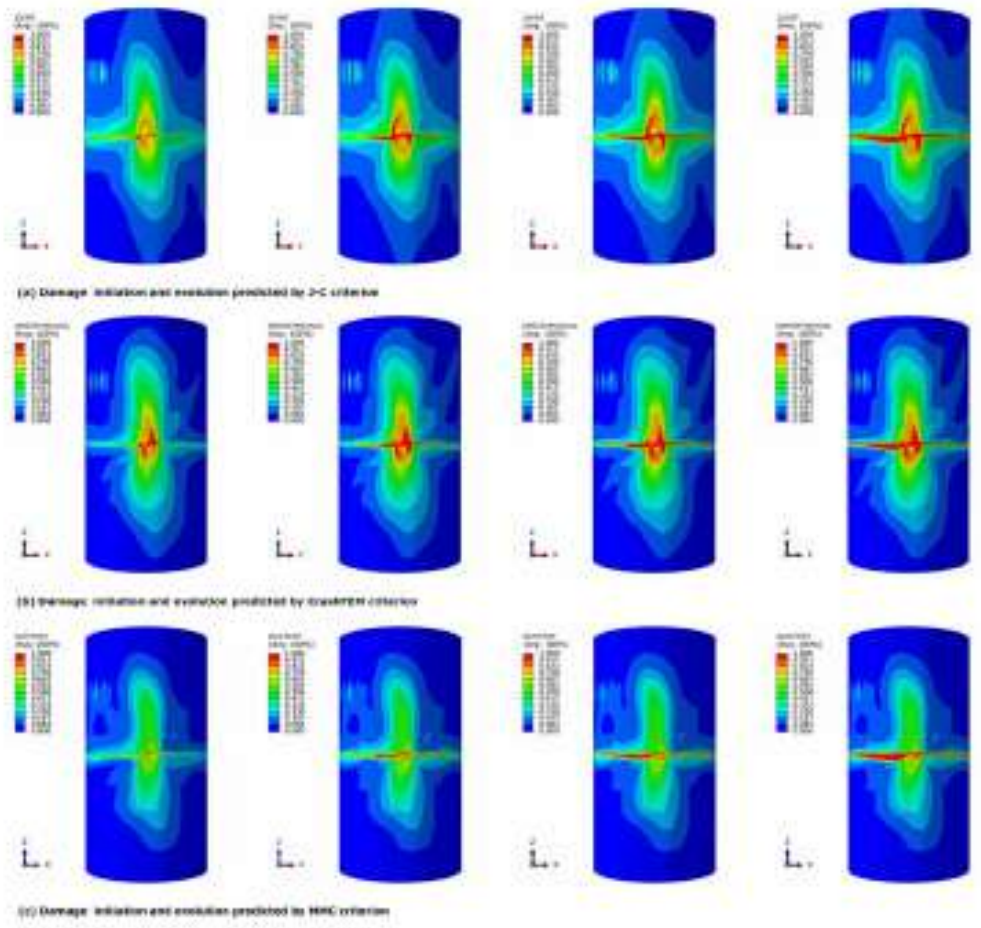

Figure 4.18: Damage distribution for the shearing process considering the three fracture criteria

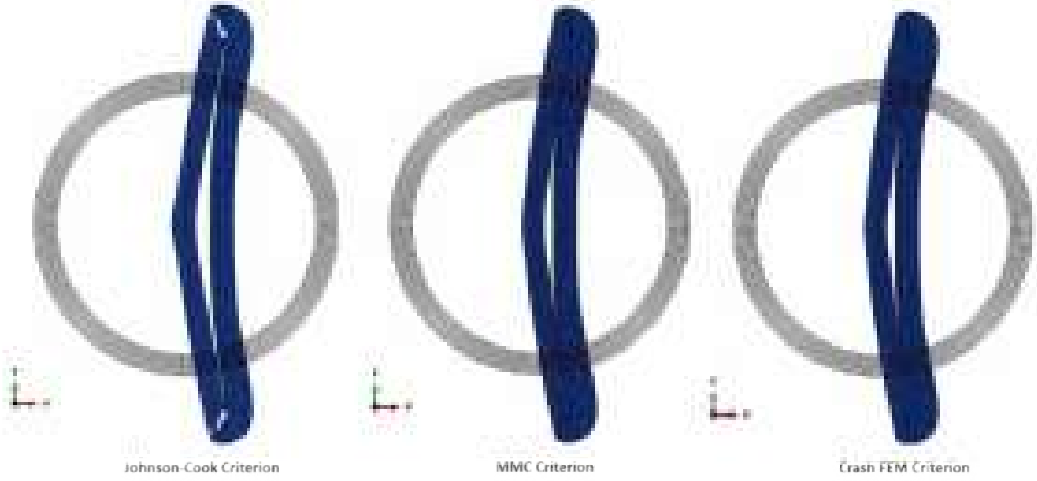

Figure 4.19: Cut off deformation of pipe cross-section after rupture

structure geometry, loading, and boundary conditions are the same for three FE models. It can be observed that the blue line in Figure 4.20 representing the J-C fracture criterion has a much smaller peak value than the others. This peak value also corresponds to a lower BOP ram displacement value, which means that the pipe is easier and faster cut by the same rams when predicted by the present Johnson-Cook fracture criterion. The MMC criterion predicts the largest shear force for the current pipe size and material.

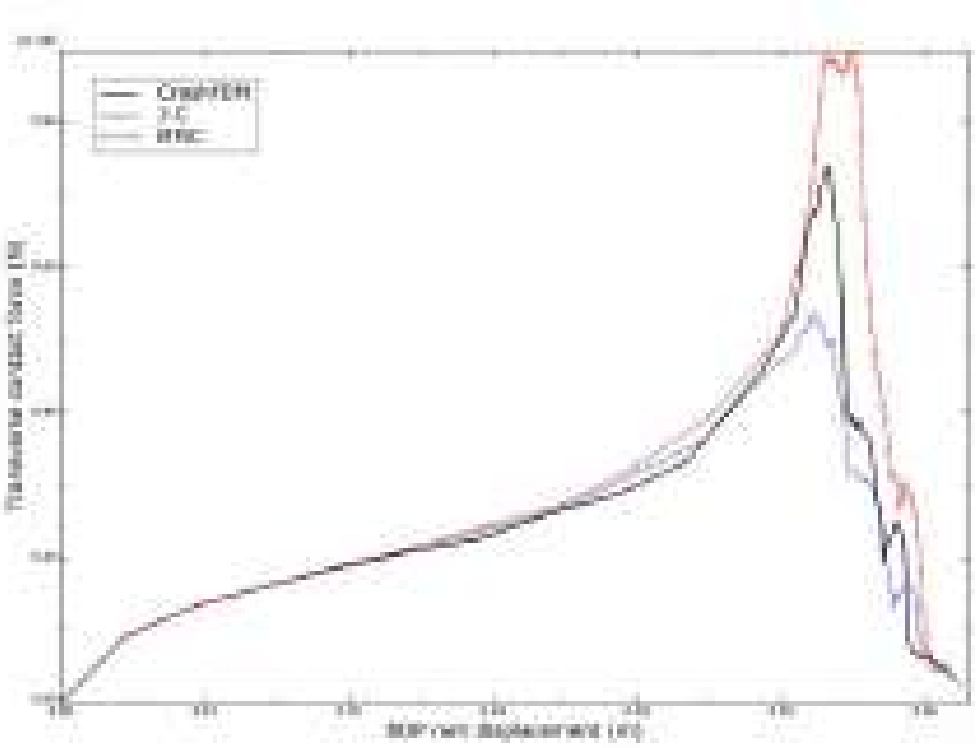

Figure 4.20: Transverse contact force curve concerning ram displacement

Due to the difficulty in obtaining BOP shear test data of TRIP690 material, the experimental data of a close grade AHSS for drill pipe, API E75 grade material, was selected to compare and discuss the accuracy of FE simulation results for different criteria. Figure 4.21 records the experimental shear force data points with an API E-75 grade drill pipe[9], sheared by a Hydril blind shear ram. With the same dimension of the pipe adopted in this chapter, the actual drill pipe shear data shown in Figure 4.21 should provide a closed shearing force with the current simulation results. From those data points, it should be noted that experimental data of each test is not exactly the same. The shearing force in the shear ram test range from 1522.40 to 1766.48 kN, with an average value of 1611.19 kN. The reason may come from the human operation error and imperfections in adjacent locations of the same drill pipe [20]. It can be observed that the simulated result obtained with the MMC

criterion is 1745.2 kN, which is just a little smaller than the upper bound for E75 experimental data, and the shearing force predicted by the CrashFEM criterion is 1519.5 kN, which is very close to the lower bound of the experimental value. The J-C criterion calculates a much smaller shearing force than the experimental value, 1056.3 kN. The difference of predicted shearing force using MMC, CrashFEM, and J-C criteria to average test value is 8.32%, -5.69%, and -34.44%, respectively.

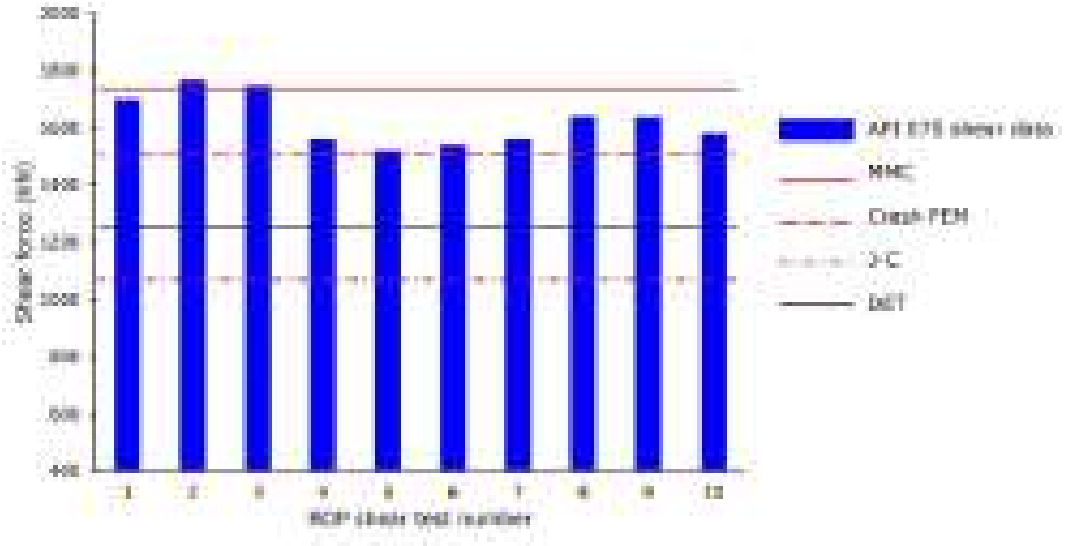

Figure 4.21: Predicted ram shearing force compared with E75 shear ram test data

4.6 Stress and deformation of the shear ram

The above discussions consider that the shear rams are rigid bodies and do not undergo any deformation. Considering that the ram shearing process is a mutual mechanical process, which includes the failure of the drill pipe as well as local plasticity of the ram blades, analysis is also conducted with deformable shear rams. A new FE model is built according to the model described in section 4.2. The only difference is that the shear rams made of 40CrNiMo alloy are included in the simulation. The blade was simulated with J2 flow plasticity theory and isotropic hardening. The material yield stress was considered 960 MPa and the stress-strain curve was used as provided by Han et al. [4, 77]. Considering that fracture occurs after large plastic deformation, the fracture criterion is only applied to the pipe. The shear rams are simulated with C3D8R elements. The mesh size of the ram blade cutting surface is 1.2 × 1.2×3 mm, and the mesh size of pipe elements at the shear section is 2.3×2.3×2.3 mm. Considering that the sharp cutting edge may difficult the contact convergency during the pipe cut, the ram blade cutting edge is rounded with a fillet of 2 mm radius.

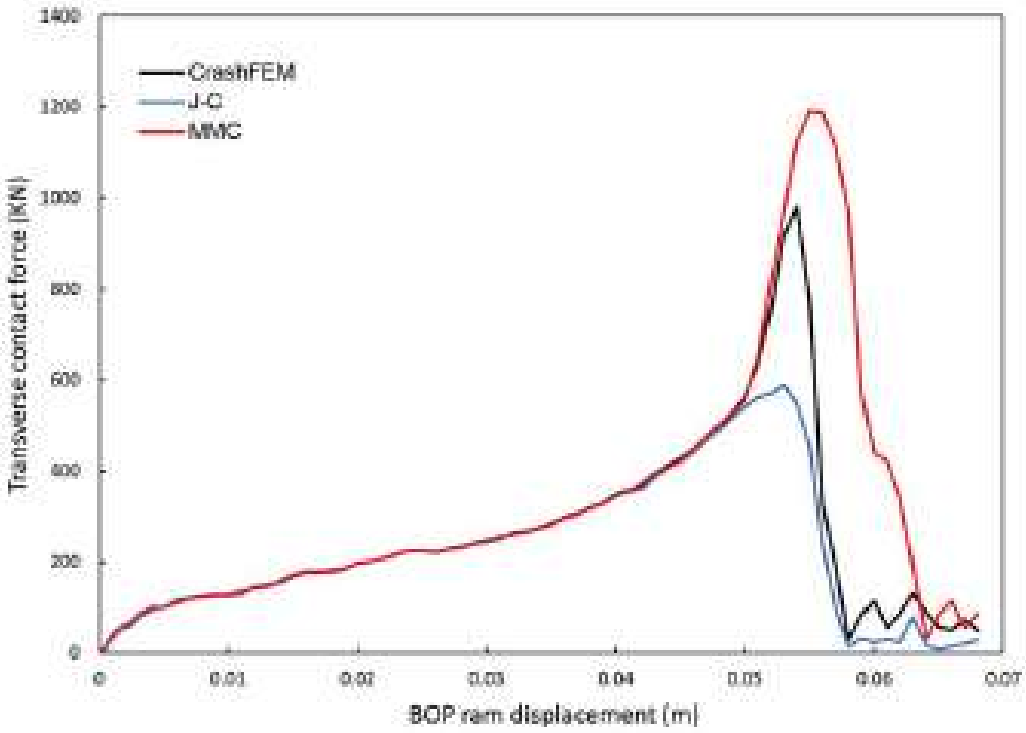

Figure 4.22: Ram shearing force curve simulated with deformable shear ram model

The shearing force curves predicted with the three fracture criteria are plotted in Figure 4.22. It can be seen from the table and the figure that the comparison between maximum shearing force values as well as ram displacements are consistent with the simulation results obtained using rigid rams, as presented in Figure 4.20. The J-C criterion predicts a much smaller peak value than the others, corresponding to a lower BOP ram displacement value.

Figure 4.23 illustrates the Von Mises stress distribution on the shear rams simulated with the three fracture criteria for the pipe material. These stress contours are plotted when the maximum stress is obtained during the shearing process for each shear ram. Simulation with each of the three fracture criteria shows consistent results where the high-stress regions are concentrated at the shearing edge surface, coincident with the pipe contact surface, even though their specific shapes vary. The peak stress value on the upper ram is generally higher than that on the lower ram, with a 3% to 6% difference, depending on the respective fracture criterion. Simulation results for each of the three fracture criteria for the pipe elements predicted that the maximum stress value on the shear rams varies. Besides, the stress distribution length along the ram blade edge reflects the different pipe flatten mode at failure, which also can be attributed to the selection of the fracture criterion. These findings may indicate that the influence of the pipe fracture criterion is consistent with that on the stress responses of shear rams, due to the mutual effect between the ram and

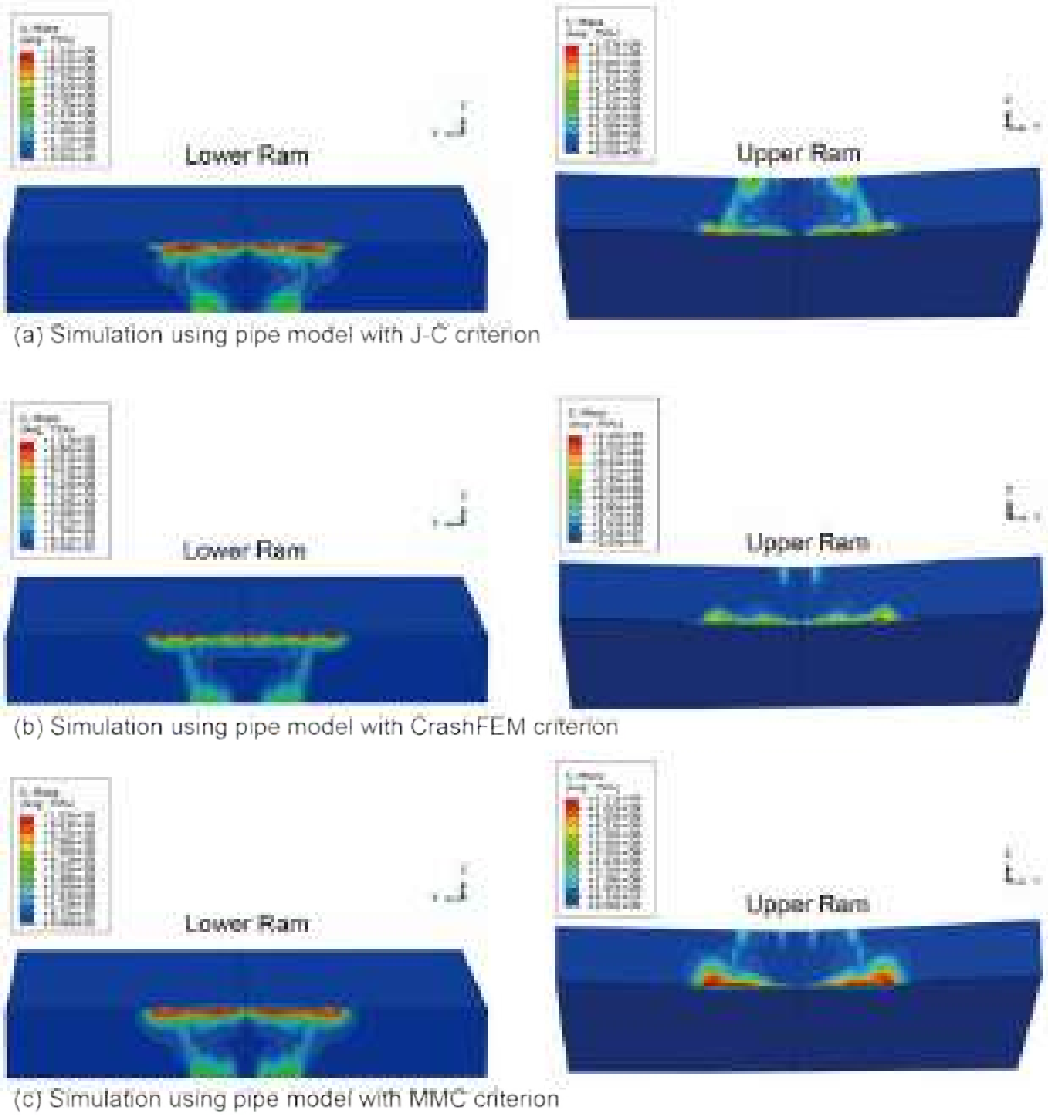

Figure 4.23: Von Mises stress of BOP shear rams simulated with three fracture criteria (in Pa)

the pipe.

Figure 4.24 records the equivalent plastic strain distribution on the shear rams simulated with the three fracture criteria for the pipe material. The maximum equivalent plastic strain values on the upper ram are generally higher than those on the lower ram, with the MMC criterion predicting the highest plastic strain. According to the simulation results, the plastic deformation only occurs in very localized regions along the blade cutting edge.

Simulation results employing three different fracture criteria are summarized in Table 4.4, including the predicted maximum shearing force, the ram displacement at the maximum shearing force, the peak stress value of the shear rams, and the maximum equivalent plastic strain after the pipe separation.

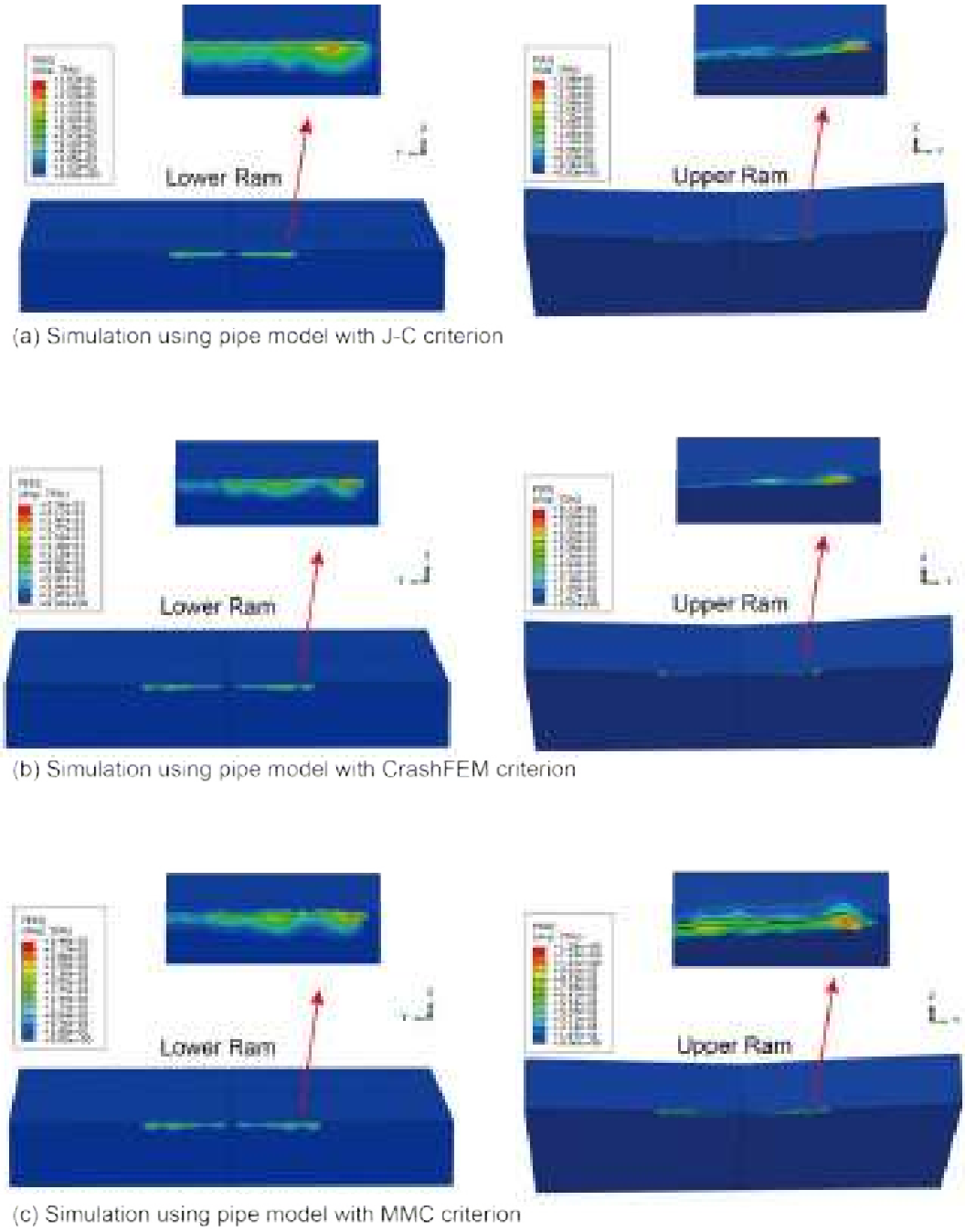

(a) Simulation using pipe model with J-C criterion

(b) Simulation using pipe model with CrashFEM criterion

(c) Simulation using pipe model with MMC criterion

Figure 4.24: Equivalent plastic strain of BOP shear rams simulated with three fracture criteria

4.7 Summary

In this chapter, a comparative study of different fracture criteria for BOP shearing simulation is conducted. A comprehensive derivation process is introduced to obtain CrashFEM fracture parameters from fracture data available in the literature.

The selection of fracture criteria is proved to have an essential influence on the FE model for BOP shearing force prediction. According to the simulation results, the discrepancy of the predicted force value can be attributed to three main aspects.

Table 4.4: Simulation results with the FE model considering the deformation of the shear rams

Fracture criterion	Max. F_{rs} (kN)	Upper ram		Lower ram	
		Max. stress (GPa)	Max. PEEQ	Max. stress (GPa)	Max. PEEQ
J-C	1179.2	1.07	0.398	1.04	0.183
CrashFEM	1958	1.10	0.873	1.07	0.236
MMC	2380.8	1.11	1.28	1.05	0.346

PEEQ: Equivalent plastic strain

First, the differences in the shape of the fracture limit curves reflect the different mathematical aspects of each model. Second, damage initiation is predicted at different time points in the same shearing process, which means that, for the large deformation part of the pipe, stiffness degradation may begin at a different time for the same pipe element. Last, the damage distribution in the shearing area changes according to the specific fracture criterion. These phenomena further affect the stress state of pipe elements in the location close to the ram shearing position, which eventually causes inconsistency in the overall shear force.

It should be noted that modern fracture criteria usually use more than one variable to characterize the stress state, which has been proved as a necessity by many researchers [47, 48]. As for the criteria introduced for BOP shearing simulation in the current thesis, the MMC fracture criterion uses stress triaxiality, and the Lode angle parameter, CrashFEM, relies on stress triaxiality and the shear stress ratio.

Some findings obtained in this chapter can be summarized as follows:

- In the BOP ram shearing process, damage in the fracture area generally accumulates in both negative and positive triaxiality ranges. This entire range should be covered by mechanical tests for the fracture parameters' derivation.
- Both the ductile fracture mechanism and the shear fracture mechanism are reflected in the BOP shearing process; therefore, a fracture criterion considering both mechanisms is recommended, such as the CrashFEM and MMC fracture criteria.
- With the fracture parameters presented in this thesis, the CrashFEM and MMC fracture criteria predict much higher shear force than the Johnson-Cook criterion and provide closer results to API E75 material shear test data

for BOP ram shear force prediction.

- As for the Johnson-Cook criterion, both the fracture limit curve and the predicted BOP shear force indicate less reliable results. The experimental calibration process for Johnson-Cook parameters needs to be further discussed in this specific engineering application.

Chapter 5

A modified fracture parameters derivation approach and verification

As has been discussed in Chapter 3 and Chapter 4, the CrashFEM criterion considering both the ductile fracture mechanism and the shear fracture mechanism reflected in the BOP ram shearing process, it is thus adopted in the current chapter combined with the proposed fracture parameters derivation approach.

This chapter first discusses the influence of material property on shearing force and the difficulty to derive the drill pipe material directly. A modified fracture parameter derivation approach for ram shearing simulation is then proposed. This method aims to obtain practical and reliable fracture parameters for the actual drill pipe shearing application based on AHSS material fracture parameters and drill pipe material tensile test.

5.1 The Influence of material property on shearing force

The fracture criterion selection has been proved to have an influence on the BOP ram shearing force. In this section, the difference in the material property will be discussed. The fracture locus of AHSS material is not commonly provided in the literature and often differ much from one author to another for a similar grade [70–72, 78]. An investigation is conducted to compare the ram shearing force curve of three AHHS materials: TRIP 690, X70, and X100. The MMC criterion is adopted with the respective fracture parameters provided in the literature [79–81]. The same FE model and application approach are employed as in Chapter 4.

The ductile fracture limit curves of X70 and X100, which are required as a mate-

rial input data of the FE model, are plot in Figure 5.1 (a) and 5.1 (b), respectively.

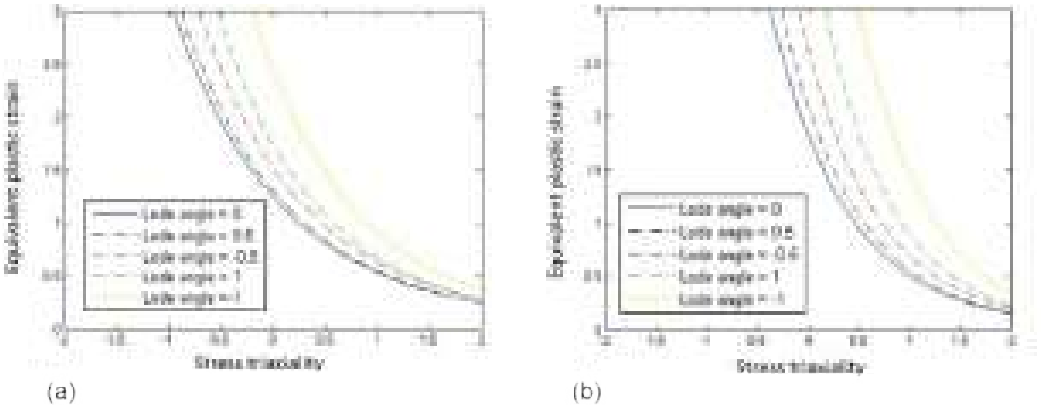

Figure 5.1: The ductile fracture limit curves of X70 (a) and X100 (b)

The ram shearing force curve with respect to ram displacement for these three materials are shown in Figure 5.2. It can be observed that the Shearing force curves of those three materials differ from each other both in shape and peak value. This discrepancy comes from the difference in the fracture limit curve as well as the plastic curve of each material. An interesting observation is that even the yield strength of X100 is almost twice larger than that of TRIP 690, their shearing force peak values are close.

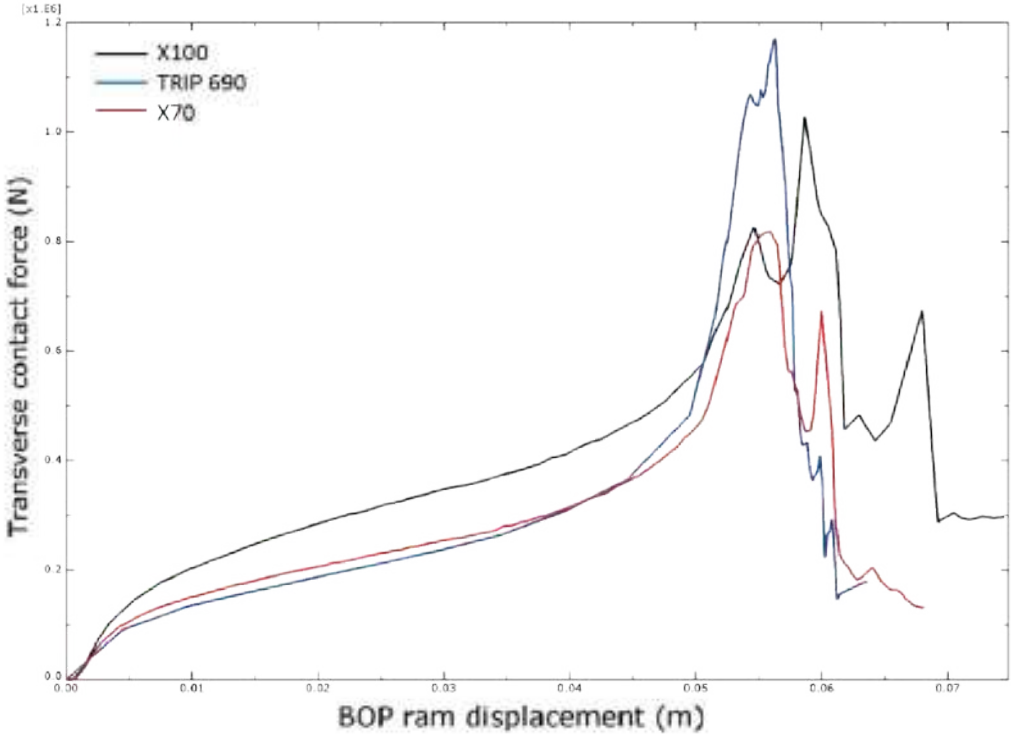

Figure 5.2: Ram shearing force curve with respect to ram displacement for these three materials

From the current comparison and discussions in previous studies, it can be seen that parameters of modern fracture criteria reflect the natural property and microstructure of the material which may not have a simple correlation with the standard mechanical property.

As required, the shear ram is designed to shear any tube inside the BOP when an emergency occurs, which theoretically includes the drill collar, cable, drill pipe body, tool joint an so on. Among those elements, the drill pipe is the most likely to be cut by the ram for its percentage of pipe length in a drill string. During the drilling operation, the drill pipe is generally under extremely high dynamic loading, including the tension, compression, friction, bending moment, torque, axial vibration, and so on. In order to guarantee the safety under such extreme working environments, API has required the drill pipe with high yield and ultimate tensile strength and classified the pipe steel into different grades according to these properties.

As for the pipe material involved in the BOP ram shearing, parameter derivation will become more complicated if the influence of the manufacturing process to actual material properties is considered.

The base metal of the drill pipe body is general Cr-Mo alloy quenched and tempered steel, the specific material differs among steel manufacturers. For example, in the literature, the base metal of drill pipe S135 steel can be 35CrMo, 36CrNiMo4, 26CrMnMo, 26MnMoV, or 42CrMo4 [4, 82–84]. Since the only requirement for the chemical components in the API standard is that the sulfur and phosphorous should be less than 0.03% (with all other elements free), the chemical composition of the base metal for drill pipe also differs from each other [85, 86]. This may induce the ductility discrepancy within the same drill pipe grade.

Modern drill pipe is made from the welding of at least three separate pieces: box tool joint, pin tool joint, and the tube. A complete manufacture process includes several steps including hot rolling, upsetting, heat treatment, quench, and temper to achieve the required dimension and high yield strengths. However, after those complicated process, as each API grade requires the range of mechanical properties, the property and structure of the same grade steel can differ from each other.

As reported by Hayriye et al.[87], the heat treatment process after friction welding was observed to have an influence on microstructure and mechanical properties. The stress relief annealing treatment caused a little decrease in yield strength and ultimate tensile strength but increase in the elongation. The ductility of samples also increased after annealing treatment which is very important for static and dynamic loads. According to the study on 26CrMoNbTiB steel by Jianjun et al.[88], with the raise of tempering temperature and the prolongation of tempering holding time, the strength of the drill pipe material was decreased, and the ductility and toughness increased.

Observing those shear ram test data, it should be noted that the maximum experimental shearing force itself has unelectable inconsistency. Repeated ram shearing experimental data have some inconsistencies, and tensile test data in adjacent locations on the same drill pipe have significant differences in the results [20].

The analysis above demonstrates the difficulty of obtaining fracture parameters of actual drill pipe material. Because drill pipe material varies in mechanical property and chemical composition, it is complicated and often impossible to precisely describe the ductile fracture locus of each drill pipe. The application of ductile fracture or damage criterion in the BOP shearing simulation to meet a high degree of reliability is, therefore, a tougher job, time-consuming, and high cost.

5.2 Correction of ductile damage limit curve for API S135 material

Due to its difficulty in using a series of fracture mechanics experiments to calibrate the fracture locus of a consistent drill pipe section material, this study proposes a practical approach to obtain the material parameters of drill pipe material, which is economical and suitable for large scale engineering applications. A ductile fracture scaling factor C_f, which is determined by the ratio of the measured value and the predicted value of an anchoring point, is proposed as follows.

$$C_f = \frac{\epsilon_f^{dp}}{\epsilon_f^{d0}} \tag{5.1}$$

where $\eta = \eta_0$ identifies the stress triaxiality in a standard tensile test for a smooth round bar specimen or a flat tensile specimen. ϵ_f^{dp} defines the measured equivalent plastic strain at damage initiation in the tensile test of drill pipe material, ϵ_f^{d0} denotes the equivalent plastic strain value predicted by the original damage limit curve of an AHSS material, at $\eta = \eta_0$.

The new ductile limit curve with correction $\bar{\epsilon}_f^D(\eta)$ is then expressed as

$$\bar{\epsilon}_f^D(\eta) = C_f \cdot \bar{\epsilon}_f^d(\eta) \tag{5.2}$$

The approach assumes that the drill pipe materials share a damage initiation curve shape with a similar AHSS material in both ductile damage and shear damage conditions. Two steps are conducted to derive the ductile damage initiation parameters of drill pipe material. The first step is to determine the damage initiation parameters for AHSS material. The curve fitting process to derive damage parameters from fracture experiments is a regression analysis of fracture test data according to the least square error method. Based on these parameters for AHSS,

the second step is to obtain the drill pipe material damage initiation curve using the tensile test data. A new damage initiation curve is attained by applying an overall scaling factor, C_f, into the ductile damage initiation curve for AHSS. The value of C_f is determined by the ratio of the measured value and the predicted value on an anchoring point. The anchoring point on the damage initiation curve is selected according to the stress state of the standard tensile test, which means the damage plastic strain value at uniaxial tension stress state is utilized. The new ductile damage initiation curve with correction is denoted by Equation 5.2. If available, a torsion test or pure shear test of drill pipe material could be used to calibrate the shear damage limit curve in the same way.

Stress state variables such as $\bar{\theta}$ and η in the damage occurrence point during the tensile test can be obtained from the numerical simulation, which follows the inverse method conducted by Bai [55]. The equivalent plastic strain at damage is obtained through analytical formulations, which will be described in the following section.

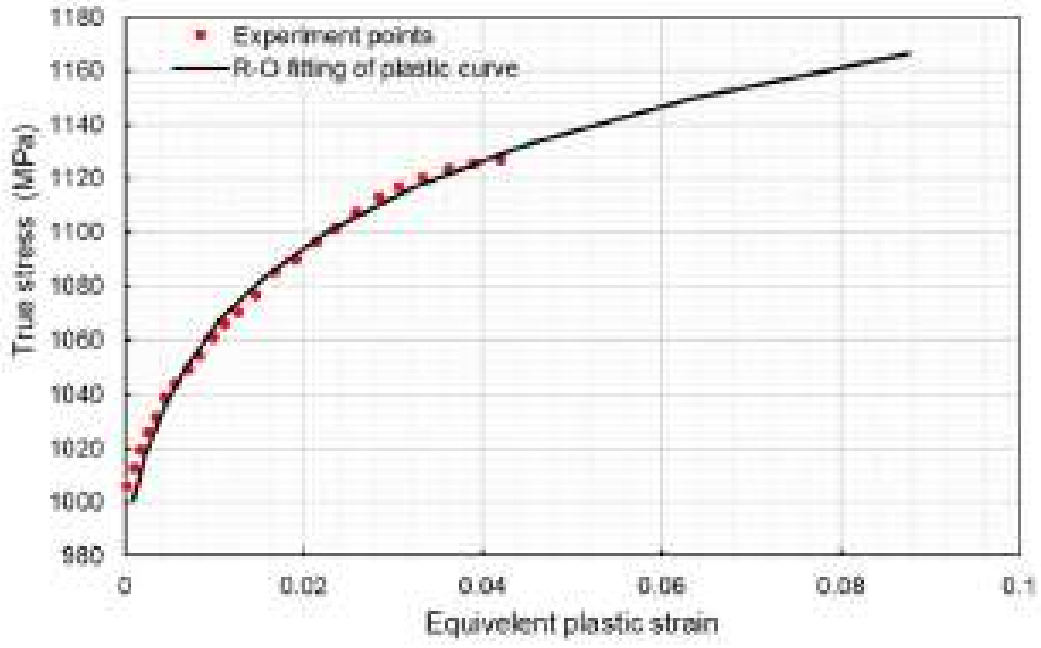

Figure 5.3: Plastic model with Ramber-Osgood fitting for S135 material

A typical S135 tensile test data[85, 89] conducted in the Subsea Technology Laboratory is adopted to obtain the true stress-strain curve. The plasticity behavior of API S135 material up to the point of necking initiation is extracted directly from the experimental data. Due to strain localization, the ultimate strength is reached at the onset of the necking. For the plastic strain beyond the necking point, Ramber-Osgood (R-O) model[90] is employed to obtain the large plastic response. Under the assumptions that the material is homogeneous with isotropy strain-hardening, the respective fit function of R-O fitting curve is

$$\epsilon = \frac{\sigma}{E}\left[1 + 1.336\left(\frac{\sigma}{\sigma_0}\right)^{21.3}\right] \tag{5.3}$$

The deformation on the shear ram blades can be neglected compared with those on the drill pipe section, therefore the rams are taken as rigid bodies. Young modulus and Poisson's ratio of the drill pipe material are assumed to be 200 GPa and 0.3, respectively.

The mechanical property obtained from the tensile test is used to obtain the new damage initiation curve. As denoted by Bai [64], for a smooth round specimen, the uniform equivalent strain at the damage in the necking cross-section can be approximately expressed by

$$\bar{\epsilon}_f = 2ln\left(\frac{a_0}{a_f}\right) \tag{5.4}$$

where a_0 is the original radius of the round bar specimen, and $a_f$is the cross-section radius at damage initiation. By correlating the damage initiation with the fracture of the specimen, the value of $\frac{a_0}{a_f}$ is calculated from the area reduction in the tensile test, which is a typical mechanical property of drill pipe material. Equation 5.4 is also used by other authors to calibrate the material ductile fracture initiation [37, 43].

In the current research, the area reduction for S135 material is 33%, which can be converted to a value of $\frac{a_0}{a_f}$ equals to 1.22, the analytical $\bar{\epsilon}_f$ value of S135 drill pipe material in the tensile test is then obtained according to Equation 5.4, where ϵ_f^{dp} equals to 0.4. As also discussed by Bai [64], the stress triaxiality of the smooth tension bar in a tension test, η_0, equals to 0.4014, and the respective ϵ_f^{d0} value in the ductile damage initiation curve is 0.625. According to Equation 5.1, the overall scaling factor C_f equals 0.64, the new ductile damage initiation curve for S135 material is obtained through Equation 5.2, denoted in Figure 5.4.

5.3 Full-scale ram shearing experiment

5.3.1 Set-up

In the actual Subsea BOP operation in offshore oil and gas exploration activity, the shearing operation is supposed to stop serious accidents, which correspond to complicated loading boundary conditions with oil and gas flow effects. According to API standard [6], the BOP shear ram test is usually conducted before a subsea BOP serves in the offshore oilfield and provides a simple loading condition for tube shearing inside BOP. These tests shall be performed without tension in the pipe and

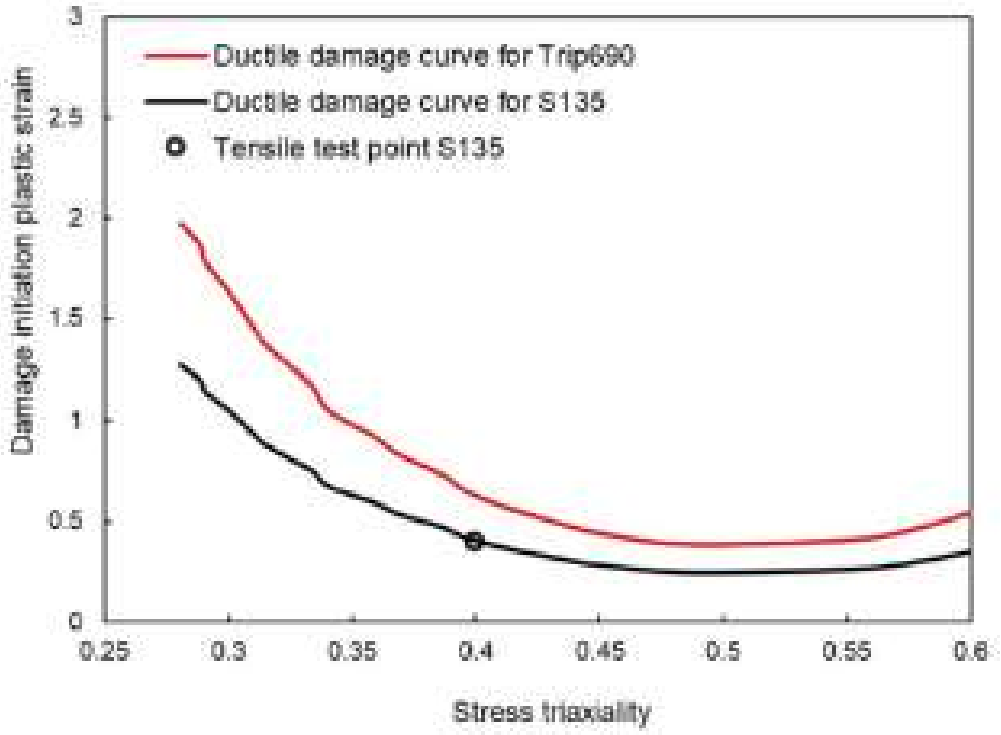

Figure 5.4: The ductile damage initiation curve for Trip690 and S135 material

with zero wellbore pressure.

In this study, a typical ram shear test is performed to investigate the shearing ability of shear ram BOP offered by Rongsheng Machinery Manufacture LTD. This is an onshore BOP rated for wellbore with a diameter of 346 mm and 34.5 MPa well pressure. The hydraulic pressure system is used to move the shear ram for shearing a section of the API 5DP S135 drill pipe body. The maximum pressure provided by the hydrostatic pump is 21 MPa, and the closing area of the ram is 0.088783 m^2. The outer diameter of the drill pipe body is 127mm, the thickness is 9.17 mm, and the total length of each drill pipe section is 3000 mm.

The experimental procedure follows the requirements of the API standard[6]. Figure 5.5 shows the schematic of the experimental equipment set-up. The drill pipe is suspended vertically by a hose facility and then lowered into the BOP bore to a proper position. The drill pipe section is centralized manually in the BOP bore under non-flowing well conditions. The BOP operating chamber is connected to the hydraulic pressure control system, which is activated through the control panel. To conduct the shear ram test, the hydraulic pressure in the BOP operating chamber is increased, so that the ram blades are pushed towards each other, flatten the drill pipe section until the drill pipe is totally cut off. An electronic recording system, including a pressure sensor, is used to record the hydraulic pressure at which the

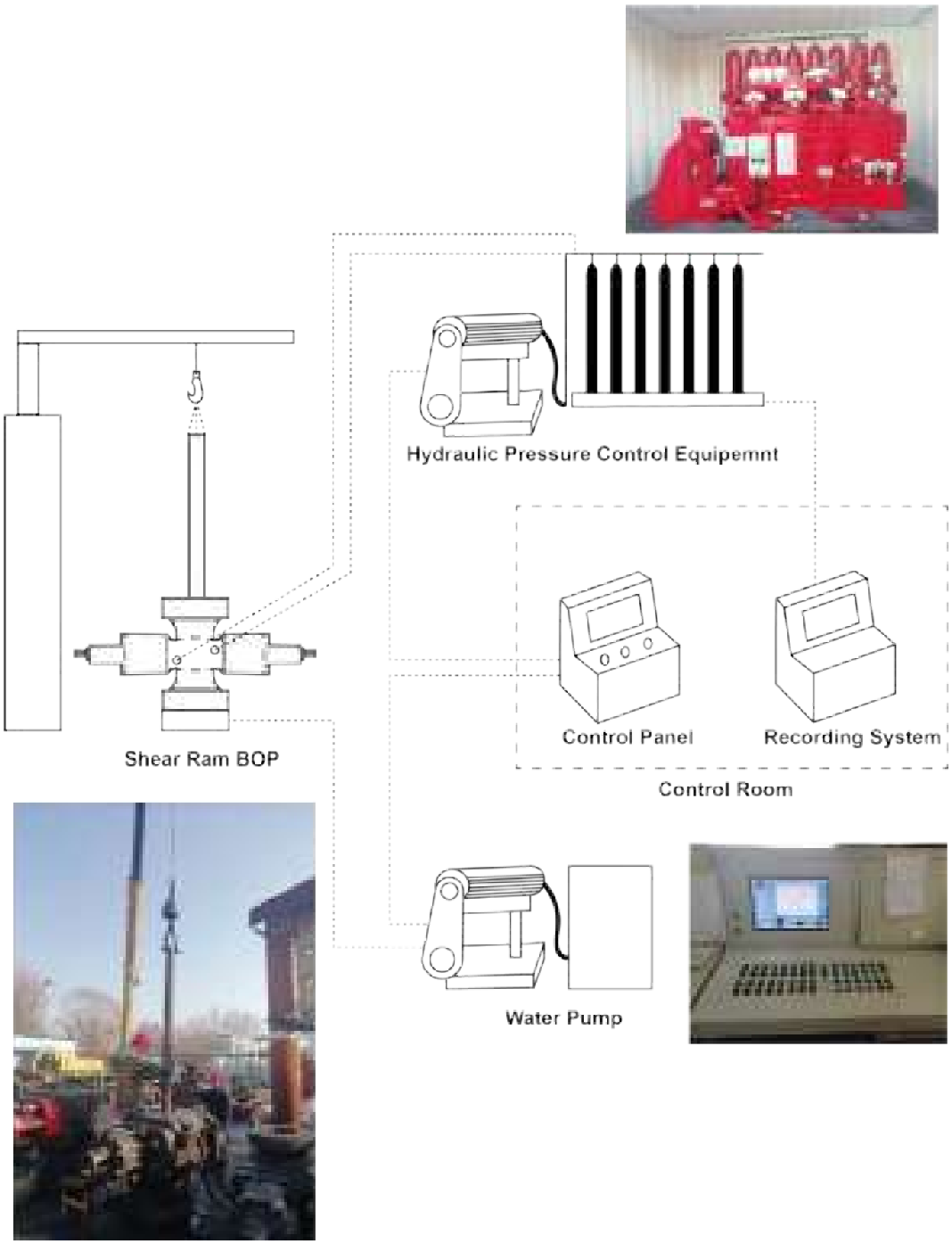

Figure 5.5: Schematic image for BOP shear ram test configuration

pipe is sheared.

5.3.2 Experimental results

The shearing experimental test takes about 1 minute, including 10 seconds from the drill pipe contact ram blades until the total rupture. Observing from the recording system, the hydraulic pressure first increases until the maximum value, generally

consistent with the time period after which the drill is cut off. Then, the pressure decreases quickly to a small value. After making sure the drill pipe is totally separated, the experiment is stopped. During this shearing process, the maximum oil pressure to cut the S135 drill pipes is 12.7 MPa. The shearing pressure curve will be further discussed together with the numerical simulation results in the following section.

Figure 5.6: Shear morphology of the drill pipe section. (a) upper and lower fish in top view, (b) upper fish in close up view

The drill pipe body shear morphology of S135 drill pipe is shown in Figure 5.6(a), large plastic deformation close to the ram contact area was observed. The cross-section of the sheared drill pipe upper fish is shown in Figure 5.6(b). It can be seen that the cross-section is flattened after the shearing process, the final shape generally follows the "double V" ram blade shape. As denoted in the figure, similar to typical punch and die process morphology, the shear cross-section is separated by several zones due to different fracture mechanics. The invade zone marks the location where the ram blade first penetrates the drill pipe material. The burr zones remain on the fracture surface after the shearing process, indicating that, before the total

separation, material in respective the zones experiences severe tearing process.

5.4 The BOP shearing numerical model

To verify the material model built in this chapter, a numerical model based on the full-scale ram shearing experiment is required. The ram blades geometry is provided by Rongsheng Inc. and adopted in the present model as well as other dimensional parameters extracted from the shearing experiment, as shown in Figure 5.7 (a). The relative position of the ram blades and the drill pipe is set-up according to the experiment. It should be mentioned that the ram body, including sealing elements, shows no effect on the shearing force, and only the upper and lower ram blades are simulated in the modeling.

5.4.1 Loading and boundary condition

The FE model is built with the following assumptions: the pipe is supposed to be fixed in the central position of BOP rams during all the shearing process. The ram velocity is constant during the shear process, the shear behavior is simulated as a quasi-static load condition, where the inertia of rams is not an influencing factor. As illustrated in Figure 5.7 (b), the constant velocity of the rams towards each other along the axis x is applied. Due to symmetry, only half of the pipe needs to be analyzed. The coupling option is applied on the top surface of the drill pipe, through which the over-constrained problem can be avoided. Automatically generated kinematic coupling equations are used to link the degrees of freedom of the surface nodes to the reference point. All of the six degrees of freedom on the reference point are fixed. The lower end of the drill pipe is free.

To obtain computational efficiency, the initial distance between the ram and the pipe is set to be infinitely small. Load rate acceleration and mass-scaling are also utilized, the total energy of the whole model is monitored to make sure the model's accuracy.

5.4.2 Element type and mesh

Simular with the model in Chapter 4, the C3D8R elements are selected to simulate the deformation and rupture of the drill pipe, R3D4 elements are used to simulate the movement of the rams. Only the pipe elements that are close to the ram blade contact area experience large plastic deformation and damage evolution. This critical region is denoted by a red rectangle in Figure 5.8. Considering several layers of elements in the middle of the critical part may be severely distorted even deleted during the ram shearing process, these layers need a very fine mesh size. By keeping

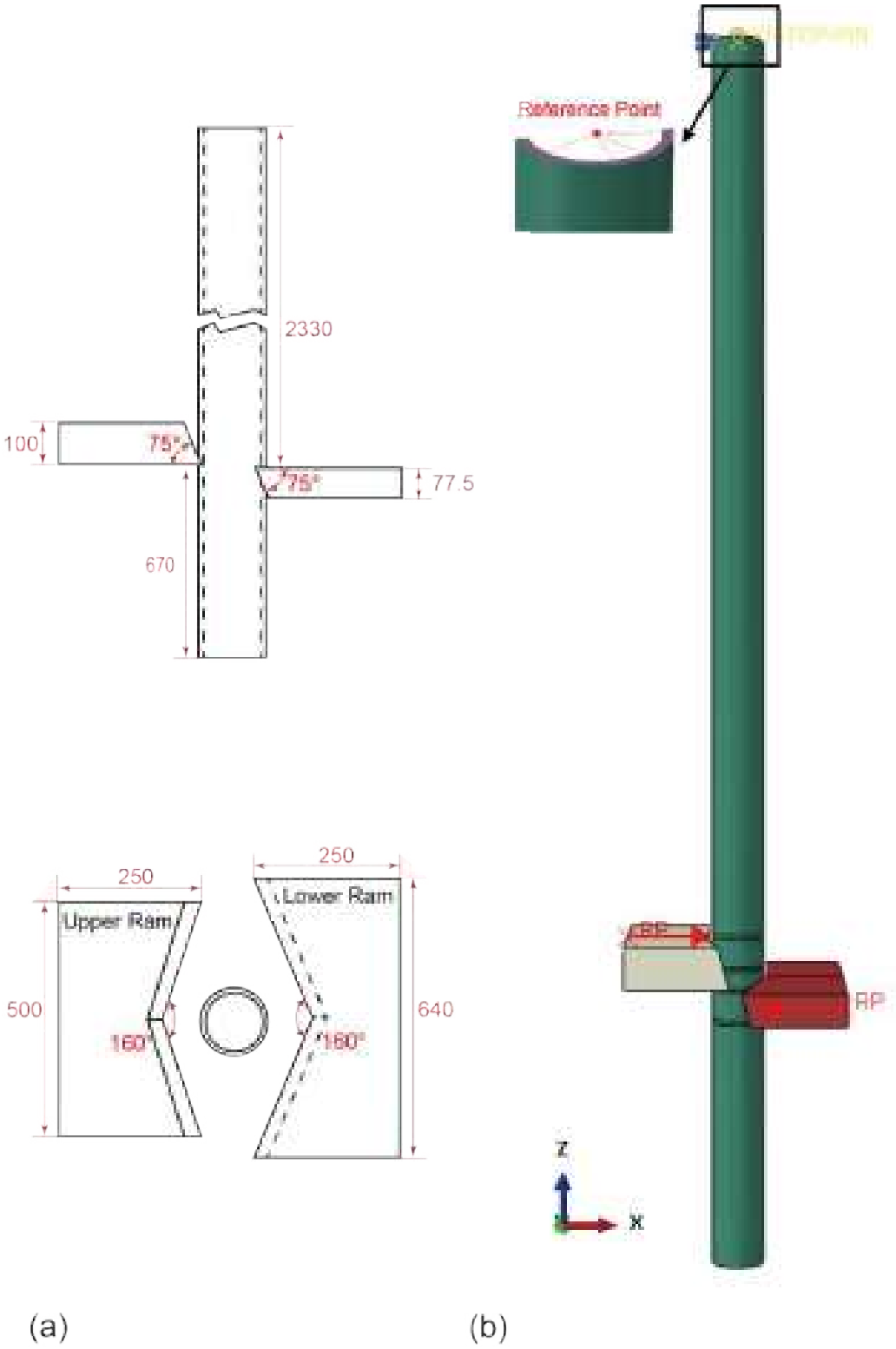

Figure 5.7: (a) Geometrical dimensions of drill pipe and BOP rams (in mm), (b) loading and boundary conditions of the ram shearing model

the other elements with a constant mesh, the element mesh of those middle layers is refined until the values of the shearing pressure are stable. A unit aspect ratio is designed for each part of the pipe element. Between the mesh regions, some transi-

tion layers are also required to obtain a continuous mesh design for the whole pipe. The final length and mesh size of the fine mesh region is shown in Figure 5.8. As discussed in Chapter 4, the converged mesh size for the ram contact regions is 0.78 mm (the number of elements through pipe thickness is 12). This mesh solution is adopted for all numerical simulations in this study.

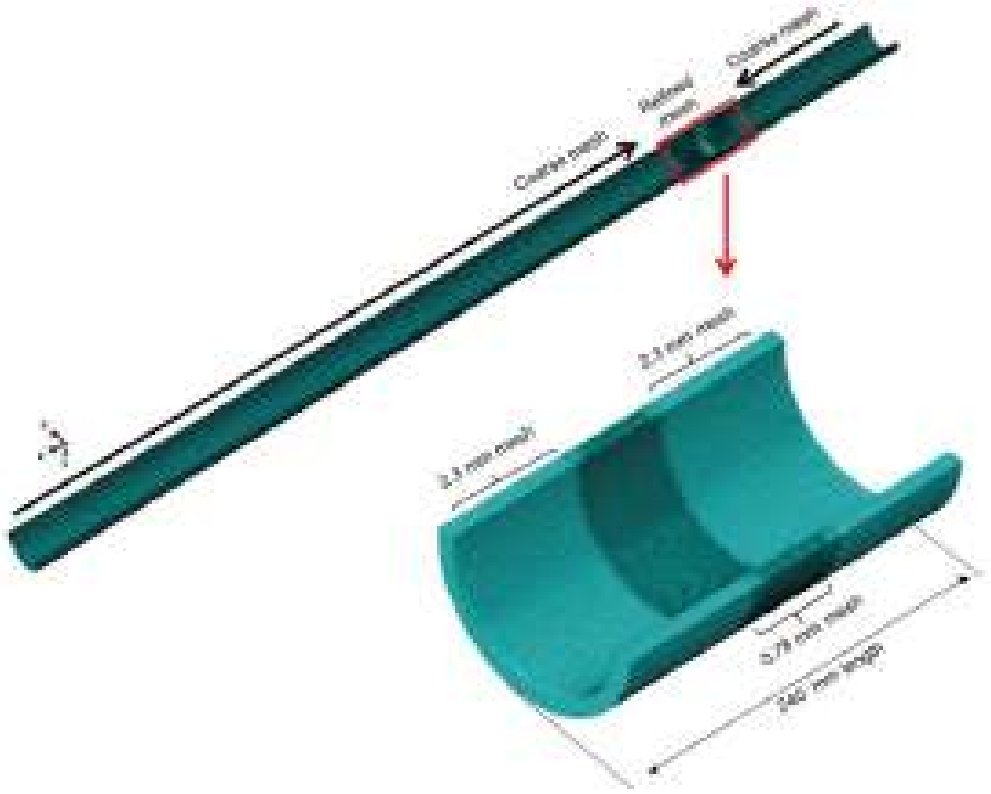

Figure 5.8: Gradual refinement of meshes with a unit aspect ratio

5.5 Simulation results

In this section, the numerical models are carried out using the finite element code ABAQUS/Explicit [74]. Some simulation results are discussed in the context of the analysis of the ram shearing process.

5.5.1 Shearing process analysis

In the numerical simulation, the initial distance between the rams and the pipe surface is 1 mm, while the clearance between the upper and lower rams is infinitely small. The rams move towards each other with a constant velocity, the response of the rams begins when parts of the ram blade first touch the pipe surface. The concept of a shearing force or shearing pressure is commonly used to describe the

force response during the ram shearing process in previous studies. Assuming a similar approach, a typical shearing pressure-time curve is plotted in Figure 5.9 (a). The curve is calculated by the numerical model described above, assuming the plastic hardening model of S135 drill pipe material and the damage initiation model corrected by S135 tensile test data. As shown in the figure, from the rams' initial contact to the pipe surface, the shearing pressure first increases to a peak value, and then, suddenly, drops to a very small value. A residual pressure may remain due to the continuous bending and the friction of the drill pipe fish. Five typical points on the curve are selected and denoted by red points in Figure 5.9 (a), while the respective stress distribution and pipe deformation combined with the relative position of the shear rams are indicated in Figure 5.9 (b).

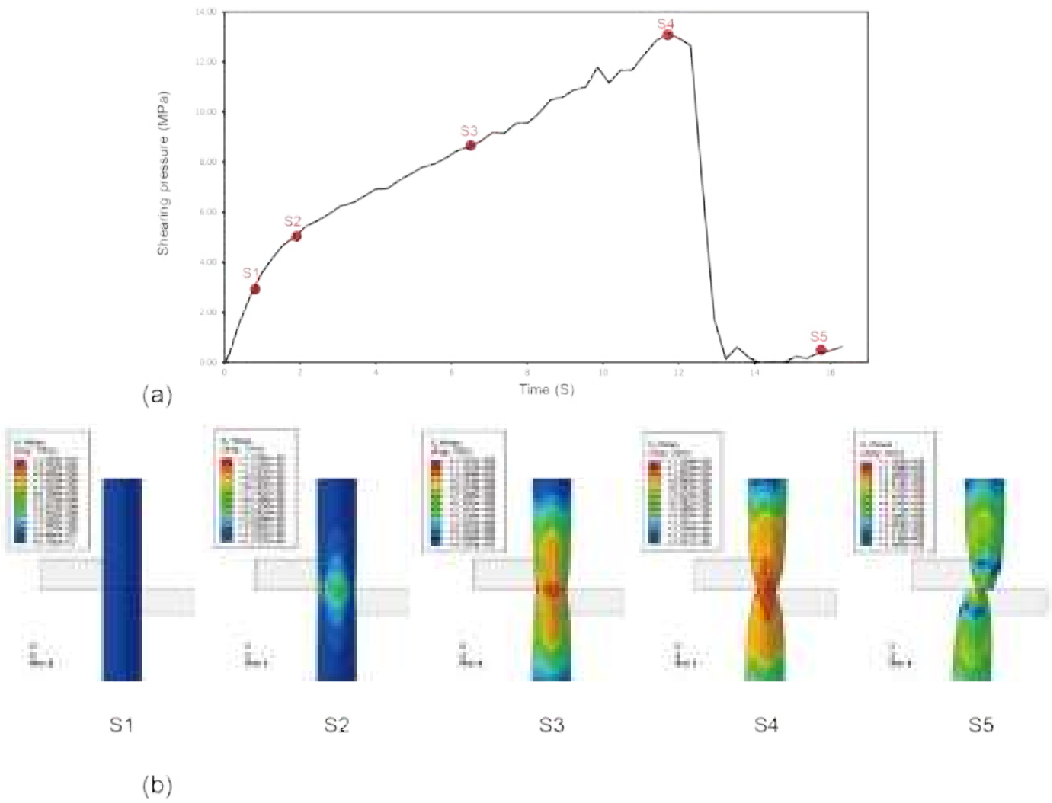

Figure 5.9: (a) Simulated shearing pressure-time curve using modified ductile damage criterion and shear damage criterion, (b) stress distribution and deformation for the pipe along the time

The details of the stress distribution along the time are described below:

- At S1, the high stress is only concentrated at the contact point, the transverse reaction force of the rams increases significantly at this stage.
- At S2, the ram begins to squeeze the pipe slightly at the contact point, and the overall deformation of the pipe is small. On the pipe surface, the range of

high-stress distribution is gradually increasing on the XZ plane, but the peak stress still happens only in the contact zone. The slope of the shear pressure decreases.

- At S3, the squeeze deformation of the pipe is further increased, and the entire pipe flattens, necking at the contact region. At this time, the high-stress region not only extends in the axial direction but also in the y-axis direction (transversal to the shear direction).
- At S4, the pipe has the largest extrusion deformation, with accentuated necking. At the shear zone, the entire circumferential direction on the pipe surface is in a high-stress region because the contact pattern becomes line-to-surface contact around the flattened pipe body. The corresponding shearing pressure also reaches a peak value. After this point, the reaction force drops sharply until the pipe was completely separated.
- At S5, the cutting process has finished, the pipe has been completely separated. At this time, the contact of the fracture cross-section of the upper and lower pipes may cause some stress concentration regions. As the rams continue to move forward, the upper pipe will bend and the lower pipe will fall due to gravity, so the average force of the rams may continue to rise. The residual pressure varies from case to case, but this does not affect the shear pressure to be considered in the analysis.

It can be seen that the slope of the curve before it drops can be generally classified into two stages. An alternative explanation is that the first slope corresponds to the elastic response of the drill pipe material, whereas the second one is more affected by the plastic response of the pipe material. This inference is consistent with the deformation characteristics of the corresponding stage in Figure 5.9 (b), as well as the analysis in previous studies [4, 42].

5.5.2 Shearing pressure curve comparison

To validate the FE model, the transverse reaction force-time curves are compared with the experimental hydraulic pressure curve. The reaction force is converted into pressure through Equation 2.4. The simulated shearing pressure curves are differentiated by damage parameter selections. One point that needs to be mentioned is that the quasi-static simulation does not focus on the actual time for cutting, thus the time-related discussion such as "which scenario denotes an earlier cut of the drill pipe" is out of the scope in the current study. The recorded time points of the experiment are plotted in Figure 5.10, whereas the time of the simulation is indicated to obtain the same rupture time point as the experiment.

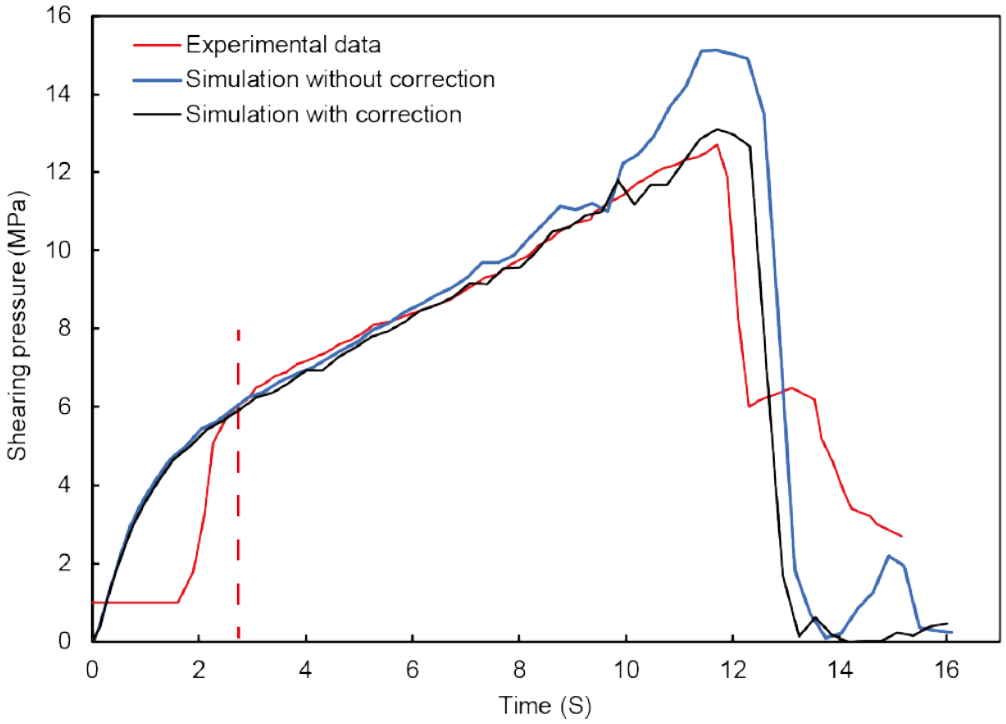

Figure 5.10: Equivalent plastic strain of BOP shear rams simulated with three fracture criteria

The experimental and simulated shearing pressure-time curves are plotted in Figure 5.10. The solid red line corresponds to the experimental curve, the blue and black lines denote the simulated curves. Specifically, the blue line denotes the simulation result with the damage initiation criteria derived from the original TRIP 690 material data, whereas the black line represents the damage initiation criteria with correction according to the S135 tensile test data. The experimental curve is read from the recorder in the whole process of the shear ram test. For the numerical simulation, the magnitude of the transverse reaction force on the two rams are not exactly the same, therefore an average value is calculated to compare with the experimental results.

As shown in Figure 5.10, the experimental curve begins from the initial value of hydraulic pressure. This is set-up manually in order to obtain the initial contact between the drill pipe and ram blades, and make sure the drill pipe is centered in the BOP wellbore. The simulated curve begins from the initial contact point and the reaction pressure increases from zero. After the time denoted by the dotted red line, the pipe element in the shear zone has a plastic response, the experimental and numerical curves become comparable. General consistency is obtained in this stage until the necking stage. Then, one can easily indicate that the black line is still consistent with the experimental curve, whereas the magnitude of shearing

pressure on the blue line is far beyond the experimental results. An important estimation method for the required shearing pressure is to extract the peak value of the pressure-time curve. Table 5.1 indicates the peak values for both simulated and experimental pressure-time curves. The discrepancy of the simulated value in relation to the experimental value is also denoted.

Table 5.1: Comparison of the maximum shearing pressure value

	Peak pressure values (MPa)	Dc (%)
Experiment	12.7	
Simulation without correction	15.12	19.7
Simulation with correction	13.11	3.2

Dc (%): The discrepancy of the simulated value with the experimental value for the respective material

From the simulation results of the S135 drill pipe material, it can be seen that the shear pressure curve basically maintains a constant slope during the second stage of the simulation with the modified damage initiation, and the peak value is effectively reduced. The modified damage initiation curve helps the shear pressure curve to obtain more consistency with the shape of the experimental curves in the post elastic region. An approximately linear curve develops until the peak appears, and it suddenly drops to a small residual pressure value. Compared with the experimental curve, the simulated pressure-time curve for S135 material shows that the correction method has obtained good accuracy in this shear ram test simulation, and the maximum shearing pressure error is only 3.2%.

5.5.3 Fracture cross-section comparison

Another effective verification method is to compare the dimensions of the pipe cross-section deformation due to the ram shearing process. As shown in Figure 5.11, the pipe cross-section after the separation in the numerical simulation with the modified damage initiation curve is compared with the experimental result of the S135 drill pipe. Table 5.2 indicates these dimensions in the experiment and numerical simulation. The largest discrepancy is 4.8%, which is acceptable considering the pipe size.

One can figure out that the upper and lower cross-sections do not perfectly match, the short axis diameter of the lower fish cross-section is large than that of the upper fish. This phenomenon may come from the post-shearing effect. The

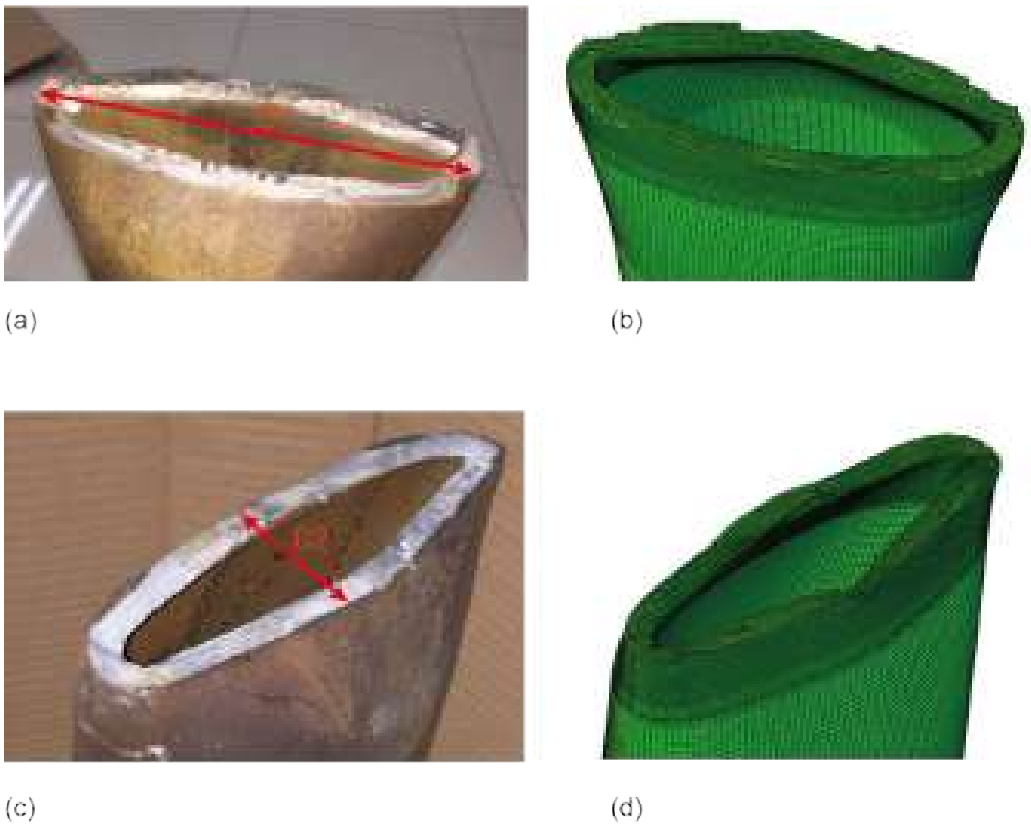

Figure 5.11: Cut off deformation after pipe separation.
(a) the upper fish cross-section in the experiment, (b) the upper fish cross-section in the numerical simulation, (c) the lower fish cross-section in the experiment, (d) the lower fish cross-section in the numerical simulation.

upper fish is further extruded by the ram blades after the shearing process, whereas the lower fish fall off by the effect of gravity.

Table 5.2: Comparison of shear cross-section dimensions

	Upper fish cross-section		Lower fish cross-section	
	D1 (mm)	D2 (mm)	D1 (mm)	D2 (mm)
Experiment	172	56	171.5	60
Simulation	170.76	56.77	169.66	57.14
Difference (%)	0.7	1.4	1.1	4.8

D1: Long-axis diameter; D2: Short-axis diameter.

5.5.4 Damage analysis of drill pipe

Based on the discussion of the pressure-time curve and the stress distribution, the damage evolution on the drill pipe during the shearing process is further investigated. As damage only initiates after large accumulated plastic deformation, five specific time points from initial necking up until complete fracture are selected to represent the full damage accumulation process. The movement direction of the upper ram is the basic reference direction. Figure 5.12 (a), (b), and (c) represent the front, back, and side views, respectively. Besides, Figure 5.12 (a) and (b) indicate the damage initiation and progress due to the motion of upper and lower ram blades, respectively. Figure 5.12 (c) represents the damage for those elements on the buckled surface. As both ductile and shear damages are taken into account in the present analysis, the vertical axis denotes the maximum damage initiation value. It can be found that at the time of 6.2 s, the damage value just initiates from zero, while the necking of the pipe already occurs. The large red area, which denotes damage value equals 1, only appeared after 13.2 s. In Figure 5.12 (a) and (b), the damage area in the ram contact zone is in the semi-oval shape, the direction of the oval line corresponds to the thickness direction of the ram blade. With further shearing by ram blades, the evolution of the damage area follows the Y axis towards both positive and negative directions. As shown in Figure 5.12 (c), the area of damage on the pipe surface in the side view first occurs as an oval shape, then extends in the Z-axis direction. More severe damages are observed after the pipe is squeezed flat enough that both ram blades contact the full edge of the cross-section.

As explained above, in the fracture region, elements experience elastic deformation, plastic deformation, and stiffness degradation due to the damage accumulation in the ram shearing process. Once the damage value arrives 1, the stiffness of the element begins to degrade according to the damage evolution law. The deletion of the elements can simulate the generation and propagation of macro-cracks. After the pipe is squeezed to the maximum extent, the damage accumulation in the contact area of the ram blade causes some elements to be deleted. These deleted elements compose an initial linear crack. At the time of 14.2 s, the cracks spread towards the pipe circumferential direction; vertical misalignment occurred on the pipe surface in the side view. The cracks are fully connected along the circumferential direction when T = 14.5 s, the pipe is divided into connected parts, and the shearing process is completed.

Observing the crack initiation and progression caused by the two ram blades, the crack size formed by the upper ram is larger, the progression process is also completed earlier. According to this simulation results, cracks close to the upper ram blade were formed before the lower ram, which causes the elements in the lower

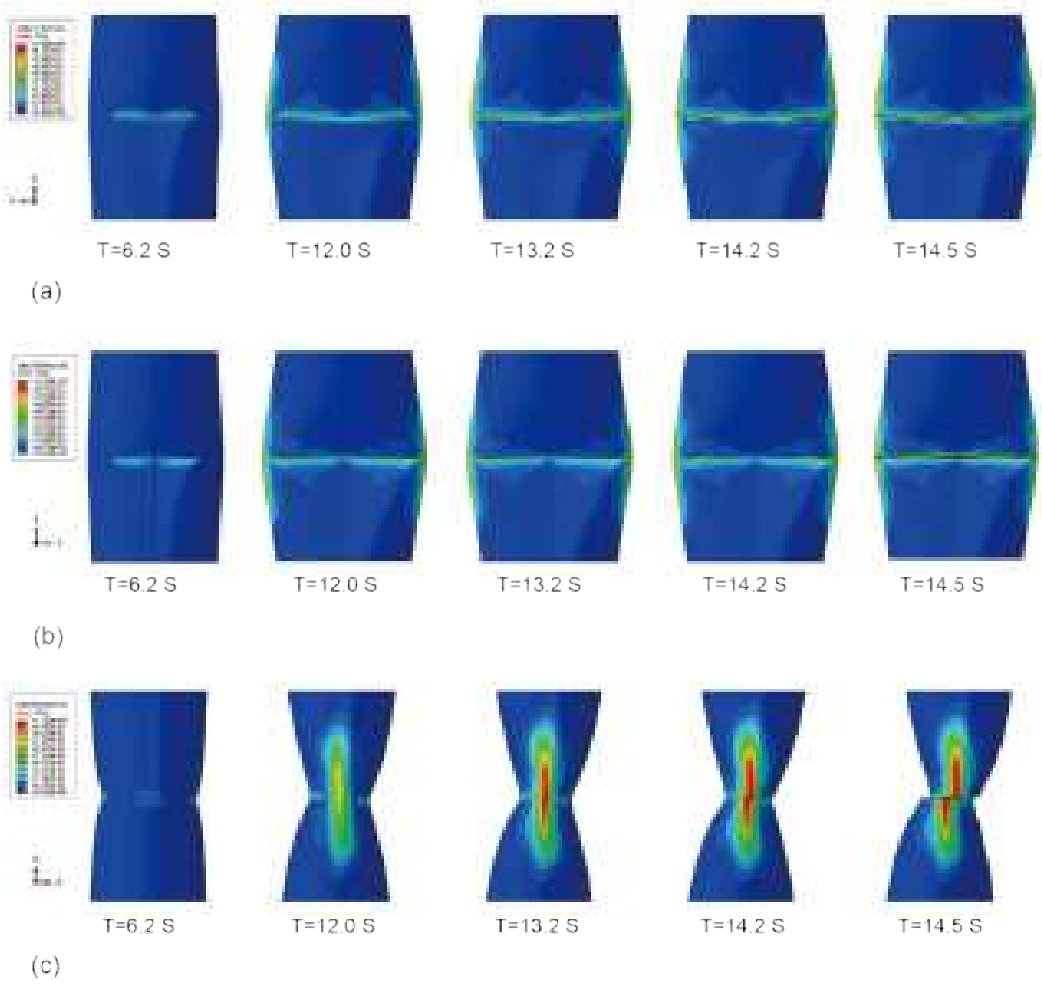

Figure 5.12: The maximum value of damage variable corresponding time and pipe deformation in (a) front view, (b) back view, (c) side view.

ram contact area to experience more tensile effects before separation. Thus, the burrs are more likely to form in this lower ram contact area. This is obvious on the fracture surface of S135 drill pipe material observed in the shearing experiment, as shown in Figure 5.6.

Damage analysis can not only help to understand the macro crack process but also capture the damage on the pipe surface during the ram extrusion process. The side-view snapshot in Chuanjun's experiment shows a very similar damage area to the results of the current simulation during the ram extrusion, as shown in Figure 5.13.

5.6 Summary

This chapter presented an experimental and numerical investigation of the ram shearing process. The experimental work follows the standard API shear ram test

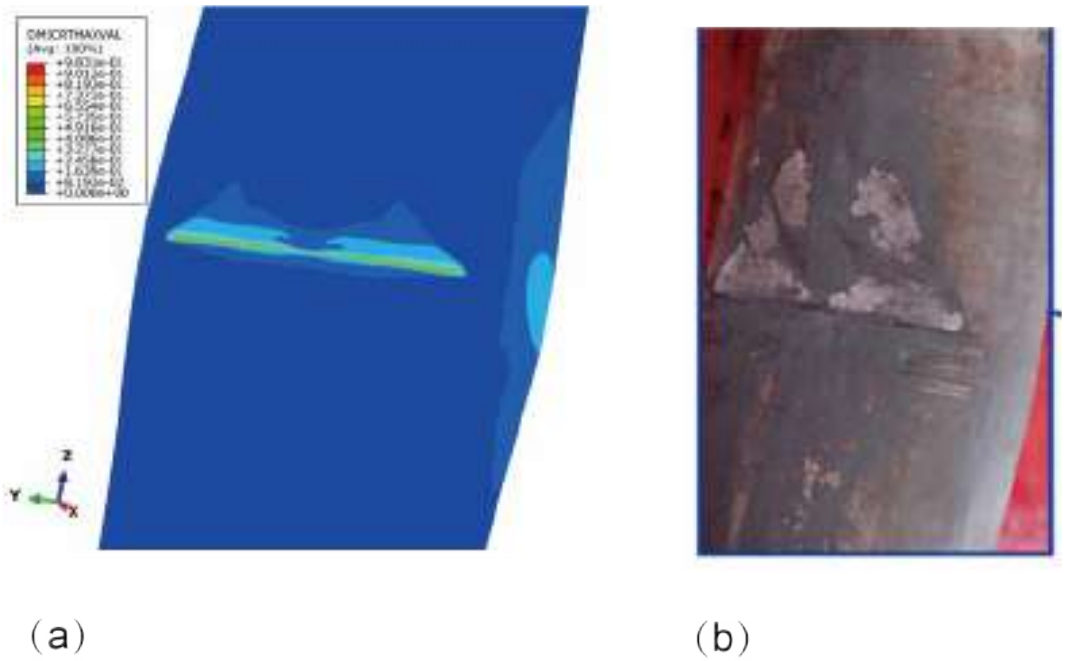

Figure 5.13: Damage on the pipe surface during the ram extrusion process

requirement, an S135 drill pipe is sheared successfully. The experimental pressure-time curve is recorded, and the peak value of the hydraulic pressure indicates the required shearing pressure to cut the pipe. A nonlinear FE model is set-up according to the ram blades dimensions and the boundary and loading conditions from the experiment. A standard tensile test data of S135 drill pipe material is utilized to obtain large plastic response. To simulate the BOP shearing process and predict the failure of the drill pipe, the ductile and shear damage criteria are employed.

The FE model is verified by a full-scale BOP ram shearing experiment by comparing the experimental shearing pressure-time curve with the simulated transverse reaction force curve. The dimension of the sheared drill pipe cross-section is also compared with the simulation result. According to the simulation result, the stress distribution, damage evolution, and macro crack propagation on the pipe during the ram shearing process are analyzed.

Chapter 6

Shear efficiency study of ram blade

As the modified fracture parameters derivation approach verified by a full-scale ram shearing experiment is provided in Chapter 5, a case study is conducted in the current chapter to demonstrate the application of the proposed FE model combined with the experiment-based fracture criterion. As demonstrates in Chapter 4, the MMC fracture criterion considers both stress triaxiality and the lode angle effect on fracture locus. The material model of TRIP 690 is adopted in the current chapter, due to the theoretical and experimental basis and complete fracture parameter verification process conducted by previous studies.

6.1 Shear efficiency correlated with ram designation

As it was concluded in the DNV report, "The inability of the BSRs to shear the off-center drill pipe contributed to the BSRs being unable to close and seal the well". After the Macondo accident, the ability of the shear rams to cut tubular successfully is of great interest to both the industry.

In the U.S., new regulations have mandated verification requirements including the shear ability of the BOP system via a proposed Safety and Environmental Management System (SEMS) program [91]. These new requirements have provided a way to identify unknown deficiencies and also encourage BOP manufacturers to increase the reliability of the BOP system. Among others, optimizing ram blade shapes in order to increase the shearing efficiency of ram blade is included in their effort.

The challenges for the conventional V-shaped ram blade identified in the previous study (assuming the width of ram covers the entire wellbore diameter) can be summarized as:

- The high required shearing force for thick and broader pipe limits the reliability

of shearing operation

- Shearing force value is strongly influenced by ductility of the pipe material which can not be fully reflected by conventional mechanical property
- The dubious centralization capability may induce the failure of the shearing and sealing operation

Based on the various shearing tests, Springett et.al claim to identify the optimum ram design of Low Force Shear (LFS) from 22 different design concepts. [14] They discuss the advantage of Low Force Shear ram of National Oil Varco (NOV) over the conventional ones based in the philosophy of final shear area reduction. The author believes that getting more of the cross-sectional area cut prior to the final rupture reduces the required shearing force. Significant improvements are reported to be obtained in shearing thin-wall drill pipes. For thick pipe, LFS roughly decreases 50% of the required shearing force of conventional V-shaped ram.

In 2014, a curved shearing blades ram designation is investigated in the study of Tulimilli et al. [16]. Based on their numerical simulated results, when the pipe is set in the center of the wellbore, the peak value of the shearing force in the ram shearing process is 27% lower than that shear by a conventional blind shear ram. The authors believe the higher contact area between the ram blade and the pipe surface helps to decrease the required shearing force. In 2015, Horstketter [29] reported that the NOV Shear All Ram with higher shearing efficiency helped the operator to complete drilling natural gas storage wells in the Netherlands. Their ram designation shares some dimensional features with the one investigated in the study of Tulimilli. The filed tests for this new ram designation include a successful shearing operation to cut a 298.5 mm OD, 65 lb/ft P-10 casing pipe in a 346mm OD wellbore. As for drill pipes with a diameter of 127 mm or larger, the Shear All Ram is reported to obtain 28% to 64% less shearing force than that predicted for conventional shear rams.

In this chapter, a case study is conducted to investigate the shearing efficiency of three ram blades by comparing the required shearing force to cut a TRIP 690 pipe. The study also demonstrates the application of the MMC criterion to BOP shearing simulation.

6.2 FE model

Base on the geometry of rams in the basic model in Figure 6.1, two modified blade edge shapes are proposed and compared with conventional double V-shaped ram. Thus, a total of three ram designs are investigated in this section, namely ram design 1, ram design 2, and ram design 3 illustrated in Figure 6.2. Their geometries are supposed to reflect some of the key features of OEM's latest shear ram dimensions.

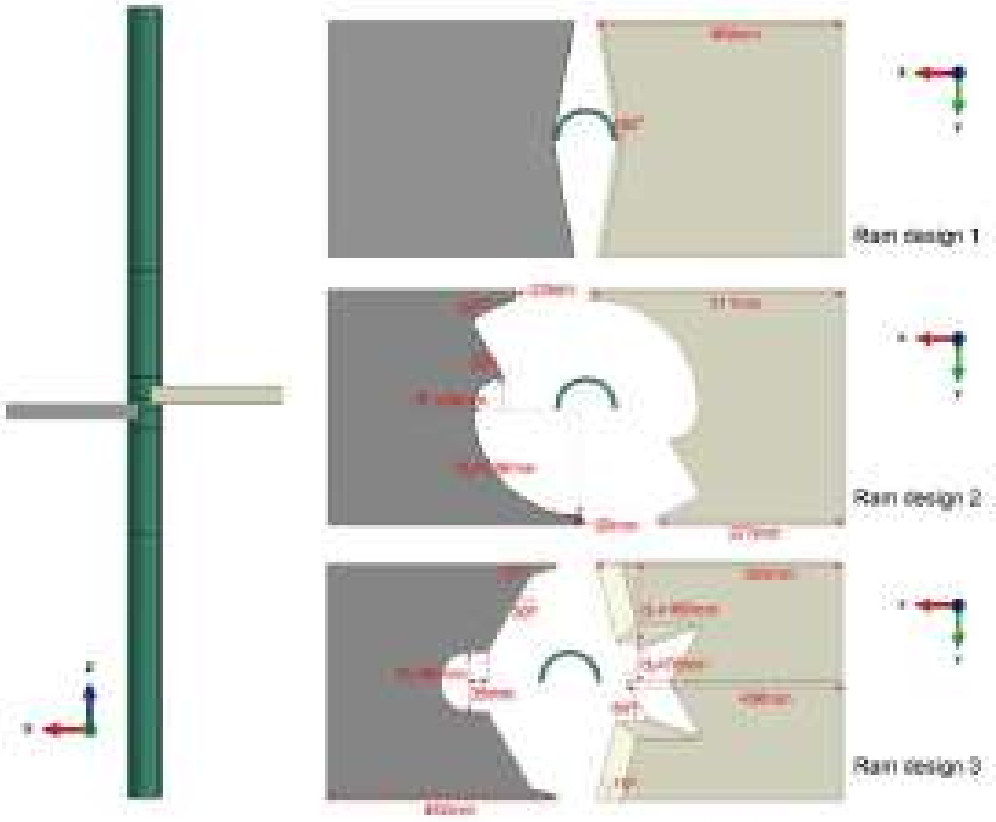

Figure 6.1: Geometrical dimensions of the drill pipe and BOP rams

Figure 6.1 illustrates the geometry of three rams under investigation in the top view and the set up of the FE model. Some characteristics can be observed from the shape of the three ram blades projected in the XY plane. It should be denoted that the discrepancy among the values of ram length in the X-axis does not affect the shearing force, while the thickness and the width in the Y-axis of the investigated upper and lower rams are consistent with that of the blind shear rams denoted in Figure 3.9. Especially, ram design 2 in Figure 6.1 includes two rams of the same dimension, but one of them is set up with 180∘ rotation around the X-axis. Each ram includes a curved face edge and cutting convex blade edge. The long curved edge on one side of each ram is designed to obtain more efficiency in pipe centralizing as rams moving forward. Besides, the convex blade next to the long curved edge is supposed to invade the material surface after the drill pipe gets stuck in the central position. For the ram design 3, the geometry of each ram is symmetrical about the X-axis, with a curved face edge and cutting convex blade edge in the center, respectively.

The rake angles of each pair of rams in current models are denoted in Figure 6.2. Accordingly, the rake angle also affects the required shearing force of each ram designation, however, considering that the calculating time of numerical simulations in this chapter would be multiply increased, and some previous studies have discussed

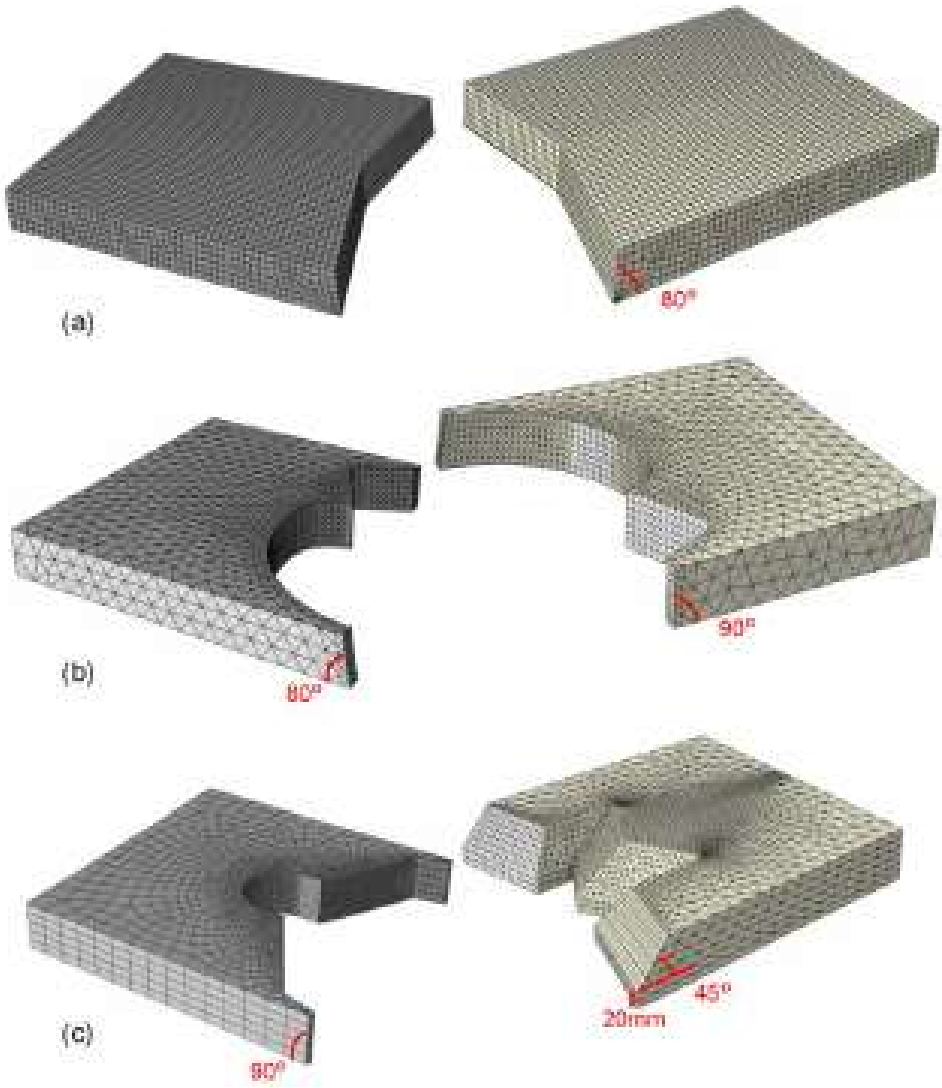

Figure 6.2: The mesh of rams for the respective model

the rake angle influence exhaustively, the current discussion focuses on comparing the blade edge shape influence with specific rake angle of each ram designation. Interested readers are referred to the numerical study of Koutsolelos[25] and the experimental study of Springett [15] for further information on the rake angle influence. R3D4 elements are used to simulate the rams under investigation. The mesh of each ram for the respective model is illustrated in Figure 6.2.

The pipe is set to be 3 m in length according to the discussion in chapter 4. To decrease the calculating time of the numerical model, the pipe is divided into 3 parts along the axial direction, as illustrated in Figure 6.3. Part 1 and part 3 is meshed with a coarse grid because they are far from the local deformation induced by ram shearing. Part 2 share the same mesh design with the former 1 m pipe model, as illustrated in Figure 3.17. Loading and boundary conditions remain consistent with the former 3 m pipe model illustrated in Figure 3.17. Only half of the pipe is

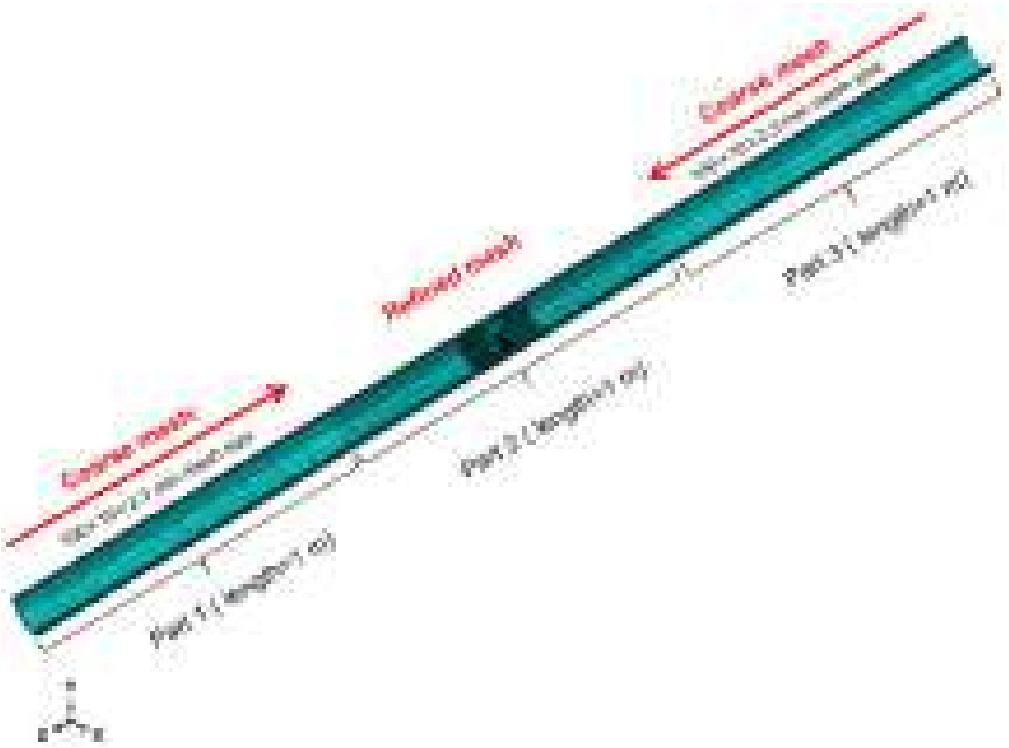

Figure 6.3: Mesh size for 3 m drill pipe

considered in the FE model.

6.3 Simulation results and analysis

Numerical simulations with three ram designations are conducted and the simulated ram shearing processes are compared and discussed. Figure 6.4 illustrates the stress distribution and pipe deformation combined with the relative position of the shear rams at the final rupture time for respective ram designation. It is visible that all of three pair of rams accomplish the shearing operation successfully, whereas the final deformation and the corresponding ram displacement is different. Besides, the cutting convex blade in ram design 2 and ram design 3 induced obvious local plastic deformation on the pipe surface, and the difference of their relative position of the ram edge cause two shear cross-section, illustrated in Figure 6.4 (b) and (c). It seems that the overall deformation on the pipe induced by ram design 3 is larger.

Figure 6.5 records the pipe cross-section in the XY plane for each model, the plane is located on the pipe symmetry center plane along the Z-axis. The cross-sections in the figure correspond to the ram displacement at peak shearing force point. According to the discussion in former chapters, these points occur right before the macrocrack initiation.

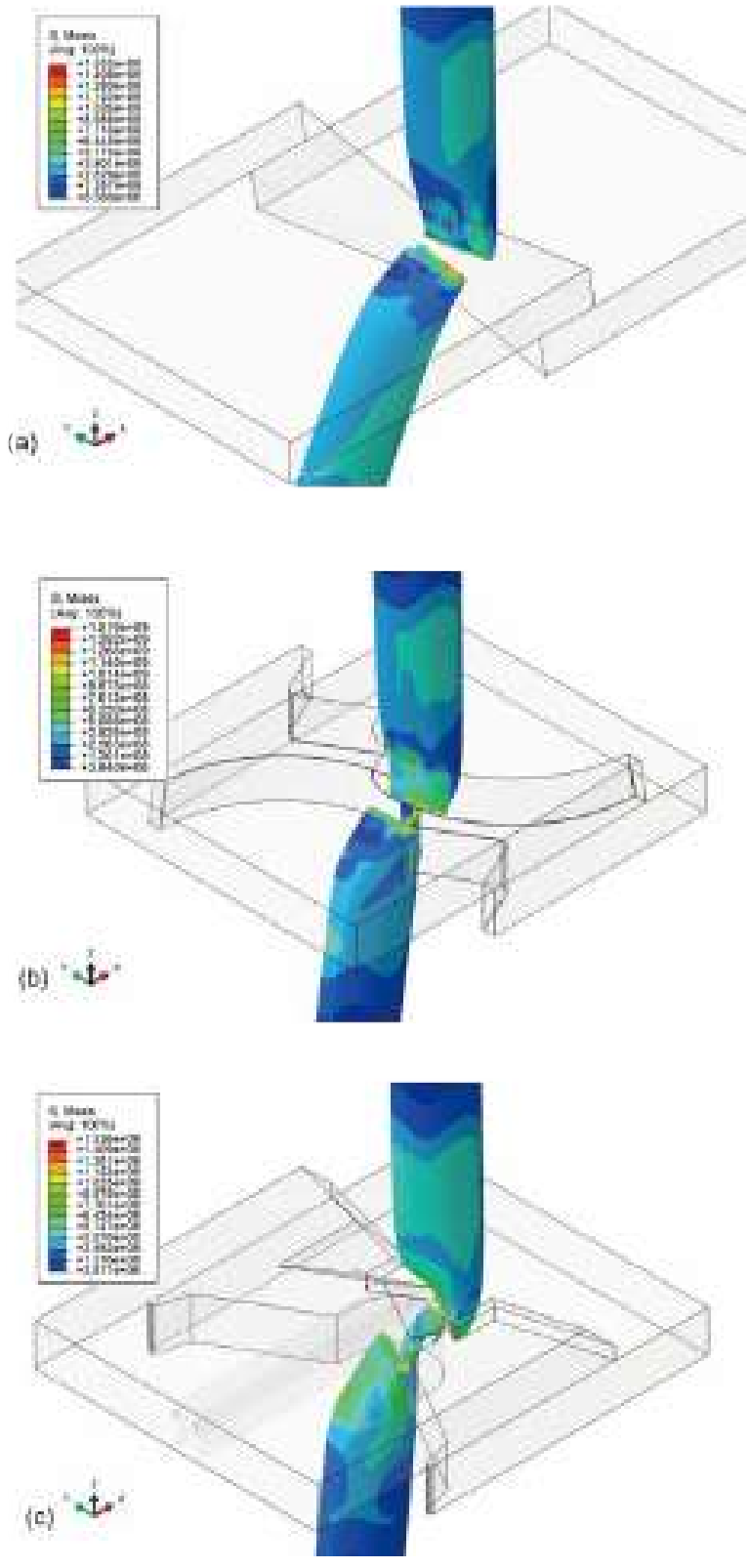

Figure 6.4: Stress distribution and deformation upon failure of the pipe

It can be seen from the figure that the pipe cross-section in each case is consistent with the shape of the ram edge at the shearing position. There are generally two types of large local shearing appearance, one is the shear effect caused the relative

movement of the ram, and the other is the direct invade caused by the convex design of the ram blade edge.

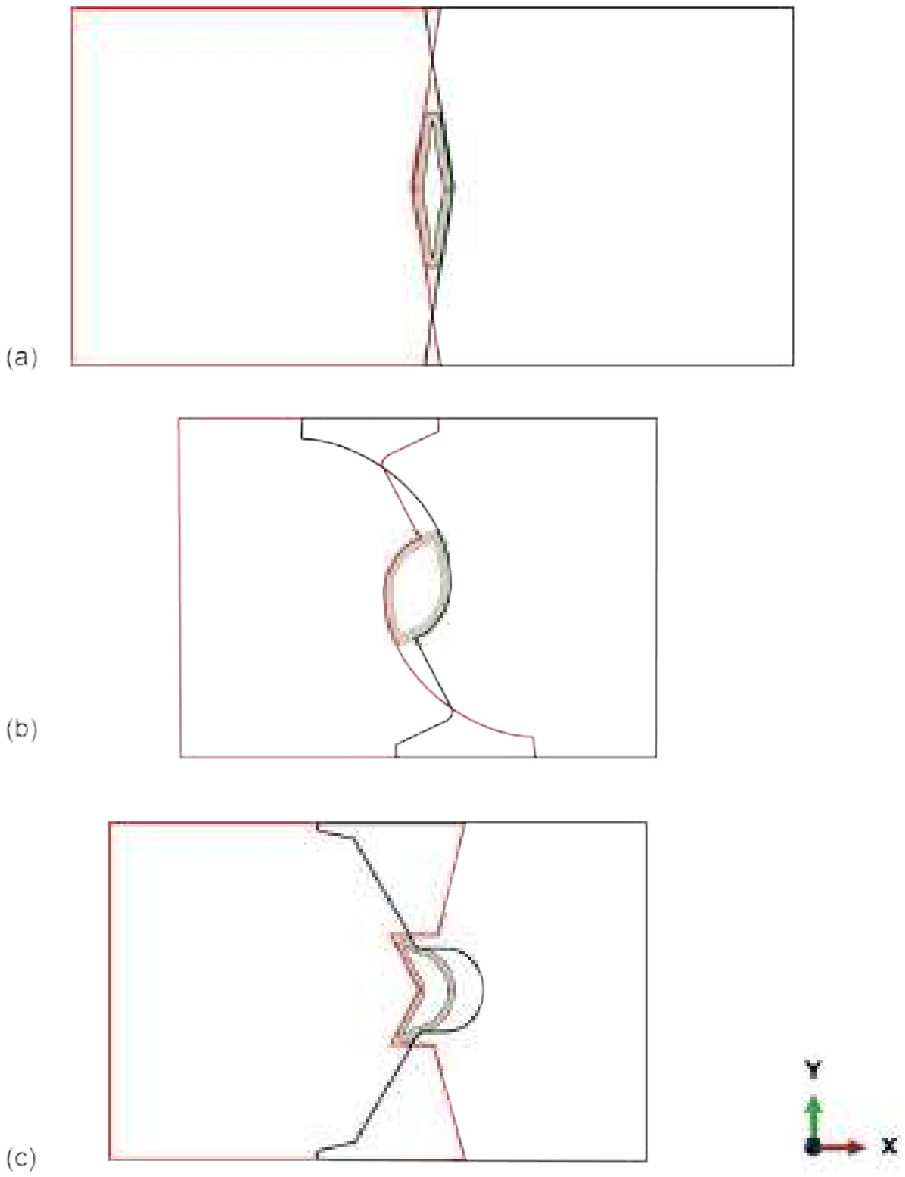

Figure 6.5: Pipe cross-sections with ram displacement at peak shearing force point

To further investigate how the blade of three ram designations deflect and shear the respective drill pipe, local enlarged side view contour of each ram shear zone is illustrated in Figure 6.6 - 6.8. The sequence in each figure consists of the ram shearing process. From the initial ram contact with the pipe until the final separation of the drill pipe, the total ram shearing process is denoted by 4 timepoints in these figures, corresponding to 25%, 50%, 75% and 100% ram displacement, respectively.

Figure 6.6 denotes the ram shearing process of ram design 1, which generally consists of the Rongshen double V-shaped ram shearing process analyzed in Chapter 5. As the V-shaped ram moving forward, both sides of the drill pipe surface are extruded to the center and almost flatten to a sheet. Since the ductility of TRIP690

is high, the shear and fracture begin after the pipe is total deformed. The high-stress distribution first occurs in the initial contact point between the pipe surface and rams, finally located on the opposite sides of the pipe cross-section due to the severe extrusion.

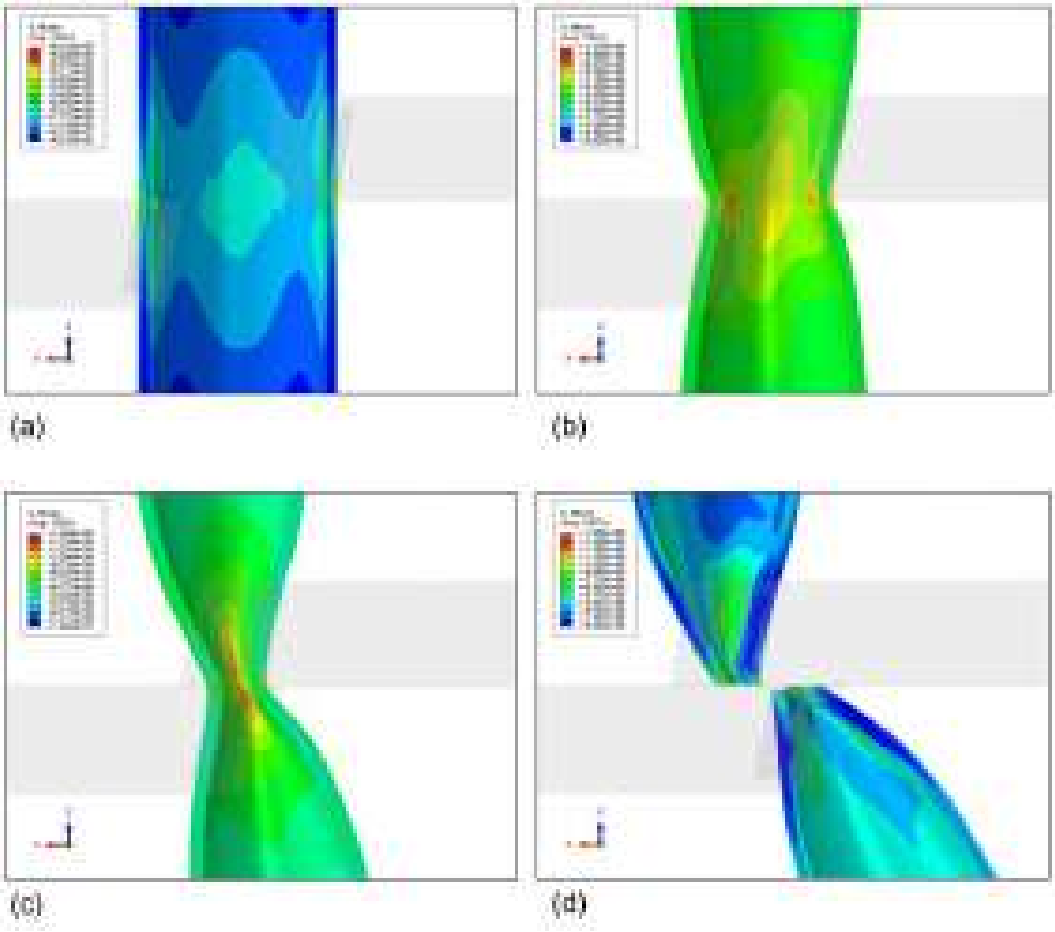

Figure 6.6: Side view contour of pipe in the shearing model with ram design 1

Figure 6.7 illustrates the ram shearing process of ram design 2. Not like the V-shaped ram edge, the long curved edge does not push the pipe surface towards the opposite side but press the pipe like a confining pressure, as shown in Figure 6.7 (b). Besides, it can be seen in Figure 6.7 (c) that the cutting convex blade invades the pipe surface like an anvil and induces stress concentration at the invades point. This may initiate a macrocrack on the pipe surface, thus the dislocation of the pipe will propagate along the circumference direction on the pipe when the curved blade moves furtherly. Under this situation, the final rupture can be seen as the result of crack propagation.

For the ram design 3 shown in Figure 6.8, a more obvious invade behavior occurs at the initial contact area between the pipe and the upper ram. With the further movement of the rams, the pipe surface is deflected seriously until the initial crack is

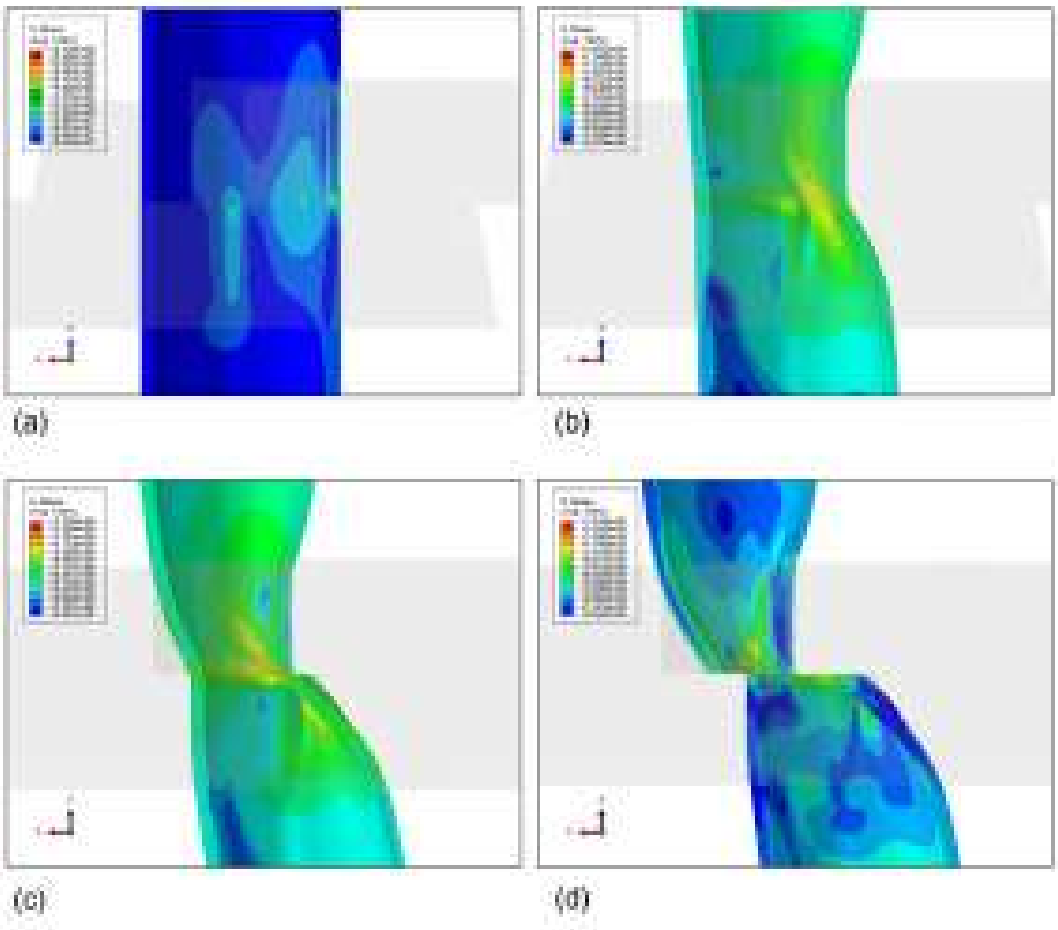

Figure 6.7: Side view contour of pipe in the shearing model with ram design 2

obtained, as shown in Figure 6.8(b). The crack propagates along the circumference direction until the total separation is complete. Note that the rake angle may influence the ram displacement corresponding to the initial crack. An early crack initiation facilitates the shearing process to complete. One can observe in Figure 6.8(d) that the tearing phenomenon is more obvious because the displacement for those elements on the right side of the pipe has a large displacement in the x axial direction. It should be noted that in this case, the pipe diameter is large than that of the curved edge of the lower ram blade. This causes the pipe to not contact the curve edge but contact with the lower ram blade in some areas instead. For a small diameter pipe or a longer curved edge designation, the ram design 3 may also shear the pipe with one curved edge and one convex blade, similar to ram design 2. In that case, the invaded zone located on the symmetry axis of the pipe cross-section.

Figure 6.9 presents the shearing force-displacement curve of BOP rams, obtained with the three ram geometry designations. It can be observed that the maximum shearing forces under three ram designation are different, the conventional double V ram, denoted by the black dotted line, requires the largest force to shear the

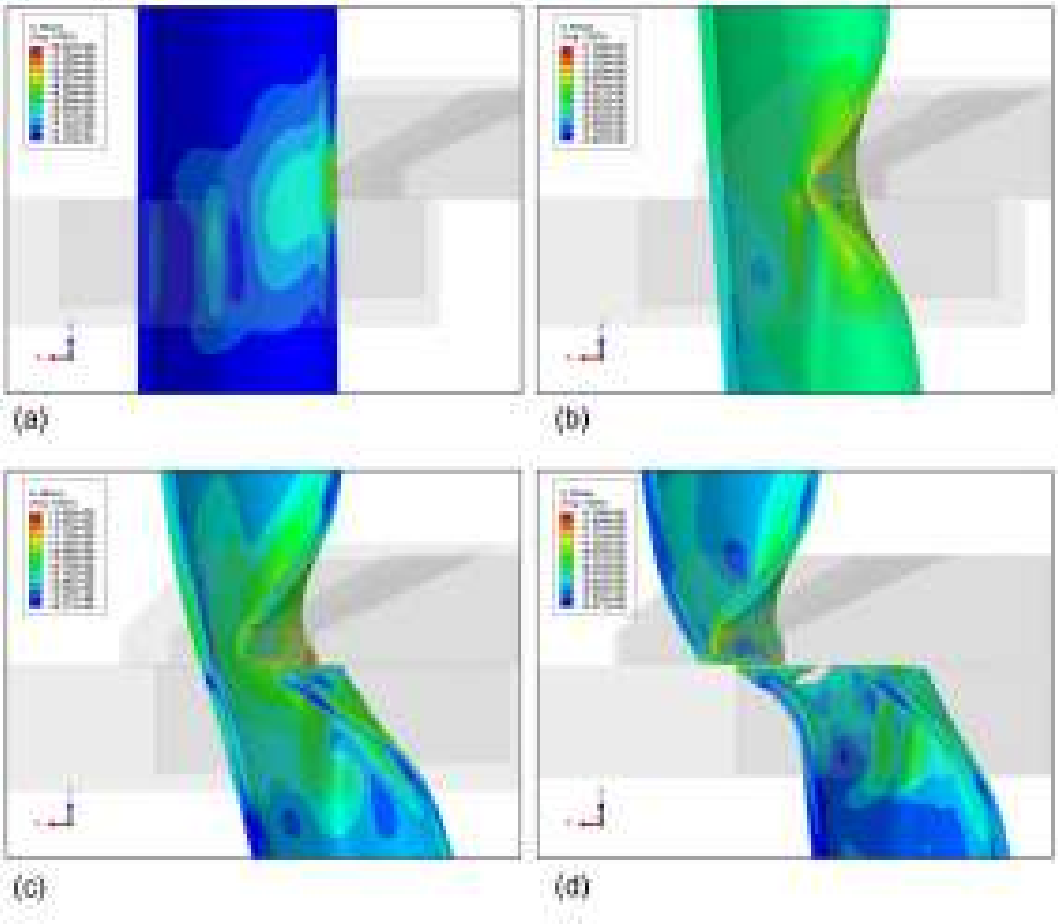

Figure 6.8: Side view contour of pipe in the shearing model with ram design 3

adopted drill pipe, while the ram 3 design requires the least shearing force, plot by the red solid line. An interesting observation is that unlike the conventional rams, the shearing forces corresponding to ram 2 and ram 3 designations have two peak values. A similar phenomenon is also reported in the experimental study of Springett [15] when presenting the shearing force curve of NOV LFS rams. The first peak value appears to correspond to the shear effect induced by the initial invade of the convex blade edge on the ram front surface. The second peak value is probably connected with the final shear of each pair of rams. According to the above analysis, it can be inferred that the stress concentration effect at the contact point of the blade edge causes macro crack initiation, denoted by the first peak value on the shearing force curve, then the crack growth along the pipe circumstantial direction and induce the curve drop to a small value. As the ram movement furtherly deform the pipe cross-section and finally separate the pipe, the curve increases to the second peak then drop to zero.

Based on the discussion of the shearing force curve and the stress distribution, the damage evolution on the drill pipe during the shearing process of each ram case is plotted in Figure 6.10. The time points of the contour plots in each figure correspond

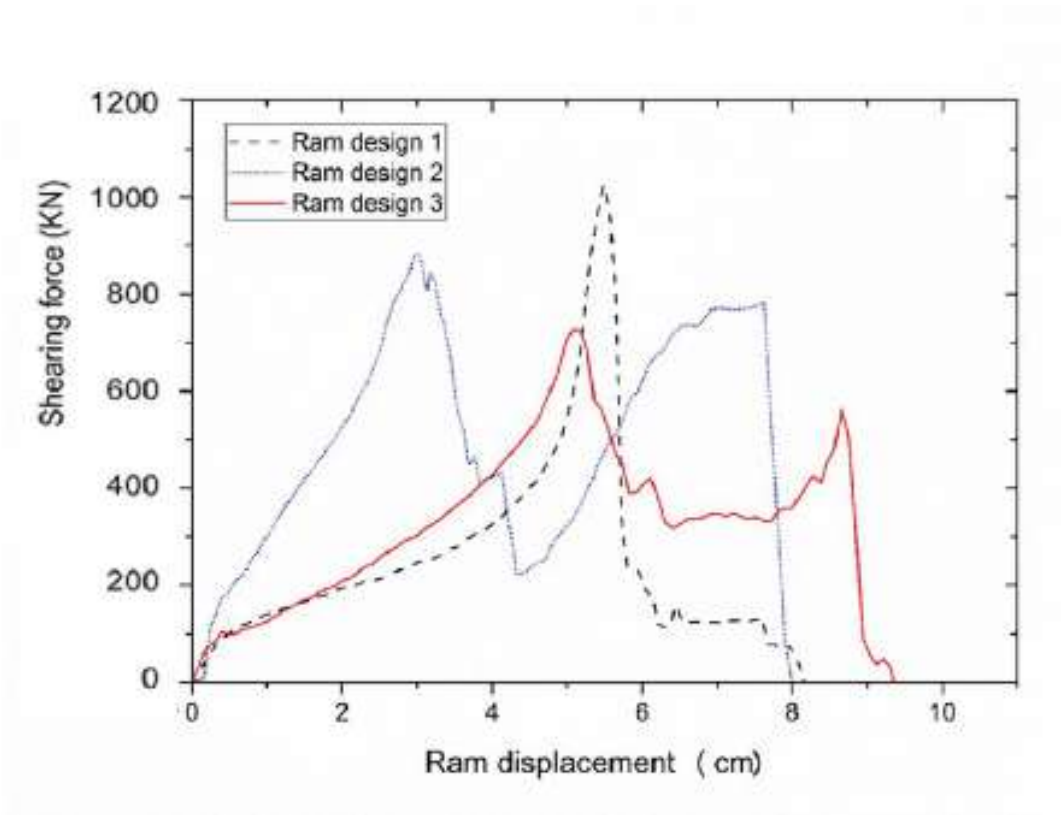

Figure 6.9: BOP ram shearing force curve with three ram designations

to the time points denoted in Figure 6.6 - 6.8. As damage only initiates after large accumulated plastic deformation, the first image of each case is eliminated, thus the remaining damage plot represents the full damage accumulation process from 25% ram placement until complete pipe reparation. To obtain a better illustration of the damage area evolution, the deformation of the pipe body and elements deletion are not shown. The three series (a), (b), and (c) correspond to damage predicted in the case of ram design 1, 2, and 3, respectively. It can be figured out that the damaged area predicted in all the three case evolute not only in the circumference direction but also along the radial direction. However, the red area which denotes the damage arrives 1 deflects the discrepancy of those pipe elements distorts due to the ram extrusion in the transverse direction in each case. In these two cases of ram design 2 and 3, damaged area distribution is more complicated because the invade of the convex blade edge on these rams induce an irregularly shaped damage distribution with a large area. In the aspect of the crack initiation, damage accumulation of ram 2 and ram 3 are satisfied for more number of elements, and the final damaged area is also larger than the ram 1 design. This may cause their final shearing force generally lower than the conventional double V ram, considering the stiffness degradation of damaged elements.

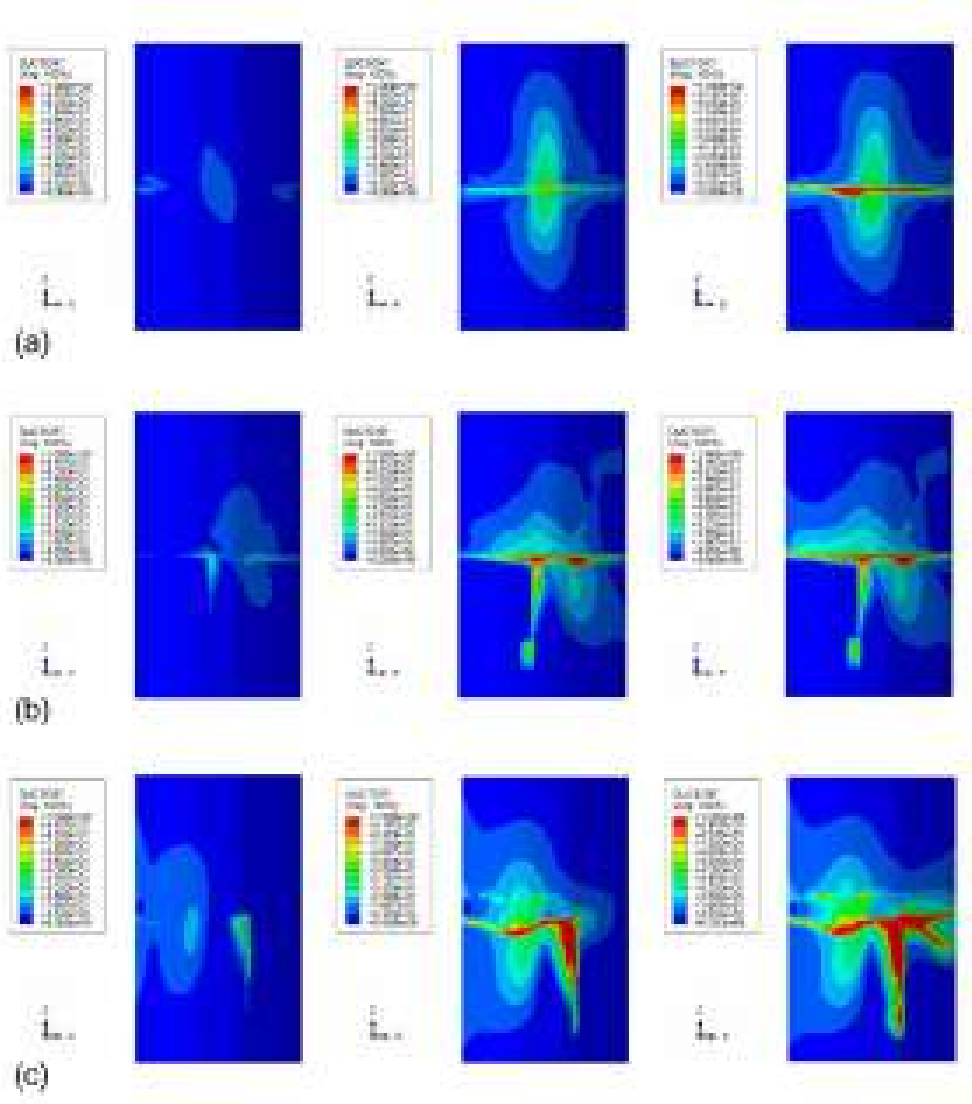

Figure 6.10: Damage evolution on the drill pipe during the shearing process for three ram designs

6.4 Summmary

This chapter demonstrates the potential of the built FE model combined with the MMC ductile fracture criterion. Considering the shearing process and ram shearing force curves of the latest ram designation are rarely provided in the literature, the analysis obtains valuable results about the shearing efficiency correlated with the ram designation. According to the simulation results, the rams with a curved face edge and cutting convex blade edge (ram design 2 and ram design 3) require 10% and 29% lower shearing force than the conventional DVS. Increased shearing efficiency can be attributed to the following aspects.

- There are generally two types of large local shearing appearance, one is the shearing effect caused the relative movement of the ram, and the other is the

direct invade caused by the convex design of the ram blade edge.

- The shape of the ram blade edge determines the pipe cross-section at the shearing position in each case, which furtherly optimizes the local shearing area for the final rupture.
- The cutting convex blade invades the pipe surface like an anvil and induces an early crack initiation, which facilitates the shearing process to complete.
- As indicated by the shearing force curve, those above effects generally divide the shearing process into two stages, the stress concentration effect at the contact point of the blade edge causes macro crack initiation, corresponding to the shearing maximum force, the final separation of the pipe is then obtained after the crack evolution along the pipe circumstantial direction, corresponding to another lower peak force.

Chapter 7

Conclusions and future studies

7.1 Conclusions

7.1.1 Maximum ram shearing force

The ram shearing process generally includes two main parts: the local pipe plastic deformation caused by the extrusion effect of the ram movement, and the failure of the pipe induced by the invading of the ram blade edge and the shearing effect of the opposite rams. By correlating the peak force of BOP ram shearing with the peak punch force in the blanking process, it is reasonable that the peak shearing force will be obtained if the decrease in load caused by the reduction of sheared area outweighs the increase in load associated with plastic hardening. The reduction of shear area is determined by the crack initiation and propagation due to ram invade, while the increased load induced by plastic deformation basically influenced by the plasticity and loading conditions of the pipe.

According to simulation results in the thesis, the following loading conditions may influence ram shearing force.

- When other influencing factors remain unchanged, the required shearing force increases when a drill pipe with the larger outer diameter need to be cut. Comparing the case of shearing ϕ127 mm with ϕ139.7 mm drill pipe, the increasing ratio of the later to the former is 10.2% according to the simulation result in the Chapter 3. To compare the case of shearing ϕ88.9 mm with ϕ127 mm drill pipe, this increasing ratio is 14.3%.

- The required shearing force without tension or compression is higher than that of pipe under compression or tension, the difference ratio range from 0.7% to 10.5% , and from 0.6% to 8%, respectively. The larger outer diameter indicates a higher difference ratio.

- In the non-centralized position inside the blade cover range, the pipe needs 17% lower shearing force to be cut. For specific well configuration, if it is in the non-centralized position beyond the width of the blade, likely the pipe will not be fully cut, and the blind shear ram may have difficulty reaching the condition to seal the well.

- Ram blade designation influence the shearing force by applying different shearing mechanics. With those specific ram designations adopted in this thesis, to shear the same centralized pipe, DVS ram requires 26% lower shearing force than BSR, while the rams with a curved face edge and cutting convex blade edge (ram design 2 and ram design 3 in chapter 6) require 10% and 29% lower shearing force than the conventional DVS.

7.1.2 Comparison and selection of fracture criteria

Constant failure criterion, such as the shear failure criterion, can be adopted to investigate the influence of pipe geometry and loading conditions on the shearing force, but not capable to estimate the ram shearing force accurately. With only one parameter to reflect the material's ductility, the criterion is very difficult to calibrate by mechanical test, the maximum shearing force strongly depends on parameter selection.

The J-C criterion seems to be not reliable according to its fracture limit curve and the predicted BOP shearing force results. Since the plastic strain rate and temperature do not vary greatly in the BOP shearing process this criterion should be applied more cautiously, because the equivalent plastic strain at the fracture is uniquely related to stress triaxiality. Using only the stress triaxiality to predict the fracture in complicated loading conditions is often insufficient.

Modern fracture criteria such as CrashFEM and MMC criteria usually use more than one variable to characterize the stress state and are suitable for BOP ram shearing simulation due to the complicated stress state in the shearing process. Based on the TRIP 690 fracture limit curve-fitting optimization introduced in Chapter 4, most of the experimental data points corresponding to various stress states are passed through by these fracture curves. Both of these criteria provide close results to API E-75 material shear test data for BOP ram shear force prediction.

For the comparison of the predicted force value with the respective criterion, the difference of predicted shearing force using MMC, CrashFEM, and J-C criteria to average test value is 8.32%, -5.69%, and -34.44%, respectively. The discrepancy can be attributed to three main aspects. First, the difference of the shape for the fracture limit curves reflects the mathematic aspect differs from each model. Second, the damage initiation is predicted at different time points in the same shearing

process, which means that, for the large deformation part of the pipe, the stiffness degradation may begin at a different time for the same pipe element. Last, the damage distribution in the shearing area changes according to the specific fracture criterion. These phenomena further affect the stress state of pipe elements in the location close to the ram shearing position, which eventually causes inconsistency in the overall shearing force.

7.1.3 Fracture criterion application and damage parameters derivation

A thorough FE model was set up to simulate the BOP shearing process. Progressive damage framework and individual fracture criterion are implemented in Abaqus/Explicit with mesh sensitivity studies. To capture the damage initiation and failure process on the pipe, a modified derivation process for the CrashFEM criterion is proposed to obtain the ductile damage limit curve of actual drill pipe material. A full-scale BOP shearing experiment is conducted to verify the proposed approach. According to the simulation results, the following conclusions may be drawn:

- The proposed new damage initiation curve of S135 drill pipe material provides simulation results consistent with the experimental results, the shape of the simulated shearing pressure curve agrees with the shape of the experimental pressure-time curve in the post-elastic region.
- The peak value of the shearing pressure-time curve is sensitive to the ductile damage initiation curve. Compared with the experimental curve, the simulated pressure-time curve for S135 material in Chapter 5 shows that the proposed correction method for ram shearing simulation lower the maximum shearing pressure error from 19.7% to 3.2%.
- For the double V ram shearing process, high stress is concentrated at the contact point in the initial cutting stage. As the rams further squeeze the pipe, high-stress regions occur both in circumferential and axial direction because of the line-to-surface contact pattern around the flattened pipe body.
- The difference ratio of the pipe fish cross-section between the simullation and experiment range from 0.7% to 4.8%. The damage regions on the pipe surface caused by the ram squeeze develop in the circumferential direction, while the buckle of the pipe induces a damage region along the axial direction.
- According to the numerical simulation, the macro-crack on the pipe body surface at the upper ram contact area is completed earlier that the lower ram,

which causes the element in the later zone to experience more tensile effects and generate more burrs.

7.2 Suggestions for future studies

To further investigate the fracture theory in ram shearing simulation, the following topics are suggested for future studies.

- Calibration of fracture parameters of actual drill pipe material with several fracture tests. These test results may bring further understanding of the ductility of drill pipe material and also will help to obtain fracture locus under a wide range of stress state.
- Design a small scale shearing specimen with actual drill pipe material which can characterize the stress state of ram shearing with a less experimental cost. The original scale of the ram shearing experiment makes it difficult to verify the simulation result.
- Correlating the fracture parameters calibration with more standard mechanical properties of drill pipe material such as the Charpy value and elongation. An easier calibration of the actual drill pipe material fracture parameters will surely facilitate the application of the fracture criteria.
- Plasticity model of the actual drill pipe material considering the differences between tension and compression. Since the damage in the pipe fracture area accumulates in both negative and positive triaxiality ranges, this plastic model may capture the plastic deformation of the drill pipe to be sheared.

Bibliography

[1] ISMAIL, Z., KONG, K. K., OTHMAN, S. Z., et al. "Evaluating accidents in the offshore drilling of petroleum: Regional picture and reducing impact", *Measurement*, v. 51, pp. 18–33, 2014.

[2] ESTEFEN, S. F., LOURENÇO, M. I. *Safety of Subsea Exploration and Production Operations*. Relatório Técnico PENO-19367, COPPE/UFRJ, 2016.

[3] SANTOS, O. L. A., BRASILEIRO, P. "Ways to successfully reduce well blowout events", .

[4] HAN, C., YANG, X., ZHANG, J., et al. "Study of the damage and failure of the shear ram of the blowout preventer in the shearing process", *Engineering Failure Analysis*, v. 58, pp. 83–95, 2015.

[5] *Investigation Report Volume 2, Explosion and Fire at the Macondo Well*. Relatório Técnico 2010-10-I-OS, U.S. Chemical Safety and Hazard Investigation Board, Washington, D.C., 2010.

[6] *Specification for Drill-through Equipment*. Api specification 16a,4th edition, 2017.

[7] *Macondo Well Incident,Transocean Investigation Report, Volume I*. Relatório técnico, Transocean, 2011.

[8] KACHICH, A. "Double Shearing Rams For Ram Type Blowout Preventer". .

[9] CHILDS, G., SATTLER, J., WILLIAMSON, R. *Shear Ram Capabilities Study for U.S. Minerals Management Service*. Relatório Técnico 3-4025-1001, West Engineering Service, 2004.

[10] GRÖNDAHL, M., PARK, H., ROBERTS, G., et al. "Investigating the Cause of the Deepwater Horizon Blowout". 2010. Disponível em: <`http://www.nytimes.com/interactive/2010/06/21/us/%0A20100621-bop.html`>.

[11] *Forensic Examination of Deepwater Horizon Blowout Preventer, Final Report for United States Department of the Interior*. Relatório Técnico EP030842, DET NORSKE VERITAS, 2011.

[12] BOARD, M., COUNCIL, N. R., OTHERS. "Macondo Well Deepwater Horizon Blowout: Lessons for Improving Offshore Drilling Safety". National Academies Press, 2012.

[13] LINDLEY, R. A., BRAUN, J. C. *Best Practice for Verification Test Protocol of Blowout Preventer (BOP) Shear Rams Used for US OCS Oil and Gas Operation*. Relatório técnico, Argonne National Laboratory, 2017.

[14] CHILDS, G., SATTLER, J., WILLIAMSON, R. *Mini Shear Study for U.S. Minerals Management Service*. Relatório Técnico 2-1011-1003, West Engineering Service, 2002.

[15] SPRINGETT, F. B., ENSLEY, E. T., YENZER, D., et al. "Low force shear rams: The future is more". In: *SPE IADC Drilling Conference and Exhibition*. Society of Petroleum Engineers, 2011.

[16] TULIMILLI, B. R., NAIK, P., CHAKRABORTY, A., et al. "Design Study of BOP Shear Rams Based on Validated Simulation Model and Sensitivity Studies". In: *ASME 2014 33rd International Conference on Ocean, Offshore and Arctic Engineering*. American Society of Mechanical Engineers Digital Collection, 2014.

[17] TULIMILLI, B. R., NAIK, P., CHAKRABORTY, A., et al. "Experimental and Numerical Investigation of BOP Shear Ram Performance". In: *ASME 2014 33rd International Conference on Ocean, Offshore and Arctic Engineering*. American Society of Mechanical Engineers Digital Collection, 2014.

[18] EVANGELATOS, G., POLLOCK, T. N., PAYNE, M. L., et al. "Advanced Model for the Prediction of Tubular Shear Mechanics". In: *SPE Deepwater Drilling and Completions Conference*. Society of Petroleum Engineers, 2014.

[19] ROBERT, B. A., ABERNETHY, B. "The new Weibull handbook", *North Palm Beach*, pp. 13–46, 1996.

[20] H., E., JR., T. C. "BOP Shearing: FEA Modelling with Void Coalescence Ductile Fracture Theory". In: *Offshore Technology Conference Asia*, 2016.

[21] *Evaluate Oil and Gas Industry's Ability to Perform BOP Shearing Tests Under Simulated Blowout Flow Conditions*. Relatório Técnico 100102.01-DG-RPT-0001, Wood Group Kenny, 2015.

[22] ABERNETHY, R. *Shear ram blowout preventer forces required*. Relatório técnico, Barringer & Associates Inc Florida, 2010.

[23] *BOP Shear and Pressure Testing of Intelligent Completion Tubing– Results and Lessons Learned*. Relatório técnico, Woodside, 2014.

[24] TEKIN, A., CHOI, C., ALTAN, T., et al. "Estimation of shear force for blind shear ram blowout preventers", *Research on Engineering Structures & Materials*, v. 1, pp. 39–51, 2015.

[25] KOUTSOLELOS, E. *Numerical Analysis of a Shear Ram and Experimental Determination of Fracture Parameters*. Master thesis.

[26] ZHU, L., ESTEFEN, S. F., DE MOURA JORGE, N. "Numerical Simulation of Shear Ram Performance". In: *37th International Conference on Ocean, Offshore & Arctic Engineering*, 2018.

[27] TEKIN, A. *Estimation of Shear Force and Optimization of Ram Geometry*. Master thesis.

[28] *Assessment of BOP Stack Sequencing, Monitoring and Kick Detection Technology*. Relatório Técnico 12-1841-DG-RPT-0003, Mcs kenny, 2013.

[29] HORSTKETTER, R., EGERAAT, S. V., OTHERS. "Norg Wells: An Evolutionary Step in Pipe Shearing Technology". In: *SPE/IADC Drilling Conference and Exhibition*. Society of Petroleum Engineers, 2015.

[30] LIU, Z., GUO, J., GUO, T., et al. "Force prediction in blow-out preventer shearing of drill pipes", *Engineering failure analysis*, v. 74, pp. 159–171, 2017.

[31] MCCLENEY, A., GREEN, S., MUESCHKE, N. "Modeling of Subsea BOP Shear and Sealing Ability Under Flowing Conditions". In: *Offshore Technology Conference*, 2018.

[32] GREEN, S. T., MUESCHKE, N., MCCLENEY, A., et al. *SUBSEA BOP STACK SHEAR/SEAL CAPABILITY MODELING TOOL*. Relatório Técnico E15PC00006, Southwest Research Institute, 2017.

[33] GRIFFITH, A. A. "VI. The phenomena of rupture and flow in solids", *Philosophical transactions of the royal society of london. Series A, containing papers of a mathematical or physical character*, v. 221, n. 582-593, pp. 163–198, 1921.

[34] BAO, Y. *Prediction of ductile crack formation in uncracked bodies*. Tese de Doutorado, Massachusetts Institute of Technology, 2003.

[35] OROWAN, E. "Fracture and strength of solids", *Reports on progress in physics*, v. 12, n. 1, pp. 185, 1949.

[36] IRWIN, G. R. "Analysis of stresses and strains near the end of a crack transversing a plate", *Trans. ASME, Ser. E, J. Appl. Mech.*, v. 24, pp. 361–364, 1957.

[37] RICE, J. R., TRACEY, D. M. "On the ductile enlargement of voids in triaxial stress fields", *Journal of the Mechanics and Physics of Solids*, v. 17, n. 3, pp. 201–217, 1969.

[38] MCCLINTOCK, F. A. "A criterion for ductile fracture by the growth of holes", *Journal of Applied Mechanics*, v. 35, n. 3, pp. 617–617, 09 1968. ISSN: 0021-8936.

[39] KACHANOV, L. M. "Rupture time under creep conditions", *International journal of fracture*, v. 97, n. 1-4, pp. 11–18, 1999.

[40] LEMAITRE, J. "A Continuous Damage Mechanics Model for Ductile Fracture", *Journal of Engineering Materials and Technology*, v. 107, n. 1, pp. 83–89, 01 1985. ISSN: 0094-4289. doi: 10.1115/1.3225775.

[41] YU, J.-L., JONES, N. "Numerical simulation of impact loaded steel beams and the failure criteria", *International Journal of Solids and Structures*, v. 34, n. 30, pp. 3977–4004, 1997.

[42] KOFIANI, K. N., KOUTSOLELOS, E., WIERZBICKI, T., et al. "Shear-generated fracture in predicting oil leak in accidents involving sinking platforms". In: *The Twenty-first International Offshore and Polar Engineering Conference*. International Society of Offshore and Polar Engineers, 2011.

[43] JOHNSON, G., COOK, W. "Fracture characteristics of three metals subjected to various strains, strain rates and temperatures and pressures". 1985.

[44] PARDOEN, T., HUTCHINSON, J. "An extended model for void growth and coalescence", *Journal of the Mechanics and Physics of Solids*, v. 48, n. 12, pp. 2467–2512, 2000.

[45] YU, S., XIE, X., ZHANG, J., et al. "Ductile fracture modeling of initiation and propagation in sheet-metal blanking processes", *Journal of materials processing technology*, v. 187, pp. 169–172, 2007.

[46] HAMBLI, R., RESZKA, M. "Fracture criteria identification using an inverse technique method and blanking experiment", *International journal of mechanical sciences*, v. 44, n. 7, pp. 1349–1361, 2002.

[47] BAO, Y., WIERZBICKI, T. "A comparative study on various ductile crack formation criteria", *J. Eng. Mater. Technol.*, v. 126, n. 3, pp. 314–324, 2004.

[48] BAO, Y., WIERZBICKI, T. "On fracture locus in the equivalent strain and stress triaxiality space", *International Journal of Mechanical Sciences*, v. 46, n. 1, pp. 81–98, 2004.

[49] EL-MAGD, E., GESE, H., THAM, R., et al. "Fracture criteria for automobile crashworthiness simulation of wrought aluminium alloy components", *Materialwissenschaft und Werkstofftechnik: Materials Science and Engineering Technology*, v. 32, n. 9, pp. 712–724, 2001.

[50] HOOPUTRA, H., GESE, H., DELL, H., et al. "A comprehensive failure model for crashworthiness simulation of aluminium extrusions", *International Journal of Crashworthiness*, v. 9, n. 5, pp. 449–464, 2004.

[51] XUE, L. "Damage accumulation and fracture initiation in uncracked ductile solids subject to triaxial loading", *International journal of solids and structures*, v. 44, n. 16, pp. 5163–5181, 2007.

[52] XUE, L. "Constitutive modeling of void shearing effect in ductile fracture of porous materials", *Engineering Fracture Mechanics*, v. 75, n. 11, pp. 3343–3366, 2008.

[53] BAI, Y., WIERZBICKI, T. "A new model of metal plasticity and fracture with pressure and Lode dependence", *International journal of plasticity*, v. 24, n. 6, pp. 1071–1096, 2008.

[54] WIERZBICKI, T., BAO, Y., LEE, Y.-W., et al. "Calibration and evaluation of seven fracture models", *International Journal of Mechanical Sciences*, v. 47, n. 4-5, pp. 719–743, 2005.

[55] BAI, Y., WIERZBICKI, T. "A comparative study of three groups of ductile fracture loci in the 3D space", *Engineering Fracture Mechanics*, v. 135, pp. 147–167, 2015.

[56] WALTERS, C. L. *Development of a punching technique for ductile fracture testing over a wide range of stress states and strain rates*. Tese de Doutorado, Massachusetts Institute of Technology, 2009.

[57] CHOTTIN, J., HUG, E., RACHNIK, M. "Damage accumulation in DP1000 sheets submitted to various stress states Steel Res". In: *Int. Spec. Ed. ICTP Conf*, pp. 895–900, 2011.

[58] BEHRENS, B.-A., BOUGUECHA, A., VUCETIC, M., et al. "Characterisation of the quasi-static flow and fracture behaviour of dual-phase steel sheets in a wide range of plane stress states", *Archives of Civil and Mechanical Engineering*, v. 12, n. 4, pp. 397–406, 2012.

[59] KOFIANI, K. N. *Ductile fracture and structural integrity of pipelines & risers*. Tese de Doutorado, Massachusetts Institute of Technology, 2013.

[60] PICKETT, A. K., PYTTEL, T., PAYEN, F., et al. "Failure prediction for advanced crashworthiness of transportation vehicles", *International Journal of Impact Engineering*, v. 30, n. 7, pp. 853–872, 2004.

[61] LEPPIN, C., KUTSCHER, M., FEUERSTEIN, M., et al. "Fracture prediction for crashworthiness assessment of aluminum bumper systems", *Bamberg: LS-DYNA Anwenderforum*, 2008.

[62] ISIK, K., SOYARSLAN, C., RICHTER, H., et al. "Analysis of formability of advanced high strength steel sheets with phenomenologically based failure criteria with separate treatment of instability, shear and normal fracture". In: *LS-DYNA 8th European users conference, Strasbourg, France*, 2011.

[63] DELL, H., GESE, H., KESSLER, L., et al. *Continuos Failure Prediction Model for Nonlinear Load Paths in Successive Stamping and Crash Processes*. Relatório técnico, SAE Technical Paper, 2001.

[64] BAI, Y. *Effect of loading history on necking and fracture*. Tese de Doutorado, Massachusetts Institute of Technology, 2007.

[65] WIERZBICKI, T., SUH, M. "Indentation of tubes under combined loading", *International Journal of Mechanical Sciences*, v. 30, n. 3-4, pp. 229–248, 1988.

[66] PAPA, I., FORMISANO, A., LOPRESTO, V., et al. "Low velocity impact behaviour of reinforced plastic laminates: Indentation and penetration laws validated for different fibres and matrices", *Composites Part B: Engineering*, v. 164, pp. 61–66, 2019.

[67] WANG, K., WIERZBICKI, T. "Experimental and numerical study on the plane-strain blanking process on an AHSS sheet", *International journal of fracture*, v. 194, n. 1, pp. 19–36, 2015.

[68] ATKINS, A. "On cropping and related processes", *International Journal of mechanical sciences*, v. 22, n. 4, pp. 215–231, 1980.

[69] SLATER, R., JOHNSON, W. "The effects of temperature, speed and strain-rate on the force and energy required in blanking", *International Journal of Mechanical Sciences*, v. 9, n. 5, pp. 271–276, 1967.

[70] ISSA, D. L. *Testing and prediction of failure of AHSS sheets at die radius and sidewall using novel fracture apparatus*. Tese de Doutorado, Massachusetts Institute of Technology, 2009.

[71] LIAN, J., SHARAF, M., ARCHIE, F., et al. "A hybrid approach for modelling of plasticity and failure behaviour of advanced high-strength steel sheets", *International Journal of Damage Mechanics*, v. 22, n. 2, pp. 188–218, 2013.

[72] LIAN, J., WU, J., MÜNSTERMANN, S. "Evaluation of the cold formability of high-strength low-alloy steel plates with the modified Bai–Wierzbicki damage model", *International Journal of Damage Mechanics*, v. 24, n. 3, pp. 383–417, 2015.

[73] KIRAN, R., KHANDELWAL, K. "A triaxiality and Lode parameter dependent ductile fracture criterion", *Engineering Fracture Mechanics*, v. 128, pp. 121–138, 2014.

[74] ABAQUS, V. "6.14 Documentation", *Dassault Systemes Simulia Corporation*, v. 651, pp. 6–2, 2014.

[75] LI, Y., WIERZBICKI, T. "Prediction of plane strain fracture of AHSS sheets with post-initiation softening", *International Journal of Solids and Structures*, v. 47, n. 17, pp. 2316–2327, 2010.

[76] BESSON, J. "Continuum models of ductile fracture: a review", *International Journal of Damage Mechanics*, v. 19, n. 1, pp. 3–52, 2010.

[77] XIANPING, H. *Working mechanism of the shear ram blowout preventer and Structure Improvement*. Tese de Doutorado, Southwest Petroleum University, 2014.

[78] HANCOCK, J., MACKENZIE, A. "On the mechanisms of ductile failure in high-strength steels subjected to multi-axial stress-states", *Journal of the Mechanics and Physics of Solids*, v. 24, n. 2-3, pp. 147–160, 1976.

[79] KOFIANI, K., WIERZBICKI, T., NONN, A., et al. "Experiments and fracture modeling of high-strength pipelines for high and low stress triaxialities". In: *The Twenty-Second International Offshore and Polar Engineering Conference*. International Society of Offshore and Polar Engineers, 2012.

[80] NONN, A., KALWA, C. "Modelling of damage behaviour of high strength pipeline steel". In: *Proc. of ECF18, 363_proceeding. pdf, 18th European Conference on Fracture, Dresden, Germany*, 2010.

[81] TANGUY, B., LUU, T. T., PERRIN, G., et al. "Plastic and damage behaviour of a high strength X100 pipeline steel: Experiments and modelling", *International Journal of Pressure Vessels and Piping*, v. 85, n. 5, pp. 322–335, 2008.

[82] ZAMANI, S. M., HASSANZADEH-TABRIZI, S. A., SHARIFI, H. "Failure analysis of drill pipe: A review", *Engineering Failure Analysis*, v. 59, pp. 605–623, 2016.

[83] HAN, Y., ZHAO, X., BAI, Z., et al. "Failure analysis on fracture of a S135 drill pipe", *Procedia Mater. Sci*, v. 3, pp. 447–453, 2014.

[84] LIU, W., LIU, Y., CHEN, W., et al. "Longitudinal crack failure analysis of box of S135 tool joint in ultra-deep well", *Engineering Failure Analysis*, v. 48, pp. 283–296, 2015.

[85] MISCOW, G., DE MIRANDA, P., NETTO, T., et al. "Techniques to characterize fatigue behaviour of full size drill pipes and small scale samples", *International Journal of Fatigue*, v. 26, n. 6, pp. 575–584, 2004.

[86] SPEC, A. "5D Specification for Drill pipe", *Fourth Edi—tionEM]. Washington IX*, 1999.

[87] EMRE, H. E., KAÇAR, R. "Effect of post weld heat treatment process on microstructure and mechanical properties of friction welded dissimilar drill pipe", *Materials Research*, v. 18, n. 3, pp. 503–508, 2015.

[88] REN, W., WANG, J., REINIKAINEN, T. "Application of ABAQUS/Explicit submodeling technique in drop simulation of system assembly". In: *Proceedings of 6th Electronics Packaging Technology Conference (EPTC 2004)(IEEE Cat. No. 04EX971)*, pp. 541–546. IEEE, 2004.

[89] MISCOW, G. F. *Fatigue of Materials Used in Drill Pipes*. Tese de Doutorado, Federal University of Rio de Janeiro, 2015.

[90] KIM, Y.-J., HUH, N.-S., KIM, Y.-J., et al. "On relevant Ramberg-Osgood fit to engineering nonlinear fracture mechanics analysis", *J. Pressure Vessel Technol.*, v. 126, n. 3, pp. 277–283, 2004.

[91] SATTLER, J. P., OTHERS. "BOP Performance-Developments and Consequences in a Post-Macondo World". In: *SPE/IADC Drilling Conference*. Society of Petroleum Engineers, 2013.